THÈSE

PRESENTEE A

L'UNIVERSITE DE PAU ET DES PAYS DE L'ADOUR

ECOLE DOCTORALE DES SCIENCES EXACTES ET DE LEURS APPLICATIONS

PAR

MUHAMMAD SULTAN

POUR OBTENIR LE GRADE DE

DOCTEUR

Spécialité : Physique

───────────────────

TOWARDS A HIGH PRESSURE PIEZOELECTRIC AXIAL VIBRATOR RHEOMETER

───────────────────

Soutenue le **Mardi 02 Octobre 2012**

Après avis de:

M. A. BAYLAUCQ	Ingénieur, HDR - TOTAL SA	
Mme. J. FERNANDEZ	Professeur - Université Saint-Jacques de Compostelle	**Rapporteurs**

Devant la Commission d'examen formée de:

M. G. GALLIERO	Professeur - Université de Pau et des Pays de l'Adour	**Président**
M. A. BAYLAUCQ	Ingénieur, HDR - TOTAL SA	
Mme. J. FERNANDEZ	Professeur - Université Saint-Jacques de Compostelle	
M. A. GRACIAA	Professeur - Université de Pau et des Pays de l'Adour	**Examinateurs**
M. F. MONTEL	Expert - TOTAL SA	
M. M. MILHET	Ingénieur de Recherche - Université de Pau et des Pays de l'Adour	

- 2012 -

ACKNOWLEDGEMENTS

Table of Contents

List of Figures

List of Tables

Nomenclature

Abbreviations

API   American petroleum institute

EV   Equipement variation

AV   Appraiser variation

R&R   Reproducibility and repeatability

s.d.   Standard deviation

Small Letters

d   Gap size or sample thickness (mm)

d_{spacer} Spacer thickness (mm)

d_{eff} Effective thickness (mm)

h   Spacer thickness (mm).

t   Time (seconds)

n   Flow behavior index

f Frequency (Hz)

f_0 Resonance frequency of the piezo sensor (Hz)

k Complex compressibility of the sample (Pa^{-1})

k' Real part of complex compressibility

k'' Imaginary part of complex compressibility

V_0 Surrounding volume (cm^3)

Capital Letters

A   Area of the vibrating plate (cm^2)

V   Volume of sample injected (µL).

T_r Relaxation time (s)

M   Consistency coefficient

ΔP_c Pressure difference at the tube ends

R   Radius of vibrating disc (mm).

$\dfrac{U}{U_0}$ Ratio between the tension received by piezo detectors in the loaded mode and

their tension in the empty mode.

K Bulk modulus (modulus of incompressibility) (Pa)

K_0 Stiffness coefficient of the piezo sensor (N.m^{-1})

K_1 Stiffness coefficient of shaft (N.m^{-1})

Q_0 Quality factor of the piezo (unitless)

F Objective function for minimization

V_p P-wave velocity (m.s^{-1})

Symbols

$G(T_r)$ Relaxation modulus

$H(T_r)$ Distribution of relaxation time

E   Elastic modulus (in case of tensile stress) or Young's modulus (N/m^2 or Pa)

$G(\omega)$ Complex shear modulus as a function of frequency (Pa)

$G'(\omega)$ Storage modulus (due to elastic part) as a function of frequency (Pa)

$G''(\omega)$ Loss modulus (due to viscous part) as a function of frequency (Pa)

$J(\omega)$ Complex shear compliance as a function of frequency (Pa^{-1})

$J'(\omega)$ Shear compliance (due to elastic part) as a function of frequency (Pa^{-1})

$J''(\omega)$ Shear compliance (due to viscous part) as a function of frequency (Pa^{-1})

K^* Complex spring constant of the sample (N/m² or Pa)

K^*_{gap} Complex spring constant of the gap (N/m² or Pa)

$K^*_{surrounding}$ Complex spring constant of the surrounding (N/m² or Pa)

K_L Compressibility of the sample (Pa⁻¹)

Log f   Logarithmic of frequency (Hz)

Greek symbols

γ Shear strain

γ_0 Constant strain

γ_s Strain or deformation due to spring

γ_d Strain or deformation due to dashpot

$\dot{\gamma}$ Shear strain rate (s⁻¹)

$\dot{\gamma}_s$ Rate of strain due to spring

$\dot{\gamma}_d$ Rate of strain due to dashpot

ε Tensile strain

$\dot{\varepsilon}$ Tensile strain rate (s⁻¹)

ϵ Gap correction (micro meter)

δ Phase angle (rad)

η Viscosity (Pa.s)

$\eta(\omega)$ Complex dynamic viscosity as a function of frequency

$\eta'(\omega)$ Dynamic viscosity (due to viscous part) as a function of frequency

$\eta''(\omega)$ Dynamic storage viscosity (due to elastic part) as a function of frequency

ρ Density (kg/m3)

σ Stress (Pa) (tensile case)

σ_0 yield stress or apparent yield stress

σ_s stress due to spring

σ_d stress due to dashpot

τ Stress (Pa) (shear case)

ω Angular frequency '$2\pi f$'(rad/s).

$\Delta\varphi$ Phase difference between output signals of sensor in the loaded and empty case.

INTRODUCTION

Liquids and solids deform under the application of stress. Upon the removal of applied stress, a solid will regain its original form, while a liquid will not. They are characterized by their properties of viscosity and elasticity. But there exists another class of materials which are called complex fluids. These are the materials which have both liquid like and solid like properties, and therefore are viscoelastic in nature. Typical examples of such fluids include heavy oils, polymer solutions and colloidal suspensions. Rheology, defined as the "***study of the flow and deformation of materials***" [Barnes H.A., 2000], is associated to the study of complex fluids. It comes from Greek words: ***rheo*** means flow, and ***logo*** means science.

Rheology is one of the very few disciplines whose origin can be traced to an exact date: April 29, 1929. A plasticity conference was held on October 17, 1924. A high level of interest was shown in this subject which led to a Third Plasticity conference in 1929. It was decided to form a permanent organization for the development of the new discipline of rheology. The preliminary scope of The Society of Rheology was set up by a committee, which then met on April 29, 1929 at Columbus, Ohio. Some of the famous participants included Eugene C. Bingham, Winslow H. Herschel, Marcel Brillouin, Herbert Freundlich, Wolfgang Ostwald, Ludwig Prandtl and Markus Reiner. E.C. Bingham chose the name "Rheology" on the advice of his friend Crawford and a definition was accepted as "the study of the flow and deformation of matter". Heraclitus quote"$\pi\alpha\gamma\tau\alpha\ \rho\epsilon i$" or "everything flows" was taken to be the motto of the subject.

From historical point of view, the theory of rheology had been started very long ago. In 1678, Robert Hooke was the first to speak of rheology in his book ***"True Theory of***

Elasticity"[Barnes H.A. et al, 1989]. This theory is summarized as follows: *"If you double the tension you double the extension"*, which means the stress is proportional to the strain.

Nine years later, Isaac Newton published *"Principals of Natural Philosophy of Mathematics"* a hypothesis associated with the simple shear state. According to him "The resistance which arises from the lack of slipperiness of the parts of the liquid, other things being equal is proportional to the velocity with which the parts of the liquid are separated from one another". This slip is what we call now 'viscosity'. This is the key property in relation to rheology.

About 300 years ago, the studies related to rheology were limited to the application of Newton's law for liquids and Hook's law for solids. At the start of nineteenth century, the scientists started to have doubts about the universal validity of these linear laws. In 1807, the elastic (Young's modulus) was identified as the constant of proportionality by the great English polymath Thomas Young.

In 1835, W. Weber conducted a series of experiments with silk threads. He observed that a longitudinal load produced an immediate extension, followed by a further extension with time. The removal of the load produces an immediate contraction, followed by the gradual contraction to attain the original position. It was indeed the study of stress relaxation for viscoelastic materials.

In 1839, Hagen was the first who did a clear study for the viscosity of a liquid. Further research related to capillary flow was done by Poiseuille (1841). Both Hagen and Poiseuille showed that flow in a capillary tube is proportional to the pressure gradient and the fourth power of the tube radius. In 1845, the complete mathematical description

of Newtonian fluids was possible, thank to the NAVIER-Stokes equations.

In 1867, J.C. Maxwell in his article "On the dynamical theory of gases" which was published in 'Encyclopedia Britannica' proposed a mathematical model to describe the fluids that have elastic properties. In 1878, Boltzmann gave his 'Principal of superposition, according to which "the value of a characteristic function of a system is equal to the sum of all changes induced in the system by the driving functions which have been applied to it throughout its history". Thus generalizing the concept of linear viscoelasticity. In 1888, the major contribution was from Thomson who introduced the concept of the distribution of relaxation times. The well-known 'spring and dashpot' analogy for the Maxwell model was not introduced until 1902 by Pointing and Thomson. In addition, Bingham proposed in 1922 a 'yield stress' to describe the flow of paints to explain the apparent plasticity of certain fluids.

Crude oil can be divided into two kinds according to their flow ability (Zhang J.J. and Liu X., 2008). One is the light crude oil, also called the conventional oil with low viscosity. The other is the heavy crude oil, also called the heavy oil or unconventional oil with high viscosity. The term heavy oil is used as a generic term for heavy oils, extra-heavy oils and bitumen.

The oil industry uses the API (American Petroleum Institute) gravity to differentiate between petroleum fluids (light oil / heavy). The following equation relates the density and API gravity.

$$\text{API}^{\circ} = \frac{141.5}{\rho} - 131.5 \qquad (1)$$

Where ρ is the density of oil at 15°C. The lower the value of density, the higher the API gravity will be.

According to equation 1, the heavy oils have API gravity between 10 and 22. For comparison, Brent from the North Sea, which serves as a reference in the ratings in European markets, is a light oil of 38° API. The extra-heavy oils and bitumen have an API° less than 10 (figure 1), which correspond to the density of water. These are the hydrocarbons which are heavier than water. The bitumen distinguishes themselves from extra-heavy oils, not by their density or chemical characteristics, but by the viscosity which is higher in the conditions of pressure and temperature of the petroleum reservoir.
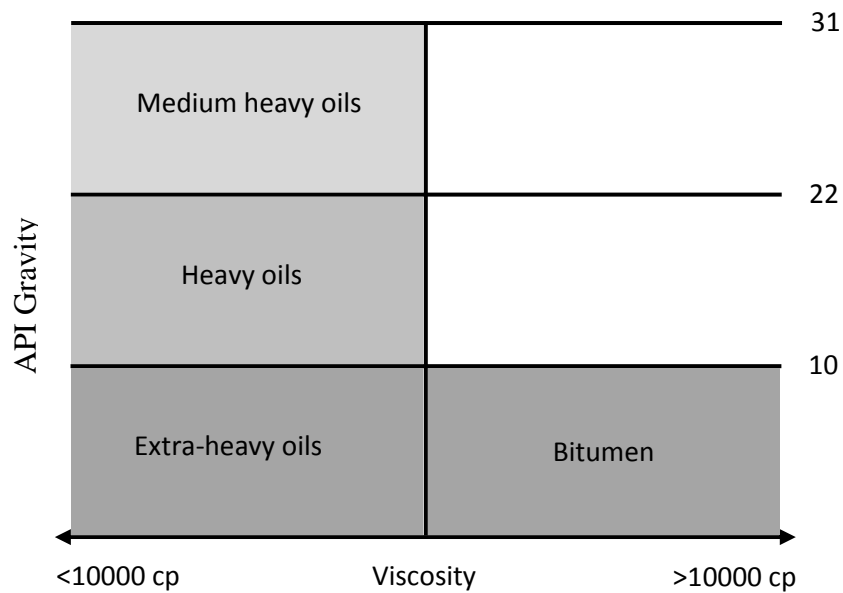
Fig.1: Classification of heavy oils as a function of API gravity

The oil industry recommends three segmentation of crude oils say A, B and C based on the viscosity in terms of content and API gravity. We can summarize these properties by saying that for oil of class A (medium heavy oils), production is easy and the recovery rate can be improved. Instead, the flow of oil provided in class B (heavy oils) is difficult, but the cold production is possible. Recoveries are low. Finally, class C (bitumen) does not flow in reservoir conditions. Heavy oils are widely distributed around the globe and have been found in various countries (figure 2).

Fig.2: Graphical distribution of heavy crude oil resources (Kimber K. D., 2007)

As far as the color, while these oils have a consistency similar to honey, the most oils flowing like syrup while bitumen remain frozen at normal temperature (figure 3). Their exploration remains limited because the countries that possess them have preferred to focus, so far, their efforts on resources easier and cheaper to retrieve.
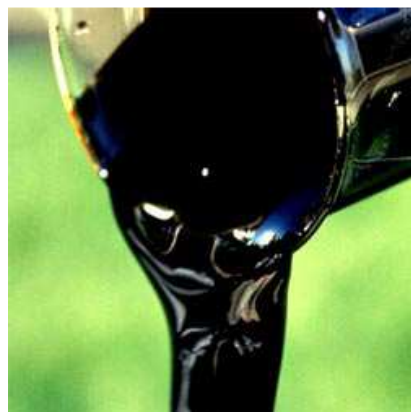
Fig.3: Bitumen at room temperature

These non-conventional oils are, for the most part, biodegraded. Located at shallow depths in unconsolidated sands and very permeable, they have been altered due to water

infiltration and bacteria; phenomenon that destroyed the lighter molecules and enriches artificially the asphaltenes and resins in oil. They contain, in addition, heavy metals, nitrogen and sulfur, which involve special treatment during the refining process.

Due to the continuous decline in the conventional oil production, the development of heavy oil is becoming important (Wang J. et al., 2006). They are important unconventional hydrocarbon resources with huge reserves (Behura J. et al., 2007). The known resources are worth about 6 trillion of barrels, an amount more than three times the combined world reserves of conventional oil and gas (Hinkle A. and Batzle M., 2006). Some of the largest known deposits are in the Athabasca sands in Canada, Faja del Orinoco inVenezuela, Alaska, California, Duri field in Indonesia, Russia, and China (Curtis C. et al., 2002). As for the volumes that can be recovered with the current techniques of production, they are estimated at some 1 trillion barrels, an amount almost equal to the recoverable reserves of conventional oil.

Heavy oils are located at shallow depths as compared to conventional petroleum. Pressure and temperature of the reservoirs are much lower than in the conventional one. Heavy oils are usually exploited through thermal recovery processes, steam flood, Steam Assisted Gravity Drainage (SAGD), Cold Heavy Oil Production with Sand (CHOPS), and injection of solvent. The major challenge for the oil industry in exploiting heavy oils comes from their high viscosity, which has a great impact on the exploitation of heavy oils (Zhao YI and Machel H. G., 2012), and causes problems in pipeline transportation (Plegue T.H. et al., 1986).

Identification of the rheological behavior of crude oil is needed for proper design of pipelines, storage and handling (Hameida A.M. and Al-Awad M.N.J., 1999). By

understanding the rheological properties of heavy oils, we can improve the characterization of reservoir viscosity. The viscosity of heavy oils depends on many factors including composition, temperature, frequency and pressure. This was the main motivation of this thesis, which has lead to the development of a High Pressure rheometer device able to work over a large range of frequency.

The first chapter of the thesis presents the main rheological techniques available that allow the measurement of rheological properties of viscoelastic substances. These techniques are very useful but face some limitations. When used in the shear mode, most of them work at low shear rates not much beyond 10 s^{-1} with the exception of capillary rheometer. At higher shear rates, flow instabilities begin to occur and the sample begins to emerge out of the gap. When used in oscillation mode, step motor rheometers are limited to low frequencies, typically lower than 100 Hz (figure 4). However, the knowledge of data at higher frequencies is required for better rheological characterization of complex fluids. The design of a device was important, which can study the rheological properties of viscoelastic substances at higher frequency range.
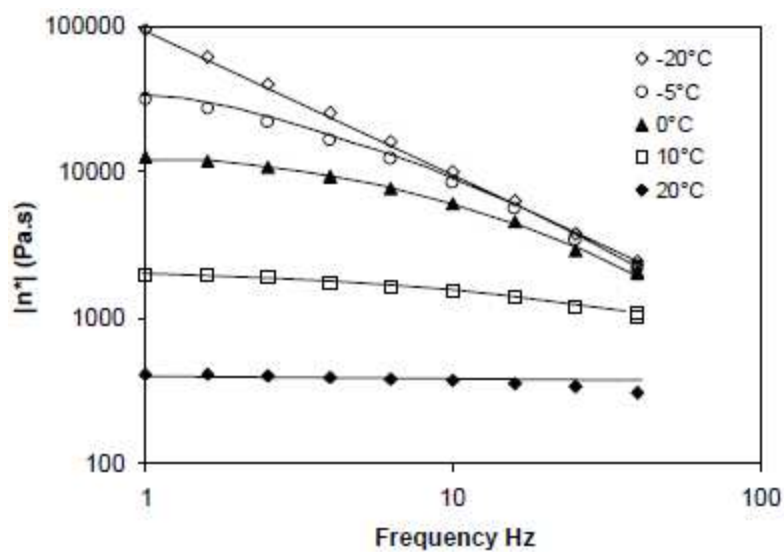
Fig.4: Temperature effect on the viscosity of a heavy oil (Henaut I. et al., 2003)

Figure 4 shows that with the decrease in temperature, not only the viscosity increases but also the rheological behavior of heavy oils becomes non Newtonian with the appearance of shear thinning behavior.

The second chapter represents the PAV (Piezoelectric axial vibrator) device. It is a kind of squeeze flow rheometer, which is used to measure the rheological properties of viscoelastic substances at high temperature (5°C to 150°C) and a frequency up to 8 kHz range, an order of magnitude greater than conventional rheometers.

The problem with PAV is that it can only study the viscoelastic properties at atmospheric pressure, whereas the study of crude oils at reservoir conditions requires a high-pressure device. Discoveries of oil and gas under high temperatures (above 150°C) or pressures (more than 100 MPa) have been made in various regions of the world. In the North Sea, the production is scheduled from deep reservoirs at 190°C and 110 MPa (Ungerer P. et al., 1998). The number of HP-HT reservoirs worldwide is numerous; however, the number of HP-HT fields in production is still very small. Therefore new equipment need to be designed, which can perform viscosity measurements at high temperatures and high pressures. Of course, there exist already many high pressure devices (Ellis J., 1976; Choi S.Y.1968; Mackley M.R. et al. 1995; Khandare P.M. et al. 2000; Saowapark S. et al., 2008; Kolitawong C. and Giacomin A.J., 2002; Donsi G. et al, 2011), but again the problem is that they cannot be used for high frequency range.

In order to attain this purpose, the atmospheric pressure PAV studied in chapter 2 was adapted in order to fit in a high-pressure cell. This high-pressure device works in the same frequency and temperature ranges as the atmospheric pressure one, but allows the study of pressurized samples up to 50 MPa (500 bars). Chapter 3 is thus about the

development of high-pressure rheometer device which needed a new design a the PAV

Cell. Finally, the thesis conclusion is added.

CHAPTER 1

CONVENTIONAL RHEOLOGY

As melt polymers and heavy oils belong to the non-Newtonian class of fluids showing the viscoelastic behavior, so a brief introduction to fluid types and viscoelastic fluids is given in the first section of this chapter. Since the rheology of materials is very important for their characterization, the rest of the chapter is devoted to the study of the theory and working principle behind the conventional type rheometers.

1.1.Types of fluids

A fluid is a substance that deforms continuously when subjected to a shear stress or tangential force (Fig. 1.1), even if the applied shear stress is very small. In simple words, a fluid is a substance which is capable of flowing and which conforms the shape of containing vessel. A real fluid is one that has some finite viscosity (resistance to flow) and thus can exert a tangential (shearing) stress on a surface with which it is in contact. The flow of real fluids is called a viscous flow. A real fluid can be further sub-divided into **Newtonian** fluids and **non-Newtonian** fluids.
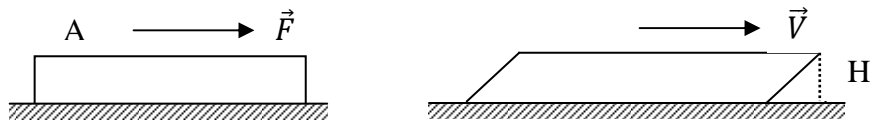
Fig. 1.1: Fluid deformation by the application of force, where the applied force per unit area is called stress ($\sigma = \frac{F}{A}$) and the resulting rate of change of deformation is called shear rate ($\dot{\gamma} = \frac{V}{H}$).

1.1.1. Newtonian Fluids

Newtonian fluids are the simplest type of fluids. They form the basis for classical fluid mechanics. These fluids obey Newton's law of viscosity given by equation 1.1. For these fluids, there is a linear relationship between shear stress and shear rate, i.e. viscosity is constant and is independent of shear rate.

$$\sigma = \eta\dot{\gamma} \qquad\qquad (1.1)$$

Where σ represents the shear stress, η the apparent viscosity and $\dot{\gamma}$ is the shear rate.

The graphical representation of shear stress versus shear rate is a straight line, which passes through the origin as shown in figure 1.2. The slope of the straight line gives the value of viscosity η for the given fluid. Thus the viscosity η is constant for Newtonian fluid at a given temperature and pressure. Newtonian's fluids can be represented by rheogram as shown in figure 1.2 given below.
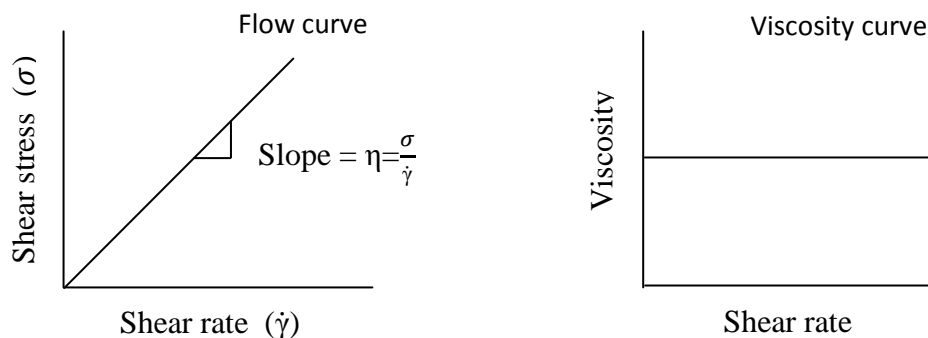
Fig. 1.2: Flow curve and viscosity curve for Newtonian fluids

Examples of Newtonian fluids are air, steam, milk, vegetable oils, fruit juices, sugar solutions, salt solutions, almost all gases and water (Schramm G., 2000, Shah N.A., 2008).

1.1.2. Non-Newtonian Fluids

All fluids that do not follow the criteria for Newtonian fluids are classified as non-Newtonian fluids. Their study is very important to petroleum engineering, as many crude oils and drilling muds show a non-Newtonian behavior (Swamee P.K., and Aggarwal N., 2011). In non-Newtonian fluids, viscosity is not constant and is a function of shear rate. In other words, there is a non-linear relationship between shear stress and shear rate. These fluids can be time independent, time dependent, or viscoelastic (Cheng L.X., 1998). In this section, we will study only time independent and time dependent fluids, while viscoelastic fluids will be discussed in the next section.

Time independent fluids are the fluids for which viscosity of the fluid is dependent on shear rate, but independent of the time of shearing.

$$\eta = \eta(\dot{\gamma}) \tag{1.2}$$

The viscosity is presented at a specific shear rate and is referred to as the "apparent viscosity", "shear viscosity" or "shear dependent viscosity". Time independent fluids are also called as generalized Newtonian fluids. They are classified into two types; power law fluids and the yield stress fluids.

1.1.2.1. Power law fluids

These are the fluids, which are represented by the popular Ostwald de Waele equation or power law equation (Elgibaly A.A.M. et al., 1997).

$$\sigma = M\dot{\gamma}^{n} \tag{1.3}$$

Where M and n are the power law model constants. M called the consistency coefficient is a measure of the consistency of the fluid, the higher the value of M, the more viscous

33

the fluid is. Whereas n is called the flow behavior index, and represents the degree of non-Newtonian behavior. For M= η and n=1 the above equation reduces to Newton's law of viscosity. Power law fluids are either shear thinning or shear thickening fluids.

Shear thinning fluids are the most widely encountered type of time-independent non-Newtonian fluids behavior, which dominate the field of rheology. They exhibit a decrease in apparent viscosity with increasing shear rates. They are obtained for 0< n<1 in the power law equation (1.3). Shear thinning fluids are called pseudo plastic fluids. Materials that exhibit shear-thinning behavior include concentrated suspensions, ketchup, mayonnaise and shampoo (Kalyon D.M. et al., 1993, Bylund G., 1995).

On the other hand, shear-thickening fluids are the opposite of shear thinning fluids, i.e. they exhibit an increase in apparent viscosity with increasing shear rates. They are obtained for n>1 in the power law equation (1.3). Shear thickening fluids are also called dilatant fluids. Examples of shear thickening fluids include wet sands (Bylund G., 1995). These fluids can be represented by rheograms shown in figure 1.3.
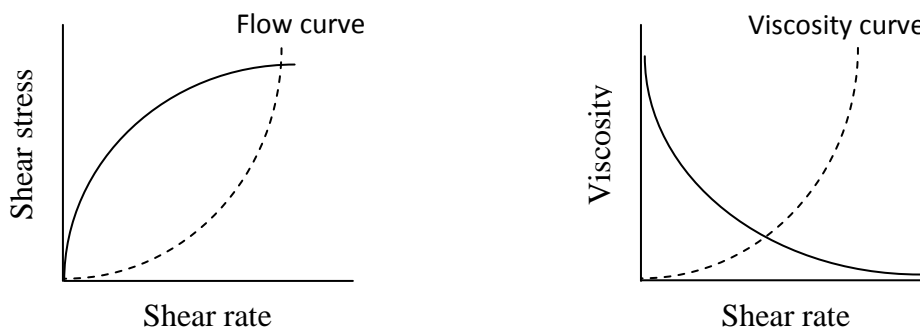
Fig. 1.3: Flow curve and viscosity curve for shear thinning fluids (solid line), and shear thickening fluids (dotted line)

1.1.2.2. Yield stress fluids

Yield stress fluids are also called viscoplastic fluids. Many materials encountered in various industries are viscoplastic. Some examples include foams, filled polymer melts, clay suspensions, paints, foodstuffs and slurries (Barnes H.A., 1999; Bird R.B. et al., 1983). These are the fluids that need a certain amount of stress before they start to deform (flow). This stress is called yield stress, and may be denoted by σ_0. Below this stress, these materials behave like solids at all. But as soon as this limit is achieved, they begin to flow like Newtonian fluid (Bingham fluids) or shear thinning fluid (plastic fluids). These fluids are represented by Herchel-Bulkley model (Nehdi M. and Rahman M.A., 2004) (equation 1.4), also called yield-power law model as it takes into account the yield stress which the power law model does not.

$$\sigma = \sigma_0 + M\dot{\gamma}^n \tag{1.4}$$

Where σ_0 is the yield stress i.e. minimum stress required to initiate flow.

Bingham plastic fluids are modelised by putting n=1 in equation (1.4), therefore, we have

$$\sigma = \sigma_0 + \eta\,\dot{\gamma} \tag{1.5}$$

In such a case M= η. Bingham plastic fluids are also called Newtonian fluids with yield stress. Their graphical representation can be seen in figure 1.4.
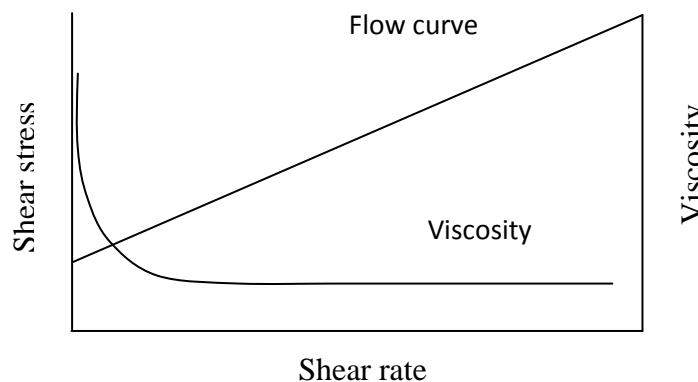
Fig. 1.4: Rheogram representing Bingham fluids

Bingham plastic model (equation 1.5) is used in the design of pipeline for non-Newtonian fluids (Sablani S.S., et al., 2003).

On the other hand, plastic fluids are modelised by putting n<1, and M= η in equation (1.4), therefore, we have

$$\sigma = \sigma_0 + \eta\,\dot{\gamma}^n \qquad n{<}1 \qquad\qquad (1.6)$$

Plastic fluids are also called shear-thinning fluids with yield stress. Their graphical representation can be seen in figure 1.5.
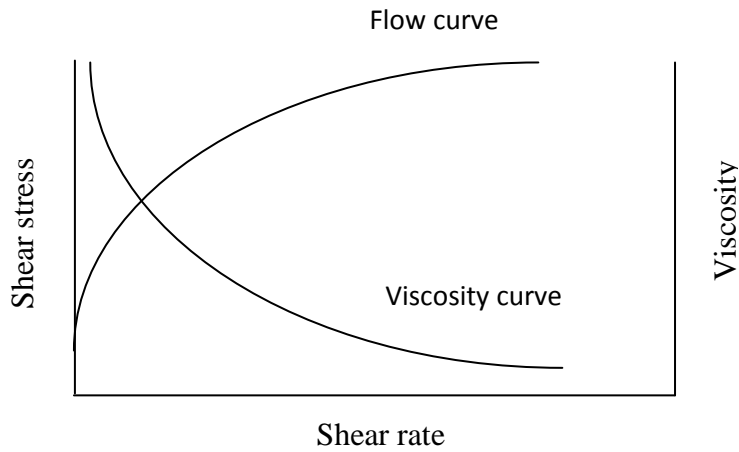
Fig. 1.5: Rheogram representing plastic fluids

1.1.2.3. Time dependent fluids

These are the fluids for which viscosity of the fluid does not depend only on shear rate but also on the time during which shear rate is applied.

$$\eta = \eta\,(\dot{\gamma}, t) \qquad\qquad (1.7)$$

It means that apparent viscosity is dependent upon the previous shear history of the fluid. There are two classifications of these fluids, thixotropic and rheopectic (Steffe J.M. and Daubert C.R., 2006).

Thixotropic fluids as drilling muds, paints, cosmetics, pharmaceuticals and grease (Sadeqi S. et al., 2011) exhibits a decrease in viscosity with time under a constant shear rate (Abu-Jdayil B., 2003), whereas rheopectic fluids are the fluids that exhibit an increase in viscosity with time under a constant shear rate. They are also called negative thixotropic or anti-thixotropic fluids. The graphical representation of these fluids can be seen in figure 1.6.
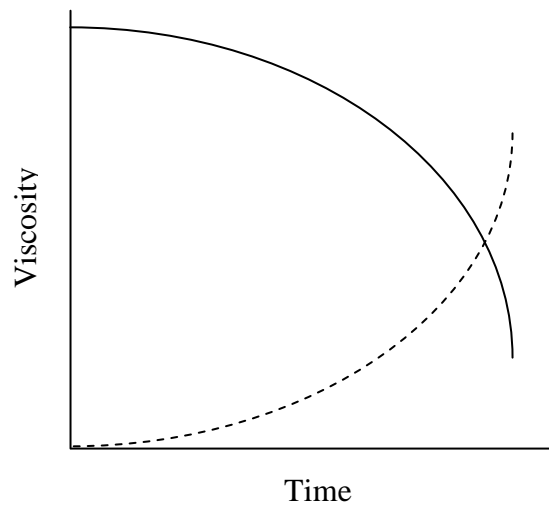
Fig. 1.6: Graphical representation of viscosity for thixotropic fluids (solid line), and rheopectic fluids (dotted line) under constant shear rate

Examples of rheopectic fluids include concentrated dispersions and waxy maize starch (Manconi M. et al., 2005; Wang B. et al., 2010).

1.1.3. Viscoelastic fluids

Classical materials are classified as viscous liquids and elastic solids (Ferry J.D., 1980). But many materials have properties between them. They are named as viscoelastic materials. In order to understand viscoelastic behavior, it is very important to understand the behavior of the classical materials.

A viscous liquid deforms continuously under the influence of an applied stress. When the applied stress is removed, it will not come back to its original undeformed state. Its deformation is permanent. It will dissipate all energy input as heat. The flow of viscous liquids is described by Newton's law. A dashpot is used to represent the viscous behavior of materials, and is shown in figure 1.7.
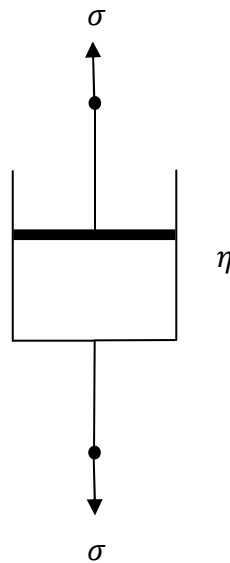
Fig. 1.7: A dashpot: mechanical analog to liquid behavior

On the other hand, a purely elastic system will deform under the influence of an applied stress. However, as soon as the applied stress is removed, it will restore its energy and will come back to its original undeformed state. Its deformation is non-permanent. Elastic responses are described by Hook's law, which constitutes a linear relationship between stress and strain as shown by equation.

$$\sigma = G\,\gamma \tag{1.8}$$

Where G is the modulus of elasticity, and γ is the deformation that occurs under the applied stress. Elastic behavior can be represented by a spring, and is shown in figure 1.8.

Fig. 1.8: A spring: mechanical analog to elastic behavior

Viscoelastic materials are capable of exhibiting both viscous and elastic properties simultaneously, e.g crude oils, asphalt, polymer melts, rubbers, grease, blood, toothpaste, ketchup and dough. Their properties depend largely on temperature and frequency. It means that within some frequency and temperature range, they will exhibit solid behavior, while for some other frequency and temperature range, they exhibit liquid behavior or a combination of both. Viscoelastic fluids flow under the influence of an applied shear stress, but when the stress is removed, they will slowly recover from some of the deformation. They store and dissipate a part of energy. Viscoelastic fluids are characterized by the complex modulus $G = G' + iG''$, the real part of which may be identified with energy storage and the imaginary part with the energy loss.

1.1.4. Viscoelastic models

To describe a viscoelastic behavior, we need a model, which consists of at least two components, one to describe elastic part represented by a spring, and the other to

describe viscous behavior represented by a dashpot. These components can be combined in many ways (Flugge W., 1967) to develop the constitutive equations for viscoelastic materials.

1.1.4.1. Maxwell Model

Maxwell model consists of a spring connected in series with a dashpot as shown in figure 1.9.
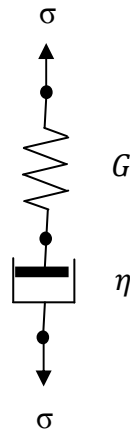
Fig. 1.9: Mechanical analog to Maxwell model comprised of a spring and a dashpot in series

In Maxwell model, the stress is the same in both elements i.e.

$$\sigma = \sigma_s = \sigma_d \tag{1.9}$$

Where σ_s and σ_d represent the stress in the spring and dashpot respectively.

The deformation (strain) of the Maxwell model is equal to the sum of the individual deformations of spring and dashpot.

$$\gamma = \gamma_s + \gamma_d \tag{1.10}$$

Where γ_s and γ_d represent the strain in the spring and dashpot respectively.

Again, from equation (1.10) we get

$$\dot{\gamma} = \dot{\gamma}_s + \dot{\gamma}_d \qquad (1.11)$$

By putting the values of $\dot{\gamma}_s = \frac{\dot{\sigma}}{G}$ and $\dot{\gamma}_d = \frac{\sigma}{\eta}$ in equation (1.11), we will have

$$\dot{\gamma} = \frac{\dot{\sigma}}{G} + \frac{\sigma}{\eta} \qquad (1.12)$$

$$\Longleftrightarrow \quad G\dot{\gamma} = \dot{\sigma} + \frac{\sigma}{\eta}G \qquad (1.13)$$

This is the standard form of Maxwell model showing the relationship between stress and strain, and clearly is an ordinary differential equation. This equation appears to be the first attempt to obtain a viscoelastic constitutive equation (Bird R.B. et al., 1987).

Creep and recovery:

In a creep test, a material is subjected to a constant stress at a given temperature, and the material's deformation as a function of time is studied.

For creep test, $\sigma = \sigma_0 = $ constant, which gives $\dot{\sigma}=0$, so equation (1.13) becomes

$$\dot{\gamma} = \frac{\sigma}{\eta} \qquad (1.14)$$

Integrating equation (1.14), we get

$$\Longleftrightarrow \quad \gamma = \frac{\sigma}{\eta}t + C \qquad (1.15)$$

Where C is the constant of integration. Its value is determined by using the initial conditions about stress and strain given in the following equations:

$$\sigma(t) = \begin{cases} 0, t < 0 \\ \sigma_0, t \geq 0 \end{cases} \qquad (1.16)$$

$$\gamma(t) = \begin{cases} 0, t < 0 \\ \frac{\sigma_0}{G}, t = 0 \end{cases} \qquad (1.17)$$

Applying these initial conditions to equation 1.15, gives $C = \frac{\sigma_0}{G}$,therefore, equation 1.15 implies

$$\gamma(t) = \sigma_0 (\frac{1}{\eta} t + \frac{1}{G}) \qquad (1.18)$$

The full description of the application of the constant stress σ_0 , and the resulting creep - recovery response for Maxwell model is shown in figures (1.10) and (1.11) respectively.
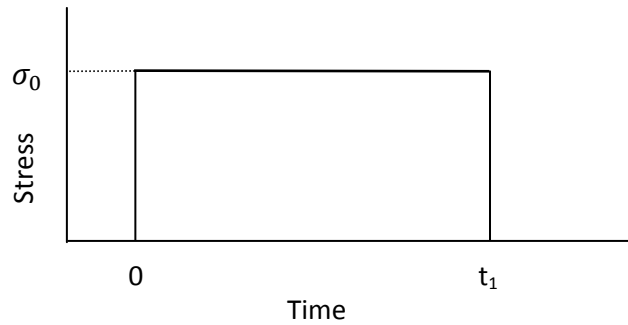
Fig. 1.10: Application of constant stress to study creep – recovery response in Maxwell model
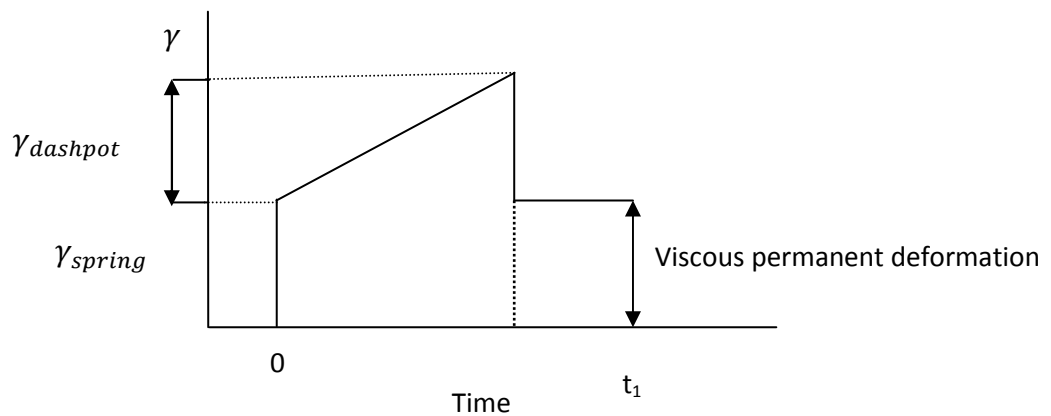
Fig. 1.11: Creep – recovery response of the Maxwell model

Stress relaxation:

In a stress relaxation test, a material is subjected to a constant strain at a given temperature, and the behaviour of stress as a function of time is studied.

For stress relaxation test, $\gamma = \gamma_0 =$ constant, which gives $\dot{\gamma}=0$, so equation (1.13) becomes

$$\dot{\sigma} + \frac{\sigma}{\eta} G = 0$$

Separating the variables and integrating, we get

$$\int_{\sigma_0}^{\sigma} \frac{d\sigma}{\sigma} = -\frac{G}{\eta} \int_0^t dt$$

$$\Leftrightarrow \quad \ln\left(\frac{\sigma}{\sigma_0}\right) = -\frac{G}{\eta} t + C \qquad (1.19)$$

Where C is constant of integration. Its value is determined by using the initial conditions given in the following.

$$\gamma(t) = \begin{cases} 0, t < 0 \\ \gamma_0, t \geq 0 \end{cases} \qquad (1.20)$$

$$\sigma(t) = \begin{cases} 0, t < 0 \\ \sigma_0, t = 0 \end{cases} \qquad (1.21)$$

We get C=0

$$\Leftrightarrow \quad \ln\left(\frac{\sigma}{\sigma_0}\right) = -\frac{G}{\eta} t$$

$$\Leftrightarrow \quad \sigma(t) = \sigma_0 e^{-\frac{G}{\eta} t} \qquad (1.22)$$

$$\Leftrightarrow \quad \sigma(t) = \sigma_0 e^{-\frac{t}{T_r}} \qquad (1.23)$$

With $T_r = \frac{\eta}{G}$ is the term constant for Maxwell model, and is called the relaxation time.

This shows that stress decreases exponentially from its initial value to zero with the time constant T_r.

The full description of the application of the constant strain γ_0, and the resulting stress - relaxation response for Maxwell model is shown in figures (1.12) and (1.13) respectively.
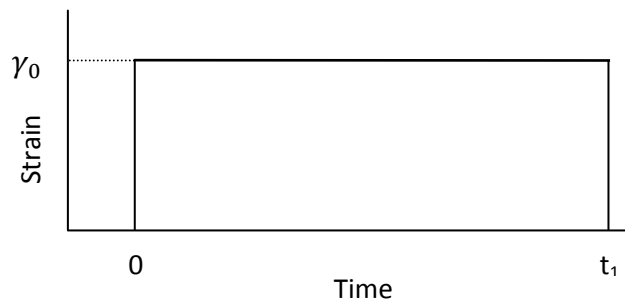
Fig. 1.12: Application of constant strain to study stress relaxation response in Maxwell model
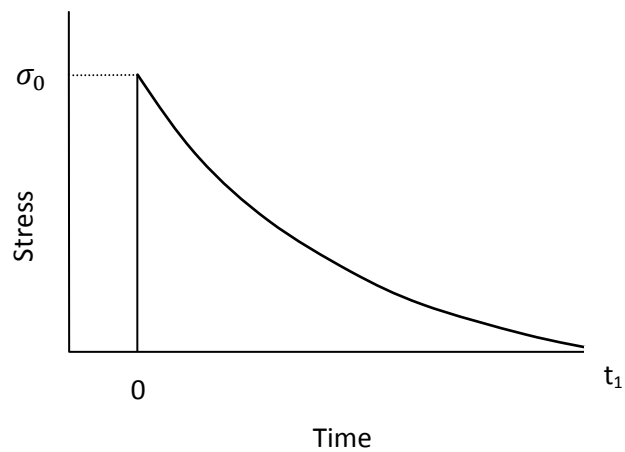
Fig. 1.13: Stress relaxation response of the Maxwell model

The above figure shows that the stress decreases as the time grows for the same strain.

Equation (1.23) can also be written as

$$\frac{\sigma(t)}{\gamma} = Ge^{-\frac{t}{T_r}} \qquad (1.24)$$

Where G is the spring constant. Here the term $Ge^{-\frac{t}{T_r}}$ is denoted by $G(t)$, and is called relaxation modulus. Therefore, equation (1.24) takes the form.

$$G(t) = Ge^{-\frac{t}{T_r}} \tag{1.25}$$

For real viscoelastic liquids, the stress relaxation curve is usually described by a series of Maxwell models in parallel.

$$G(t) = \sum G_i e^{-\frac{t}{T_{ri}}} \tag{1.26}$$

Where the various parameters are usually obtained by non-linear curve fitting.Equation (1.26) is very useful in determining the relaxation spectrum of the fluid. Relaxation spectrum shows how material softens with time.

Dynamic (oscillatory) test

The dynamic or oscillatory tests consist of applying a small sinusoidal strain (or stress) and measuring the resulting stress (or strain). Suppose an oscillatory sinusoidal strain of angular frequency ω is generated in the material.

$$\gamma = \gamma_0 \, sin\omega t \tag{1.27}$$

The stress response of the material will be of the form

$$\sigma = \sigma_0 \sin (\omega t + \delta) \tag{1.28}$$

i.e. the strain lags behind the stress by a phase angle δ. This phase angle is a determining factor for material behavior as shown in the figures 1.14 to 1.16.
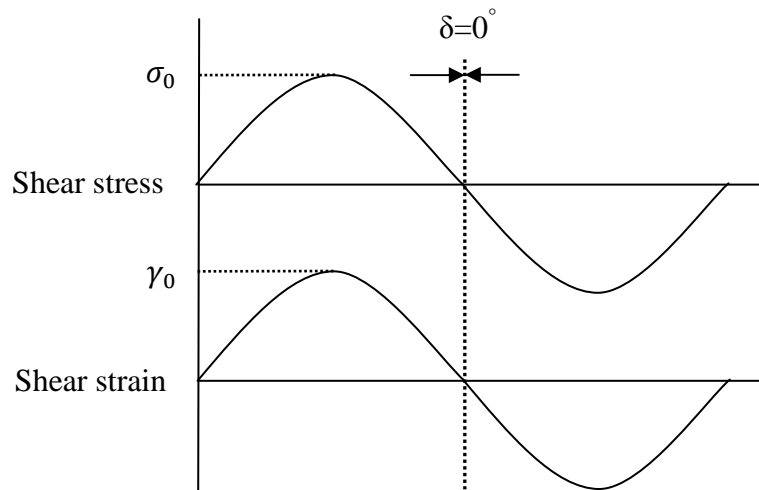
Fig. 1.14: Oscillating test representing purely elastic material
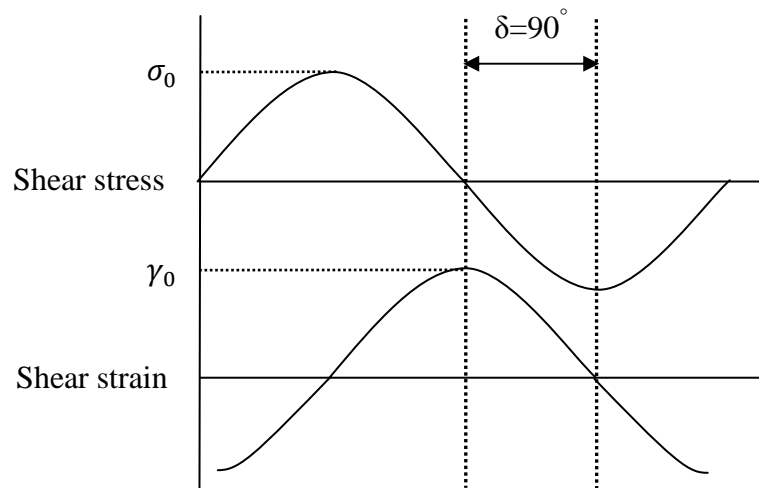
Fig. 1.15: Oscillating test representing purely viscous material
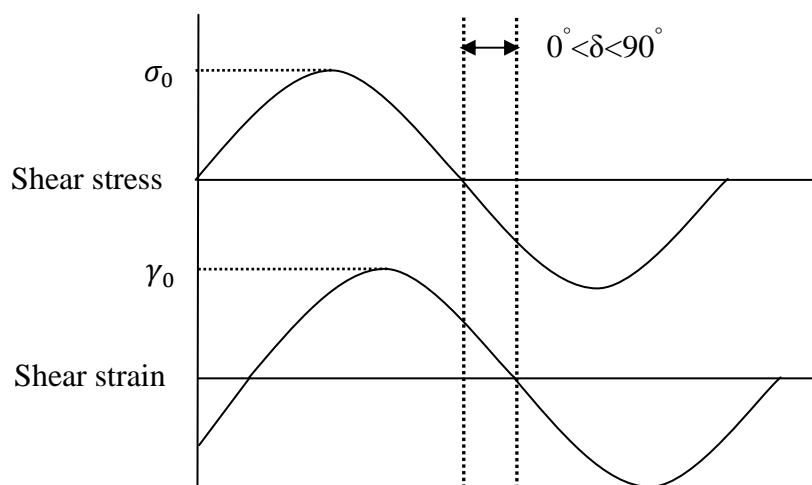
Fig. 1.16: Oscillating test representing viscoelastic material

These figures show the typical material behavior determined by the phase lag (δ) between the input stress and the output strain. If a material is purely elastic, the phase difference between the imposed stress and the resultant strain is zero degree. If the material is purely viscous, the phase difference is 90 degrees. Whereas, for viscoelastic materials, it lies between zero degree and 90 degrees.

The phase difference (δ) together with the amplitudes of stress (σ_0) and strain (γ_0) waves are used to determine the rheological properties such as G, J, and η.

$$G = \frac{\sigma_0}{\gamma_0} \qquad (1.29)$$

$$J = \frac{1}{G} \qquad (1.30)$$

$$\eta = \frac{G}{i\omega} \qquad (1.31)$$

Considering the application of the oscillatory test to the Maxwell model. For harmonic stress $\sigma = \sigma_0 e^{i\omega t}$, which derives the strain harmonically $\gamma = \gamma_0 e^{i\omega(t+\delta)}$, where ω is the angular frequency, and δ is the phase angle between the applied stress(strain) and the resulting strain (stress), equation 1.12 takes the form

$$i\omega\gamma_0 e^{i\omega(t+\delta)} = \frac{1}{G} i\omega\sigma_0 e^{i\omega t} + \frac{1}{\eta}\sigma$$

$$\Longleftrightarrow i\omega\gamma = \frac{1}{G} i\omega\sigma + \frac{1}{\eta}\sigma$$

$$\Longleftrightarrow \sigma = \frac{G\eta i\omega}{G+i\omega\eta}\gamma$$

$$\Longleftrightarrow \sigma = \left(\frac{G\eta^2\omega^2 + G^2 i\omega\eta}{G^2 + \omega^2\eta^2}\right)\gamma$$

Let $\frac{\eta}{G} = T_r$, the relaxation time, then after simplification the above equation can be written in the complex form as follows

$$\sigma = G\left[\frac{(\omega T_r)^2}{1+(\omega T_r)^2} + i\frac{\omega T_r}{1+(\omega T_r)^2}\right]\gamma$$

$$\Leftrightarrow \sigma = G^*\gamma$$

with
$$G^* = G\left[\frac{(\omega T_r)^2}{1+(\omega T_r)^2} + i\frac{\omega T_r}{1+(\omega T_r)^2}\right] \tag{1.32}$$

The real and imaginary parts of equation 1.32 can be given as.

$$
\begin{cases}
G'(\omega) = G\frac{(\omega T_r)^2}{1+(\omega T_r)^2} & (1.33) \\[3mm]
G''(\omega) = G\frac{\omega T_r}{1+(\omega T_r)^2} & (1.34)
\end{cases}
$$

This concept can be extended to any number Maxwell models connected in parallel, as shown in figure 1.17.
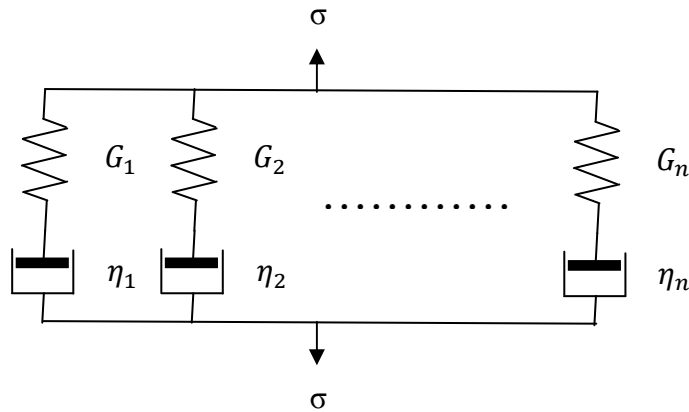
Fig. 1.17: Generalized Maxwell model: Multiple Maxwell models connected in parallel

In this case, the values of the overall storage and loss moduli, G' and G'', at angular frequency ω, are given by the following equations.

$$\begin{cases} G' = \sum G_i \frac{(\omega T_{ri})^2}{1+(\omega T_{ri})^2} & (1.35) \\[3ex] G'' = \sum G_i \frac{\omega T_{ri}}{1+(\omega T_{ri})^2} & (1.36) \end{cases}$$

1.1.4.2. Kelvin-Voigt Model

If we connect a spring in parallel with viscous damper (dashpot), we will have the simplest model for viscoelastic solid. Such a combination is called Voigt model, after the name of famous German physicist (1850-1919). The Voigt model is also known as Kelvin or Kelvin-Voigt model, linking it with Lord Kelvin (1824-1907), another Scottish physicist. It seems to be more appropriate to describe the solid dampers behavior (Lewandowski R., and Chorazyczewski B., 2010).
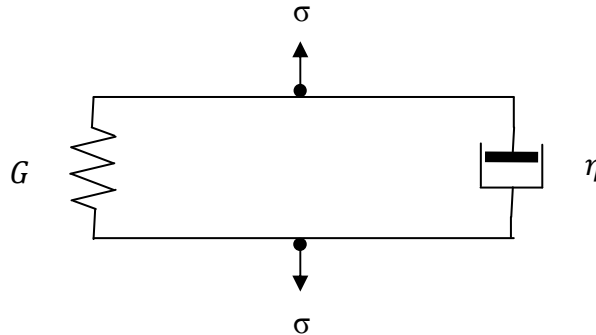
Fig. 1.18: Mechanical analog to Kelvin-Voigt model comprised of a spring and a dashpot in parallel

In case of Kelvin-Voigt model, the strain experienced by the spring is the same as that experienced by the dashpot i.e.

$$\gamma = \gamma_s = \gamma_d \qquad (1.37)$$

The stress in the Kelvin-Voigt model is equal to the sum of the individual stresses of spring σ_s and dashpot σ_d.

$$\sigma = \sigma_s + \sigma_d \qquad (1.38)$$

As $\sigma_s = G\gamma$ and $\sigma_d = \eta\dot{\gamma}$, then equation (1.38) gives

$$\sigma = G\gamma + \eta\frac{d\gamma}{dt}$$

or
$$\eta\frac{d\gamma}{dt} + G\gamma - \sigma = 0 \qquad (1.39)$$

This is the standard form of the constitutive equation for Kelvin-Voigt model showing the relationship between stress and strain, and clearly is an ordinary differential equation.

Creep and recovery:

$\sigma = \sigma_0$ (constant), so equation (1.39) gives

$$\eta\frac{d\gamma}{dt} + G\gamma - \sigma_0 = 0 \qquad (1.40)$$

This is linear non-homogeneous ordinary differential equation with constant coefficients. Its solution is given by the following equation.

$$\gamma = \frac{\sigma_0}{G} + Ae^{-\frac{t}{T_r}} \qquad (1.41)$$

The initial conditions associated with the creep are given by equations 1.16 and 1.17:

Applying these initial conditions to equation (1.41), we get $A = -\frac{\sigma_0}{G}$

Therefore, finally equation (1.41) takes the form

$$\gamma = \frac{\sigma_0}{G}(1 - e^{-\frac{t}{T_r}}) \qquad (1.42)$$

This means that the strain will grow to a constant value as time increases.

The full description of the application of the constant stress σ_0, and the resulting creep - recovery response for Kelvin-Voigt model is shown in figures (1.19) and (1.20) respectively.
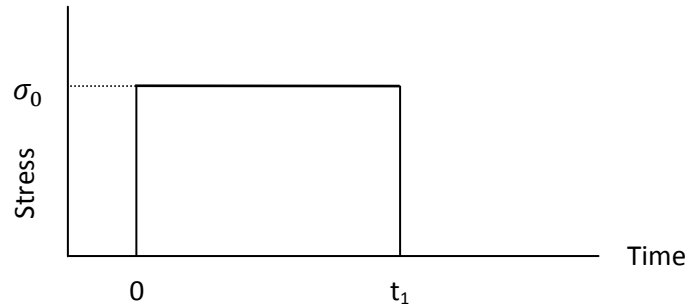
Fig. 1.19: Application of constant stress to study creep – recovery response in Kelvin-Voigt model
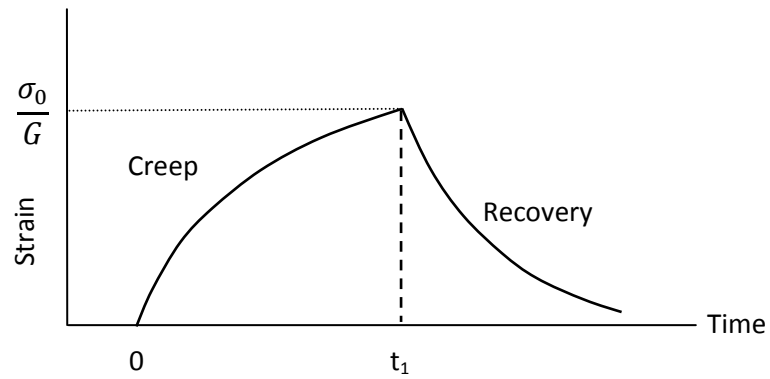
Fig. 1.20: Creep – recovery response of the Kelvin-Voigt model

Stress relaxation:

Consider next stress relaxation test. Setting the strain to be constant γ_0 (Fig. 1.21), equation (1.39) reduces to

$$G\gamma_0 - \sigma = 0 \tag{1.43}$$

$$\Leftrightarrow \quad \sigma = G\gamma_0 \tag{1.44}$$

This means that the stress is taken up by the spring and will stay constant as time grows for the same strain. Therefore, there is in fact no stress relaxation over time (Fig. 1.22).
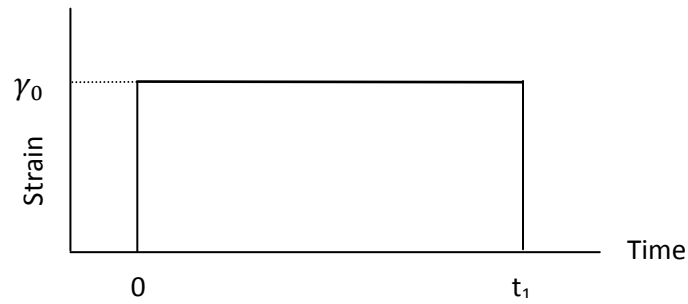
Fig. 1.21: Application of constant strain to study stress relaxation response in Kelvin-Voigt model
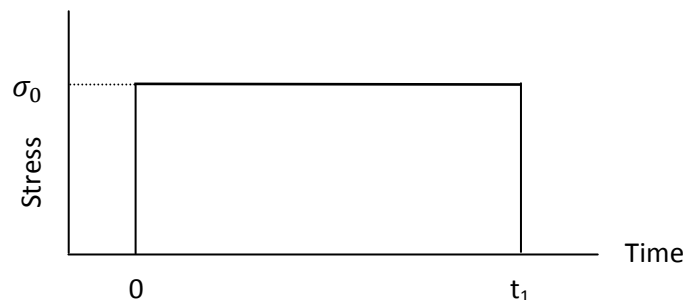
Fig. 1.22: Stress relaxation response of the Kelvin-Voigt model

Actually, in Kelvin-Voigt model, an instantaneous strain γ_0 is applied to the dashpot. Thus, the stress (proportional to $\dot{\gamma}$) exerted by the dashpot will be infinite, and will break the system. Consequently, the Kelvin-Voigt model is not able to describe the stress relaxation process.

Dynamic (oscillatory) tests:

For harmonic stress $\sigma = \sigma_0 e^{i\omega t}$, this derives the strain harmonically $\gamma = \gamma_0 e^{i\omega(t+\delta)}$
Putting these values in equation (1.39), we get

$$\sigma = \eta i\omega\gamma_0 e^{i\omega(t+\delta)} + G\gamma$$

$$\Leftrightarrow \sigma = \eta i\omega\gamma + G\gamma$$

$$\Leftrightarrow \sigma = (G + i\eta\omega)\gamma$$

$$\Leftrightarrow \sigma = G^*\gamma$$

With $\qquad\qquad\qquad G^* = G + i\eta\omega \qquad\qquad\qquad$ (1.45)

The real and imaginary parts of equation 1.45 can be given as.

$$\begin{cases} G'(\omega) = G & (1.46) \\ \\ G''(\omega) = \eta\omega & (1.47) \end{cases}$$

Which shows that under all loading, storage modulus is equal to the stiffness of the spring, whereas the loss modulus grows unbound for very high frequencies.

The actual viscoelastic behavior of materials is very complex. The simplest models, Maxwell and Kelvin-Voigt explain the basic characteristics of viscoelastic behavior. The Maxwell model, for example, has a viscous character and explains well the relaxation behavior of viscoelastic materials. On the other hand, the Kelvin-Voigt model has a solid character and explains well the retarded elasticity behavior. However, none of the mentioned models completely explains the real behavior of viscoelastic materials. There are other models with G and η constants but they are rather complex. These models include the three-element model (Standard linear solid model) and four element models (Burger's model).

1.1.4.3. Standard linear solid Model (SLS)

The Maxwell and Kelvin models are the simplest two-element models. More realistic material responses can be modeled using more elements. Standard linear solid model is a three-element model. Although it can be formed by a number of ways (Jo C. et al,

2005; Wang B. and Chen L.Q., 2009), but we will form it by connecting a Maxwell element in parallel with a spring (Kalita P. and Schaefer R., 2008; Jo C., and Naguib H.E., 2007) as shown in figure 1.23. It is used to describe both the creep and stress relaxation.
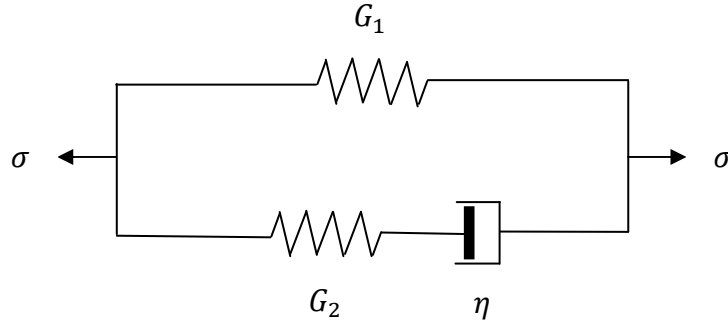
Fig. 1.23: Mechanical analog to three-element model; Maxwell element connected to a spring in parallel

The standard form of the constitutive equation for three-element model showing the relationship between the applied stress σ and the resulting strain γ, is given by the following equation.

$$\sigma + \frac{\eta}{G_2}\dot{\sigma} = G_1\gamma + \frac{\eta(G_1+G_2)}{G_2}\dot{\gamma} \tag{1.48}$$

Here, η is the dynamic viscosity of dashpot, whereas G_1 and G_2 are the moduli of elasticity of the spring, in parallel and in series to dashpot respectively. The application of oscillatory test leads to

$$G^* = \frac{G_1 G_2^2 + \eta^2 \omega^2 (G_1+G_2)}{G_2^2 + \eta^2 \omega^2} + i\frac{\eta\omega G_2^2}{G_2^2 + \eta^2 \omega^2} \tag{1.49}$$

The real and imaginary parts of equation 1.49 can be given as.

$$\begin{cases} G'(\omega) = \frac{G_1 G_2^2 + \eta^2 \omega^2 (G_1+G_2)}{G_2^2 + \eta^2 \omega^2} & (1.50) \\[4mm] G''(\omega) = \frac{\eta\omega G_2^2}{G_2^2 + \eta^2 \omega^2} & (1.51) \end{cases}$$

1.1.4.4. Burger's Model

Burger's model is a series combination of Maxwell model and Kelvin-Voigt model, named in honor of the Dutch physicist (1895-1981). It is a four-element model, comprising of two springs and two dashpots (Fig. 1.24).
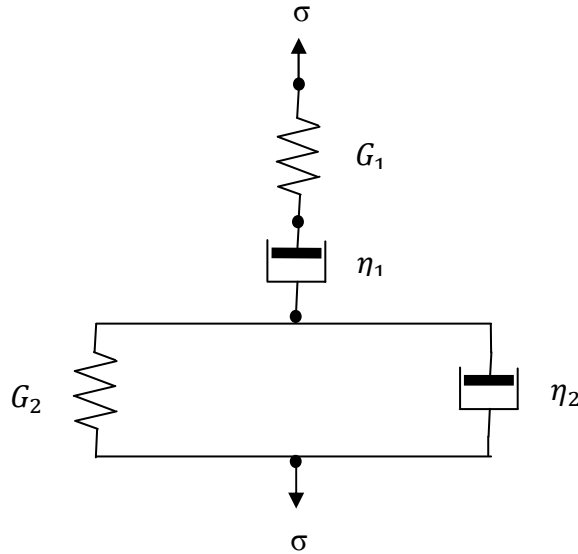
Fig. 1.24: Mechanical analog to Burger's model: Maxwell model and Kelvin-Voigt model connected in series

The standard form of the constitutive equation for Burger's model showing the relationship between applied stress σ and the resulting strain γ, is given by the following equation.

$$\eta_1\eta_2\ddot{\sigma} + [G_2\eta_1 + G_1(\eta_{1+}\eta_2)]\dot{\sigma} + G_1G_2\sigma = G_1G_2\eta_1\dot{\gamma} + G_1\eta_1\eta_2\ddot{\gamma} \qquad (1.52)$$

The application of oscillatory test leads to

$$G^* = \frac{G_1\eta_1\omega^2(G_2^2\eta_1 + G_1G_2\eta_1 + \eta_1\eta_2^2\omega^2)}{(G_1G_2 - \eta_1\eta_2\omega^2)^2 + \omega^2(G_2\eta_1 + G_1(\eta_1 + \eta_2))^2} + i\frac{G_1\eta_1\omega(G_1G_2^2 + G_1\eta_1\eta_2\omega^2 + G_1\eta_2^2\omega^2)}{(G_1G_2 - \eta_1\eta_2\omega^2)^2 + \omega^2(G_2\eta_1 + G_1(\eta_1 + \eta_2))^2}$$

With the real and imaginary parts given in the following.

$$\begin{cases} G'(\omega) = \dfrac{G_1\eta_1\omega^2(G_2^2\eta_1+G_1G_2\eta_1+\eta_1\eta_2^2\omega^2)}{(G_1G_2-\eta_1\eta_2\omega^2)^2+\omega^2(G_2\eta_1+G_1(\eta_1+\eta_2))^2} & (1.53) \\\\ G''(\omega) = \dfrac{G_1\eta_1\omega(G_1G_2^2+G_1\eta_1\eta_2\omega^2+G_1\eta_2^2\omega^2)}{(G_1G_2-\eta_1\eta_2\omega^2)^2+\omega^2(G_2\eta_1+G_1(\eta_1+\eta_2))^2} & (1.54) \end{cases}$$

There could be developed of course as many viscoelastic models as we desire by connecting spring and dashpot in varying combinations. As the number of elements used is increased, the constitutive equations representing the relationship between applied stress σ and the resulting strain (γ) become more complex.

1.2. Conventional rheometer types

A rheometer refers to a device which is used to study the rheology of materials. Rheometers are of two types: shear rheometers and extensional rheometers. They can be either stress controlled or strain controlled. Extensional rheometry is the study about tensile deformation. In these rheometers, an extensional stress or extensional strain is applied to the sample, and the resulting extensional strain or extensional stress is measured. As we are only concerned with shear rheometry, so throughout this thesis we will focus ourselves to shear rheometers.

Shear rheometers are the more widely used rheometers. In these rheometers, a shear stress or shear strain is applied to the sample, and the resulting shear strain or shear stress is measured. Shear rheometers can be further sub-divided into two types; drag flow rheometers and pressure driven flow rheometers (Macosko C.W., 1994). In drag flow rheometers, shear stress or shear strain is generated between two solid surfaces, one of which is moving and the other is at rest (e.g. rotational rheometers). In pressure driven flow rheometers, a fluid under pressure is forced to move through a thin cylindrical tube (e.g. capillary tube rheometers), and the resulting shear stress or the

shear strain is measured from the pressure difference at the tube ends. A brief classification of rheometers is given in figure 1.25.
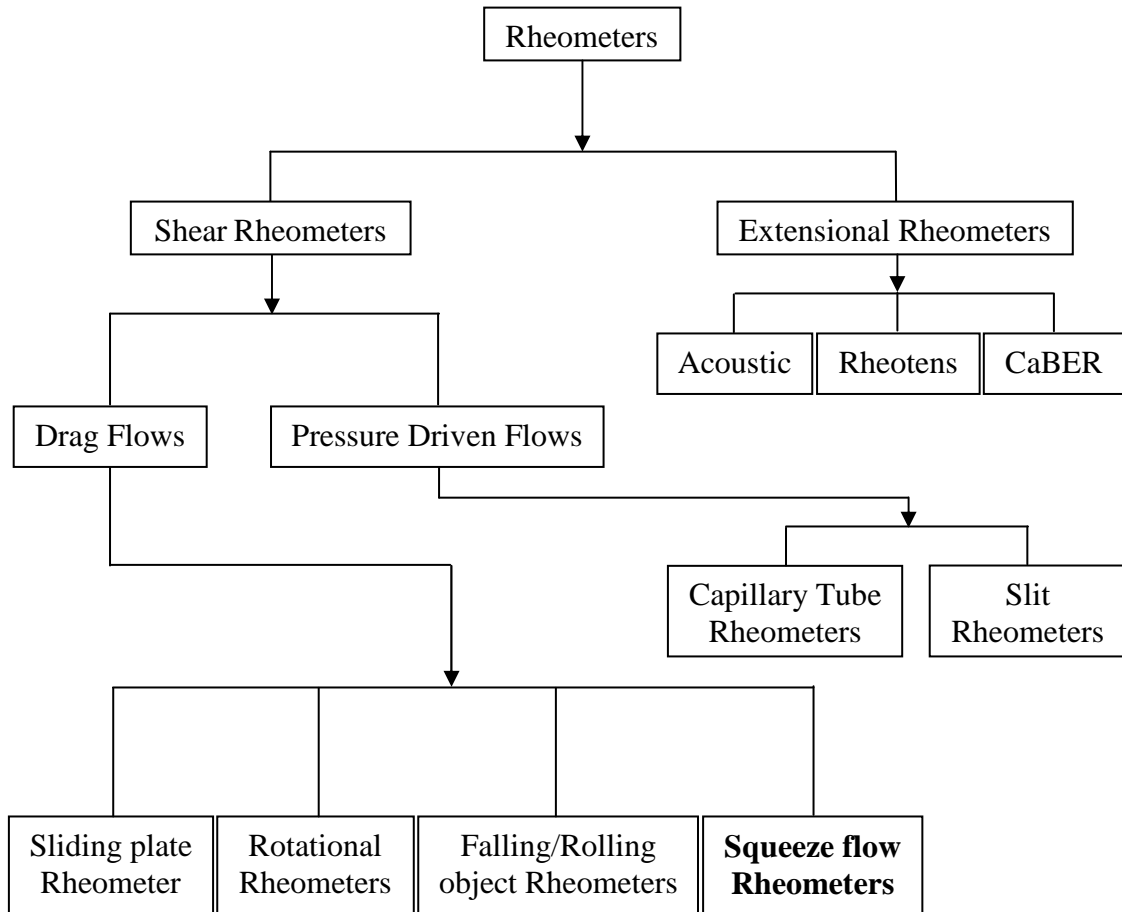
Fig.1.25: Some classical types of rheometers

In the following sections, we will study about the most commonly used rheometers.

1.2.1. Capillary tube rheometer

Capillary tube rheometer is a kind of non-rotational pressure driven flow geometry. In capillary tube rheometers, a fluid is subjected to flow through a tube of constant cross section by means of a pressure difference across the ends of tube. The flow parameters are chosen in such a way that the flow is laminar, isothermal and steady-state. Its schematic diagram is shown in figure 1.26. The main components of capillary tube

rheometer are the reservoir containing the fluid, and a capillary tube of radius R_c and length L_c which is connected to the bottom of the reservoir. Our interest lies in calculating the pressure drop ΔP_c at the tube ends and the flow rate Q, which can be used in determining the viscosity.
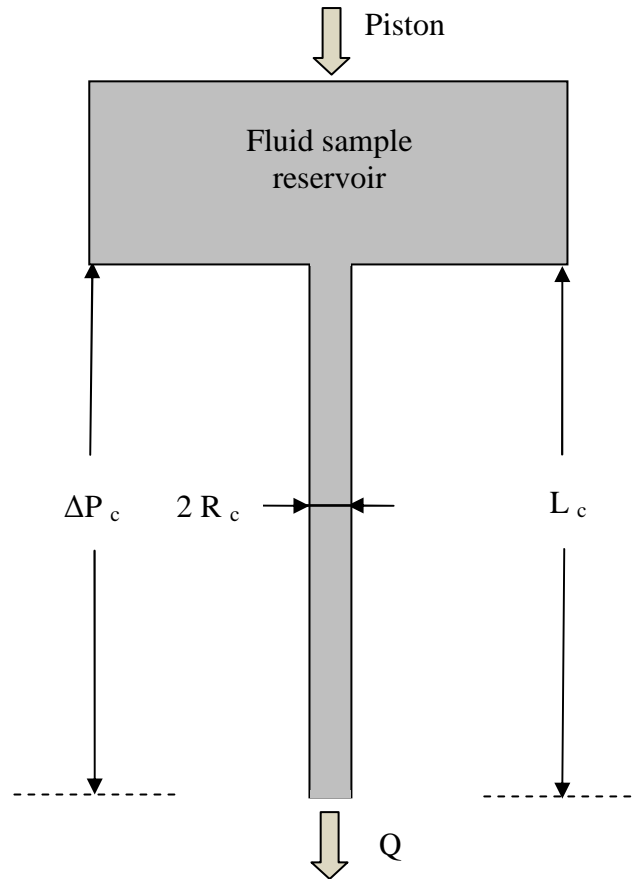
Fig.1.26: Schematic diagram of capillary tube rheometer: fluid sample
is shown by shaded area

Consider the case in which pressure is applied by means of a piston. The fluid flows slowly and steadily through capillary tube. The flow in the capillaries for Newtonian or non-Newtonian fluids is assumed to be laminar. Once the pressure drop at the tube ends is determined, the shear stress at tube wall is given by.

$$\tau_w = \frac{R_c \Delta P_c}{2 L_c} \tag{1.55}$$

In case of Newtonian flow, viscosity is independent of shear stress and shear rate. Therefore a single measurement is sufficient to calculate the viscosity. Here the flow pattern is governed by the well known Hagen-Poiseuille Equation, and the pressure drop at the tube walls is given by.

$$\Delta P_c = \frac{8Q\eta L_c}{\pi R_c^4} \qquad (1.56)$$

Where Q is the volumetric flow rate and η is the dynamic viscosity.

And the wall shear rate is given as follows (Morita A.T. et al. 2006).

$$\dot{\gamma}_w = \frac{4Q}{\pi R_c^3} \qquad (1.57)$$

Using equations 1.55 and 1.57, the viscosity is given by.

$$\eta = \frac{\pi \Delta P_c R_c^4}{8 Q L_c} \qquad (1.58)$$

In case of non-Newtonian flow, viscosity depends on shear rate. A single measurement is insufficient to calculate viscosity. A series of measurements are required at varying pressures. Here the stress-strain relationship is given by power-law relation (Elgibaly A.A.M. et al., 1997).

$$\tau_w = M(\dot{\gamma}_w)^n \qquad (1.59)$$

Where $\dot{\gamma}_w$ is the wall shear rate.

Advantages:

- It is very simple device in its design (Chhabra R.P. and Richardson J.F., 1999).
- It can operate to high shear rates (Arabo E.Y.M., 2011).
- It is suitable for high viscosity substances (Arabo E.Y.M., 2011).

Drawbacks:

- Shear rate is not uniform throughout the flow (Seyssiecq I. et al., 2003).

- It requires large sample volumes (Seyssiecq I. et al., 2003).

1.2.2. Sliding plate rheometer

Sliding plate rheometers are the simplest form of shear rheometers (Cheneler D., 2009).
A sliding plate rheometer consists of two parallel plates. Its schematic diagram is shown
in figure 1.27. The fluid sample is placed in the gap between the plates. Here the lower
plate is kept stationary, while the upper plate slides, and thus a shear flow is produced.
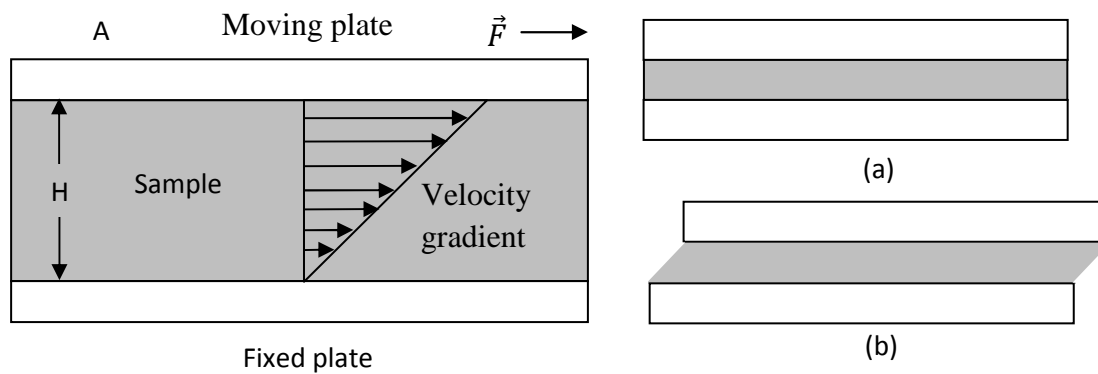
Fig.1.27: Sliding plate rheometer: (a) before the flow, (b) after the flow

Consider the case in which a fluid volume (thickness H) is placed between the plates.
When a force is applied on the upper plate, this plate will move with a velocity $\vec{V}$ in the
direction of force. After measuring the distance X moved by the upper plate, rheological
quantities can be found by the following relations.

Shear Stress: $$\tau = \frac{F}{A}$$ (1.60)

Shear Strain: $$\gamma = \frac{X}{H}$$ (1.61)

Strain rate: $$\dot\gamma = \frac{V}{H}$$ (1.62)

Where A is the area of the upper plate.

Since viscosity is the ratio between shear stress and strain rate, therefore from equations (1.60) and (1.62) we have

$$\eta = \frac{\tau}{\dot\gamma}$$ (1.63)

or $\quad \eta = \frac{FH}{AV}$ (1.64)

Advantages:

- It provides the simplest way to generate steady shear motion (Macosko, C.W. 1994).

Drawbacks:

- For large strains, it is very difficult to keep the constant gap between the plates (Macosko, C.W. 1994).

1.2.3. Rotational rheometers

In rotational rheometers, the fluid sample is placed in the narrow space between two surfaces. One of the surfaces is fixed while the other one is rotated. They are either in the form of controlled rate or controlled stress. In controlled rate form, the torque or shear stress is measured at certain pre-set speeds. While in controlled rate form, a certain pre-set torque is applied and the resulting shear rate is produced from the rotational speed of the rotating surface (Rao M.A., 1999). Traditional rotational type rheometers consist of concentric cylinder, parallel plate, and cone and plate rheometers (Steffe J.F., 1996).

1.2.3.1. Coaxial rotating cylinders (Couette Flow)

This is the very common type of rotational rheometer. It consists of two concentric-coaxial cylinders. Its schematic diagram is shown in figure 1.28. The inner cylinder is often called as 'bob' whereas the outer cylinder is called as 'cup'. The fluid sample is placed in the annulus between the two cylinders. One of the cylinders is fixed and the other is rotated with a set speed. In this way shear rate is generated in the annulus. Shear stress is calculated from the torque of the rotating cylinder and the geometrical dimensions. If we change the speed of the rotating cylinder, we can produce various torques, which can be used in determining the flow curve i.e. shear stress-shear rate curve.
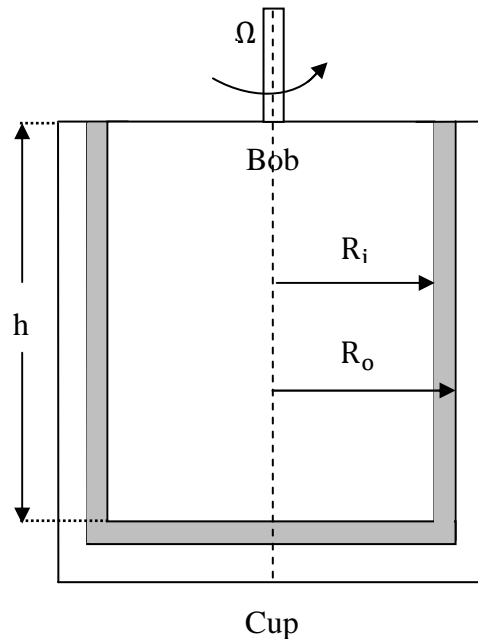
Fig.1.28: Typical concentric cylinder; fluid sample is shown by shaded area

The shear stress can be calculated as follows (Macosko C.W., 1994).

$$\tau \, (R_k) = \frac{M_k}{2\pi R_k^2 h} \qquad (1.65)$$

Where R_k could be the radius of inner or outer cylinder, depending if the bob is being rotated and cup is kept stationary and conversely. Similarly is the case for torque M_k. And h is the hight of inner cylinder. For very thin fluid annulus ($\frac{R_i}{R_o} \geq 99\%$), the shear rate can be calculated as

$$\dot{\gamma}(R_k) = \frac{\Omega \bar{R}}{R_o - R_i} \tag{1.66}$$

With

$$\bar{R} = \frac{R_i + R_o}{2} \tag{1.67}$$

Where R_i and R_o are the radii of inner and outer cylinders respectively, and Ω is the angular velocity.

From equations (1.65) and (1.66) we have the viscosity as follows

$$\eta = \frac{\tau(R_0)}{\dot{\gamma}(R_0)} = \frac{M_i(R_o - R_i)}{2\pi h R_o^2 \bar{R}} \tag{1.68}$$

Where M_i is the torque exerted on the inner cylinder.

Advantages:

- For large radii, the shear rate is nearly constant (Chhabra R.P. and Richardson J.F. 1999).

- It is useful for low viscosity samples and high shear rates (Macosko, C.W., 1994).

- It requires small sample volume (Seyssiecq I. et al., 2003).

Drawbacks:

- It is a big disadvantage of coaxial cylinder geometry that in order to change the gap between the cylinders, we have to change the cylinders (Walters K., 1975).

- The gap between the cylinders must be larger than the largest particle of the sample (Seyssiecq I. et al., 2003).

- It is difficult to clean for high viscosity fluids (Macosko, C.W., 1994).

1.2.3.2. Parallel plate rheometer

The parallel plate (disc) rheometer is also called torsional rheometer. It consists of two parallel discs. Its schematic diagram is shown in figure 1.29. The fluid sample is placed in the gap between the discs.
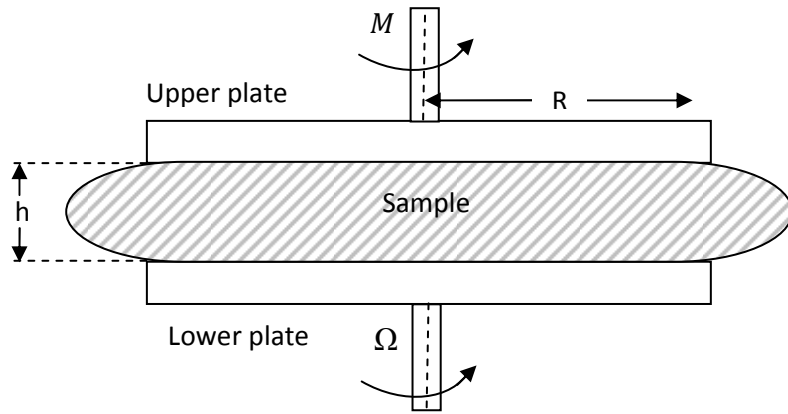
Fig.1.29: Parallel disc rheometer; fluid sample is shown by shaded area

Consider the case in which lower plate is fixed and upper plate rotates with angular speed (Ω). After measuring the torque (M) on the plate, the shear stress and shear strain can be calculated as follows.

$$\tau = \frac{2M}{\pi R^3} \tag{1.69}$$

$$\dot{\gamma} = \frac{\Omega R}{h} \tag{1.70}$$

Where R is the radius of plates and h is the distance (gap) between the plates. Using equations Eqns. (1.69) and (1.70), the viscosity is given as follows.

$$\eta = \frac{\tau}{\dot{\gamma}} = \frac{2hM}{\pi R^4 \Omega} \tag{1.71}$$

Advantages:

- It is a great advantage of parallel plate geometry that the gap between the plates can be easily changed to accommodate a huge range of materials, and a series of measurements can be performed on the same sample (Walters K., 1975).

- Very small gaps down to 5µm can be used (Henson D.J. and MacKay M.E., 1995).

- It can be used for polymer melts, blends and composites (Shenoy A.V., 1999).

- It needs a small sample volume and easy to sample loading (Macosko, C.W., 1994).

- It is less expensive and easy to clean (Shaw M.T. and Liu Z.Z., 2006).

Drawbacks:

- Shear rate is not uniform and varies in the radial position (Ortman K.C. et al., 2011).

1.2.3.3. Cone and plate rheometer

The cone and plate rheometer is widely used instrument for shear flow rheological properties of polymer systems (Shenoy A.V., 1999). It consists of a circular plate at the base and a circular cone at the top. Its schematic diagram is shown in figure 1.30. It works on the same principle as parallel plate rheometer; the only difference is a cone the upper disc is replaced by a cone. The fluid sample is placed in the gap between plate and cone, making an angle β. The cone and plate geometry produces a flow in which shear rate is nearly uniform. However, in order to ensure that shear rate is constant, the angle β should be small (<4°) (Walters K., 1975). Weissenberg Rheogonimeter can be a well-known example of cone and plate rheometer.
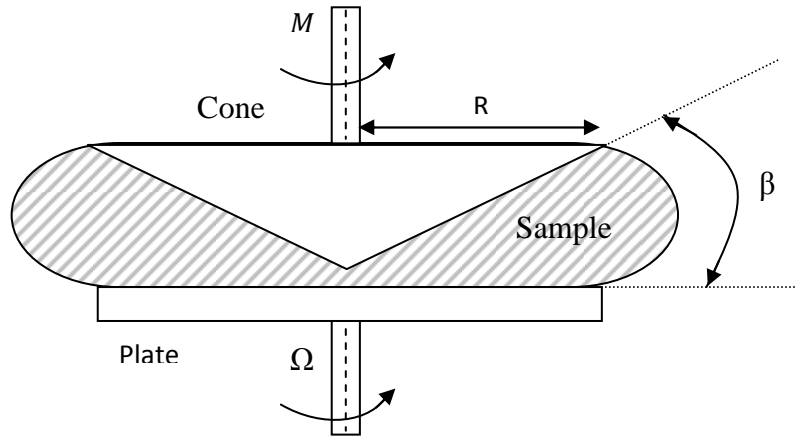
Fig.1.30: Cone and plate rheometer; fluid sample is shown by shaded area

Consider the case in which plate is kept fixed, while cone rotates with a known angular velocity (Ω). After measuring the torque (M) on the plate, the shear stress and shear strain can be calculated as follows (Macosko C.W., 1994; Walters K., 1975).

$$\tau = \frac{3M}{2\pi R^3} \tag{1.72}$$

$$\dot{\gamma} = \frac{\Omega}{\beta} \tag{1.73}$$

The viscosity is given by

$$\eta = \frac{\tau}{\dot{\gamma}} = \frac{3M\beta}{2\pi R^3 \Omega} \tag{1.74}$$

Advantages:

- It is the main advantage of cone and plate rheometer that the shear rate $\dot{\gamma}$ is nearly uniform within the fluid sample, which enables us to obtain the shear stress at a given shear rate $\tau(\dot{\gamma})$ from a single measurement (Venerus D.C., 2007).

- It is useful for normal stress measurements (Shenoy A.V., 1999).

- It requires small sample size and is easy to load and clean (Shenoy A.V., 1999).

- Maximum shear rate rachieved to 10 s^{-1} (Son Y., 2008).

Drawbacks:

- It is a big disadvantage of cone and plate geometry that in order to change the gap angle, we have to change the cone (Walters K., 1975).

- For the shear rate to be constant, the angle β between the cone and plate should be made as small as possible (Barnes H.A. et al., 1989).

1.3. Torsional resonators and quartz resonators

There exist a lot number of complex fluids for which the dynamics extends to many hours or even days. They have diverse relaxation process. High frequency rheology provides insight into microstructures of these kinds of fluids. The range of this high frequency normally extends from 10^6 Hz. Step motor rheometers are limited to frequencies $\leq 10^2$ Hz. Torsional resonators can be used to attain high frequency data. These devices are available in many geometries e.g. cylinder, tube or plate (Romoscanu A., 2003). Valtorta D. and Mazza E. (2005) used a torsional resonator device to study the viscoelastic properties of soft tissues in the linear viscoelastic range for discrete frequencies in the range from 1 kHz to10 kHz. Fritz G. et al. (2002) studied the rheology of colloidal dispersions for discrete frequencies in the range of 10^4 to 10^6 Hz. Similary, quartz resonators can also be used for very high frequency 10 MHz (Nwankwo E. and Durning C.J., 1999). Since these are only single frequency devices (page 70), they are unable to cover all the relaxation processes for complex fluids.

1.4. Squeeze flow rheometer

Squeeze flow rheometer is widely used for the rheological characterization of non-Newtonian fluids (Bird R.B. et al., 1987). Squeeze flows arise in a variety of situations, including machine bearings, human joints, manufacturing processes, lubrication systems and compression molding (Lawal A. and Kalyon D.M., 1998; Lawal A. and Kalyon D.M., 2000, Tadmor Z. and Gogos C.G., 1979). In a squeeze flow rheometer, a material is compressed between two parallel plates (Engmann J et al., 2005) of radius R separated by a gap H. Its schematic diagram is shown in figure 1.31.
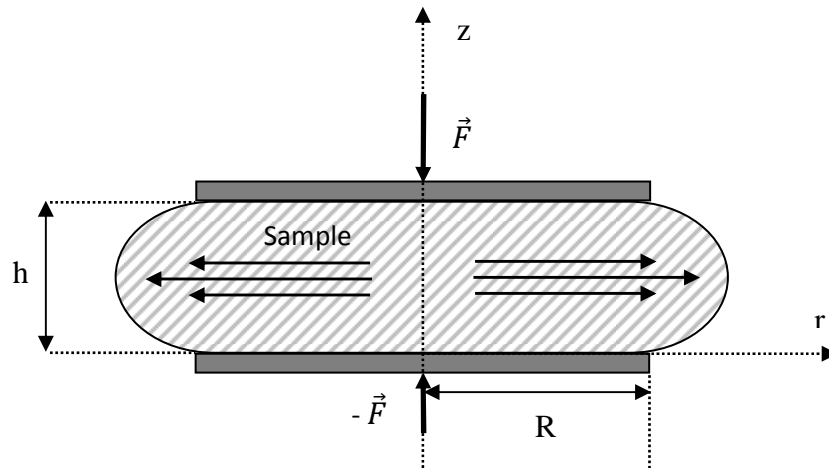
Fig. 1.31: Schematic diagram of squeeze flow between two parallel plates

Where 'R' is the plate's radius and h is the sample thickness. The plate radius is taken to be very large as compared to the sample thickness i.e. R/h>>1. Normally, the lower plate has a fixed position, while a force of magnitude F is applied in a direction perpendicular to the upper plate. The material between the plates is compressed and flows in the radial direction. Squeeze flow is carried out with the following boundary conditions.

$$\begin{cases} v_r = 0, v_z = 0 & \text{on } z = 0 \\ v_r = 0, v_z = -V_z & \text{on } z = h \end{cases} \tag{1.75}$$

Where v_r and v_z are the velocity components in the r and z direction respectively.

Neglecting the fluid inertia, the equations of momentum and conservation of mass can be written in the cylindrical form as follows (Oswald P., 2005).

$$0 = -\frac{\partial P}{\partial r} + \eta \frac{\partial^2 v_r}{\partial z^2} \quad \text{(momentum along r)} \tag{1.76}$$

$$0 = -\frac{\partial P}{\partial r} \quad \text{(momentum along z)} \tag{1.77}$$

$$\frac{1}{r}\frac{\partial}{\partial r}(rv_r) + \frac{\partial v_z}{\partial z} = 0 \quad \text{(continuity)} \tag{1.78}$$

Where p is the pressure exerted on the fluid, which is considered to be isotropic.

The interest lies in determining the total force F exerted by the fluid on the plate in the direction of plate movement, which is given in the following equation (Sherwood J.D., 2005).

$$F = 2\pi \int_0^R p(r)r\,dr \tag{1.79}$$

Solving equations (1.76, 1.77, and 1.78) using the initial conditions (Eq. 1.75), the force F (Eq. 1.79) can be found as follows (Oswald P., 2005).

$$F = \eta \frac{3\pi R^4}{2h^3}\frac{dh}{dt} \tag{1.80}$$

Although squeeze flow rheometers can also be used in steady shear mode, yet they are frequently used in dynamic (oscillating) mode to study the rheological properties of viscoelastic materials (Ahmed J. and Ramaswamy H.S., 2007; Field J.S. et al., 1996).

Advantages:

- Squeeze flow rheometer is a simple way to measure rheological properties (Meeten G.H., 2004), especially for very viscous materials.

- Oscillation squeeze flow can handle more easily the inertial effects than the torsional oscillation methods (Bell D. et al, 2005).

- It can be used for both shear and extensional forms (Coblas D. et al., 2010; Lawal A. and Kalyon D.M., 1998) depending on if there is 'no wall slip' or 'perfect wall slip'.

- It can measure rheological data for frequencies much higher than the step motor rheometers (Cheneler D. et al, 2011; Kirschemann L., 2003) and in a wide continuous range (Fig. 1.32).

Drawbacks:

- It is difficult to ensure ideal boundary conditions ("no slip" or "perfect slip") (Engmann J et al., 2005).

- The flow can be shear or extension dominated depending on the boundary conditions and geometry (i.e. ratio of gap height to plate radius) (Chan T.W., and Baird D.G., 2002).
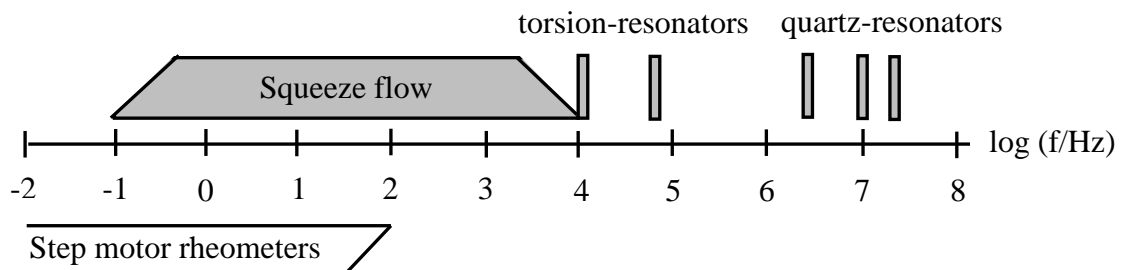
Fig. 1.32: Frequency range comparison between conventional rheometers, torsion-resonators, quartz resonators, and Squeeze flow rheometer

1.5. Chapter Summary

As we have seen, the rheometers can be used in determining viscosities of different kind of materials. However, despite their usefulness, they have also some limitations and drawbacks. When used in the shear mode, most of them work at low shear rates not much beyond 10 s^{-1} with the exception of capillary rheometer. At higher shear rates, flow instabilities begin to occur and the sample begins to emerge out of the gap. When used in oscillation mode, step motor rheometers are limited to low frequencies, typically lower than 100 Hz. However, the knowledge of data at higher frequencies is interesting for the rheological characterization of complex fluids. Sometimes, these higher frequencies can be achieved by time-temperature superposition principle, but it is not always possible if a phase or glass transition occurs in the temperature range. On the other hand, torsional resonators and quartz resonators can also be used to study rheology at high frequencies. But the problem with these devices is that these are only single frequency devices. Therefore, according to these remarks, squeeze flow rheometers seem to be the most adequate as they can extend the frequency range of step motor rheometers to an order of magnitude towards high frequency. This favors the idea to develop a squeeze flow rheometer. This rheometer will be useful to study the rheological behavior of materials over a large range of frequency (1 Hz to 8 kHz) and high temperatures (5°C to 150°C). It requires very small amount of sample (down to 10µL). Due to its smaller size and simple design, it is user friendly, very easy to transport and clean. Furthermore, its adaptation for high-pressure working seems to be possible.

CHAPTER 2

PAV: ATMOSPHERIC PRESSURE RHEOLOGY

PAV stands for piezoelectric axial vibrator. It is a kind of dynamic squeeze flow rheometer. The model employed in this work has been developed by Pechhold and Kirschenmann at the institute for Dynamic Material Testing (IdM) at University of Ulm, Germany. It is used to measure the rheological properties of viscoelastic materials at atmospheric pressure. A detailed study about the structure, theory and calibration of PAV can be found in the thesis work of **Ludwig Kirschenmann** (Kirschemann L., 2003). Here our purpose to deal with PAV is twofold. First: the study of its experimental capability by taking its basic theory and working equations. Second: its adaptation in the development of a high pressure PAV device (chapter 3).

2.1. Structure of PAV

It consists of a fixed lower plate and a vibrating upper plate between which sample is placed with the help of syringe. Circular spacers of different thicknesses varying from 15µm to 1 millimeter are used to adjust the thickness of the sample.

Fig. 2.1: Piezoelectric axial vibrator; device for atmospheric pressure rheology

The actuator/sensor of PAV probe is a thin-walled (0.5 mm thick) square copper tube, which is glued on a rigid base and above a thick ceramic plate, which transfers oscillations (fig. 2.2). On the copper tube, eight piezo elements are in pairs (inside and outside) glued on the four sides (figure 2.2. and figure 2.3.). In order to avoid a direct coupling between actuators and detectors, the copper tube possesses four partial slots (slits) alongside between the actuator piezos and the detector piezos. Two opposite pairs as actuators are connected with the reference output of the LockIn-amplifier, which supplies sinusoidal voltage. The other pairs, the detectors, detect the deflection of the copper tube, the vibrations of which are altered due to the interaction with the sample.
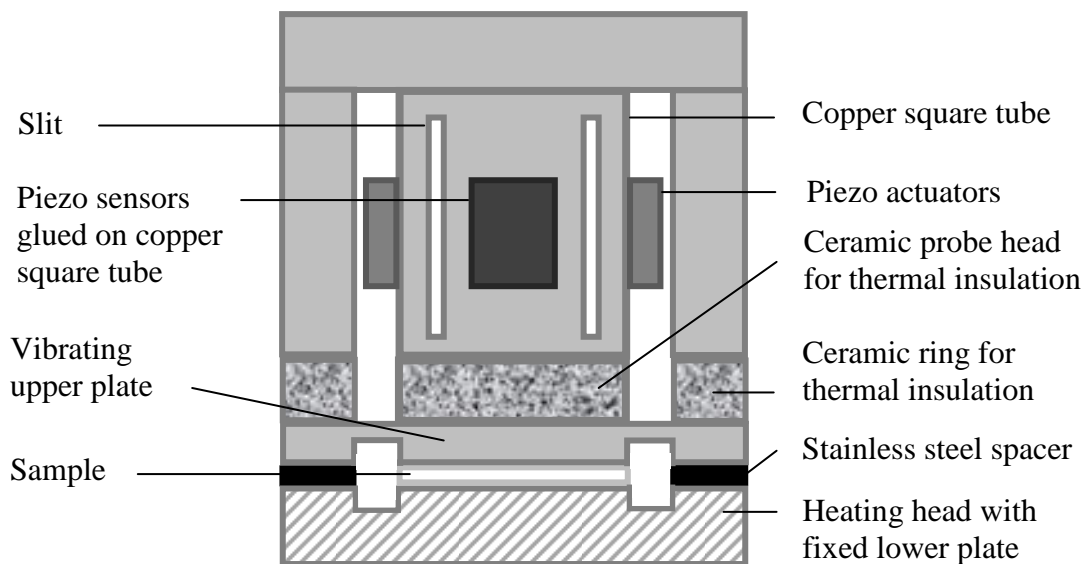
Fig. 2.2: Structure diagram of piezoelectric axial vibrator
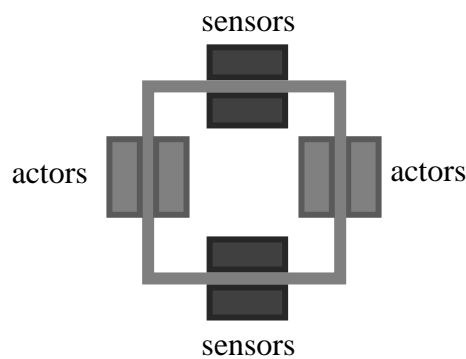
Fig. 2.3: Structure of piezos glued to square copper tube (inside & outside)

The ceramic ring as well as the ceramic probe head serves to protect the actuator/sensor unit against high temperature. It is also mentionable that the glue cannot withstand high temperatures as it possesses a glass transition temperature of 140°C, and it is possible to refresh the electronic part with a cooling water bath if necessary (Figure 2.4).
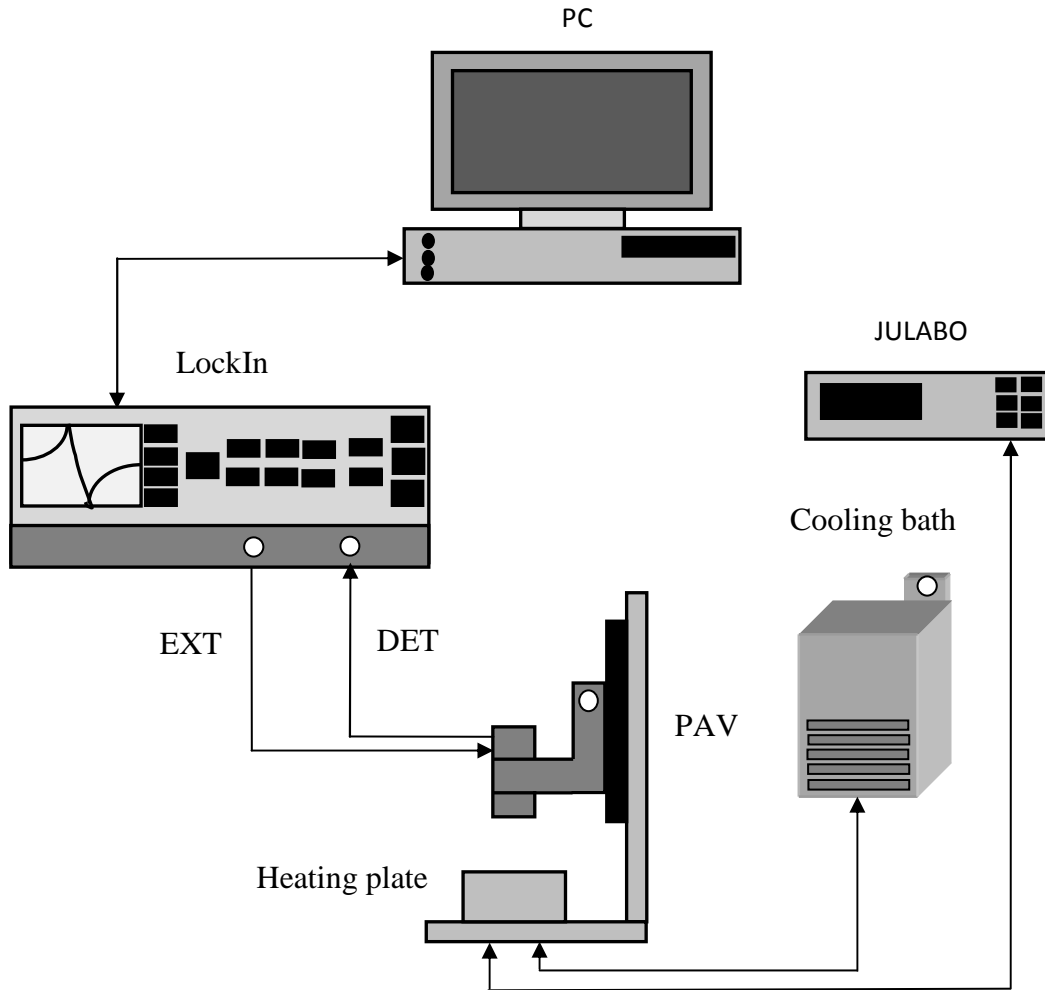
Fig. 2.4: Structure of the measuring position of PAV

Figure 2.4 shows the structure of the measuring position of PAV. It consists of a LockIn amplifier, model SR 850 of the company Standard research. A cooling bath is used for cooling purposes, while for heating purpose we use a JULABO electrical heating controller. LockIn is connected to a computer, which takes up the measured values.

2.2. Theory of PAV

In order to measure a sample, an empty measurement must be accomplished with adjusted gap d. Subsequently, a measurement with sample is taken. The LockIn amplifier supplies the excitation voltage to the excitation piezos, and measures the signals from the detection piezos. A key factor for calculating the rheological properties is the complex spring constant K^* of the sample (Fig. 2.5) which can be calculated as a function of electrical signals measured by the piezoelectric sensors. These electrical signals are: the tension received by the sensor in the empty mode U_0, the tension received by the sensor in the loaded form U, the phase difference between output signals of sensor in the loaded and empty case $\Delta\varphi$, and the excitation frequency f.

These values are useful in calculating the value of $\frac{K_0}{K^*}$, which in real and imaginary parts is given in the followings (Kirschemann L., 2003).

$$\left(\frac{K_0}{K^*}\right)' = \frac{U}{U_0} \cdot \frac{1}{1-\frac{f^2}{f_0^2}} \cdot \frac{\frac{1}{1+B\left(1-\frac{f^2}{f_0^2}\right)}\left(cos\Delta\varphi-\frac{U}{U_0}\right)+\frac{sin\Delta\varphi}{Q_0\left(1-\frac{f^2}{f_0^2}\right)}}{1-2\frac{U}{U_0}cos\Delta\varphi+\left(\frac{U}{U_0}\right)^2} - \frac{B}{1+B\left(1-\frac{f^2}{f_0^2}\right)} - \frac{K_0}{K_1} \cdot \frac{1}{\left(1-\frac{f^2}{f_1^2}\right)} \qquad (2.1)$$

$$\left(\frac{K_0}{K^*}\right)'' = \frac{U}{U_0} \cdot \frac{1}{1-\frac{f^2}{f_0^2}} \cdot \frac{\frac{sin\Delta\varphi}{1+B\left(1-\frac{f^2}{f_0^2}\right)}-\frac{1}{Q_0\left(1-\frac{f^2}{f_0^2}\right)}\left(cos\Delta\varphi-\frac{U}{U_0}\right)}{1-2\frac{U}{U_0}cos\Delta\varphi+\left(\frac{U}{U_0}\right)^2} \qquad (2.2)$$

Where

K_0 (N/m): Coefficient of stiffness of the piezo sensor.

f_0 (Hz): Resonance frequency of the piezo sensor.

f_1 (Hz): Resonance frequency of shaft.

$B = \frac{A}{1-A}$, and A is a coefficient obtained by calibration.

Q_0 = Quality factor of the piezo.

We will see in the coming section how equations (2.1) and (2.2) will be very helpful in the calculation of rheological quantities.
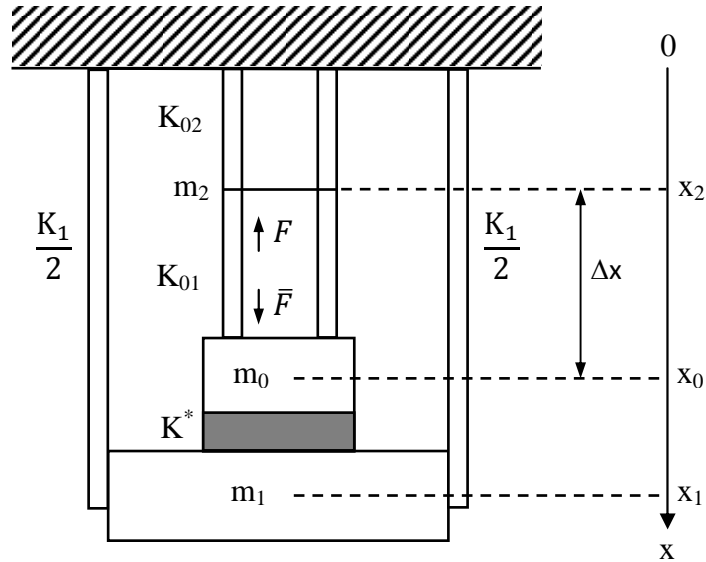
Fig. 2.5: Mechanical equivalent diagram of PAV

Figure 2.5 shows the mechanical equivalent diagram of PAV. In this figure, m_0 represents the mass of the probe head, m_1 the mass of heating plate and m_2 the mass of the lower part of the active probe length and the upper part of the passive length. K_1 denotes the spring constant of the slits, K_{01} the spring constant of the active part of the copper tube, K_{02} the spring constant of the passive length of the copper tube, and K^* the desired complex spring constant of the sample. Then, x_1 is the deflection of heating plate, x_0 the deflection of the probe plate, and x_2 the deflection of the passive part of the probe. $F, \bar{F}$ is the pair of exciting forces.

2.3. Computation of rheological quantities J, G, and η

The dynamic vibration of upper plate of PAV creates a dynamic squeeze flow as shown in figure 2.6.
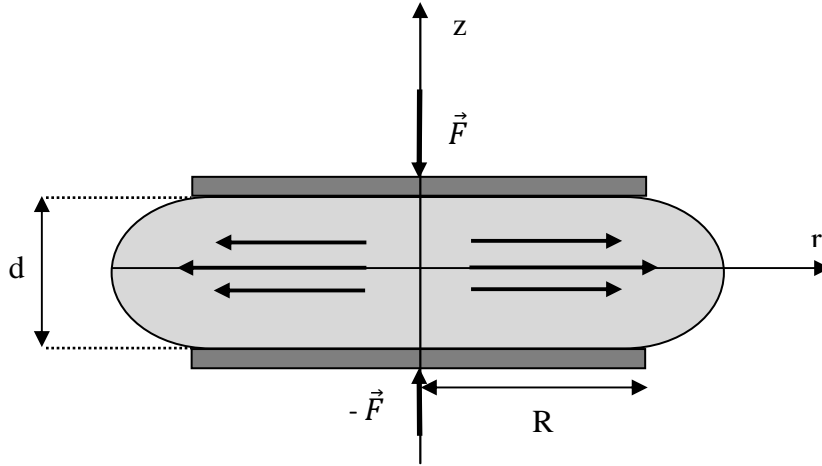
Fig. 2.6: Dynamic squeeze flow between two parallel disks each with radius R. The static plate spacing is d, and the dynamic amplitude is Δd.

From the continuum mechanical calculation for the dynamic squeeze flow within the range of linear viscoelasticity and with the assumption that no wall slip is present, the complex spring constant K^* of a sample of density ρ can then be calculated by using the equation 2.3(Kirschemann L., 2003).

$$\frac{1}{K^*} = \frac{2}{3\pi} \cdot \frac{d^3}{R^4} \cdot \frac{\frac{1}{G}\left[\left(1+\frac{G}{3K}\right)\cdot\left(1+\frac{\rho\omega^2 d^2}{10G}+\cdots\right)+\frac{G}{K}\cdot\frac{3}{2}\cdot\frac{R^2}{d^2}\left(1+\frac{2}{3}\cdot\frac{d^2}{R^2}\cdot\frac{1+\frac{G}{3K}}{1-\frac{2G}{3K}}\right)\right]}{\left(1+\frac{4G}{3K}\right)\left(1+\frac{4}{3}\cdot\frac{d^2}{R^2}\cdot\frac{1-\frac{G}{6K}}{1-\frac{2G}{3K}}\right)}$$

(2.3)

Where, K represents the bulk modulus and G the shear modulus of the sample. Whereas R is the radius of the disc, d is the sample thickness, and $\omega = 2.\pi.f$ is the angular frequency.

Consider first approximation: if the sample is incompressible i.e. $\frac{G}{K} \ll 1$, then equation 2.3 becomes.

$$\frac{1}{K^*} = \frac{2}{3\pi} \cdot \frac{d^3}{R^4} \cdot \frac{\frac{1}{G}\left(1+\frac{\rho\omega^2 d^2}{10G}+\cdots\right)}{\left(1+\frac{4}{3}\cdot\frac{d^2}{R^2}\right)}$$

(2.4)

Consider second approximation: if the sample thickness d is very small as compared to the disc radius R (i.e. $\frac{d}{R} \ll 1$), then equation 2.4 becomes

$$\frac{1}{K^*} = \frac{2}{3\pi} \cdot \frac{d^3}{R^4} \cdot \frac{1}{G}\left(1 + \frac{\rho\omega^2 d^2}{10G} + \cdots\right) \tag{2.5}$$

$$\Rightarrow K^* = \frac{3\pi}{2} \cdot \frac{R^4}{d^3} \cdot \frac{G}{\left(1+\frac{\rho\omega^2 d^2}{10G}+\cdots\right)} \tag{2.6}$$

Let $J = \frac{1}{G}$ then we receive from equation (2.6) the following quadratic equation in J

$$J^2 + \frac{1}{\beta} \cdot J - \frac{c}{\beta} \cdot \frac{K_0}{K^*} \tag{2.7}$$

Where

$$\begin{cases} \beta = \frac{\rho\omega^2 d^2}{10} & (2.8) \\\\ c = \frac{3\pi}{2} \cdot \frac{R^4}{K_0 d^3} & (2.9) \end{cases}$$

Solving equation 2.7 for $J = J' - iJ''$, we obtain (Kirschemann L., 2003)

$$\begin{cases} J' = c\left(\frac{K_0}{K^*}\right)'\left(1 - \beta c\left(\frac{K_0}{K^*}\right)'\right) + \beta\left[c\left(\frac{K_0}{K^*}\right)''\right]^2 & (2.10) \\\\ J'' = -c\left(\frac{K_0}{K^*}\right)''\left(1 - 2\beta c\left(\frac{K_0}{K^*}\right)'\right) & (2.11) \end{cases}$$

Once the values of J' and J'' are known, we can calculate complex shear modulus $G^* = G' + iG''$, and complex dynamic viscosity $\eta^\star = \eta' - i\eta''$ of the sample using the the following equations.

$$G' = \frac{J'}{J'^2+J''^2} \ , G'' = \frac{J''}{J'^2+J''^2} \tag{2.12}$$

And $\qquad\qquad\qquad \eta' = \frac{G''}{\omega} \ , \eta'' = \frac{G'}{\omega} \tag{2.13}$

Taking into account the compressibility of the sample

If the thickness of spacer is very very small (300µm or lower), then the product term $\left(\frac{G}{K} \cdot \frac{R^2}{d^2}\right)$ is in indeterminate form, and cannot be neglected. Therefore, equation 2.3 becomes:

$$\frac{1}{K^*} = \frac{2}{3\pi} \cdot \frac{d^3}{R^4} \cdot \frac{1}{G}\left[\left(1 + \frac{\rho\omega^2 d^2}{10G} + \cdots\right) + \frac{G}{K} \cdot \frac{3}{2} \cdot \frac{R^2}{d^2}\right] \qquad (2.14)$$

Furthermore, for very very small 'd', the inertial term containing the product $(\rho\omega^2 d^2)$ in the above equation can be neglected as compared to 1. Therefore, we come up with the following equation.

$$\frac{1}{K^*} = \frac{2}{3\pi} \cdot \frac{d^3}{R^4} \cdot \frac{1}{G}\left[1 + \frac{G}{K} \cdot \frac{3}{2} \cdot \frac{R^2}{d^2}\right] \qquad (2.15)$$

Putting $J = \frac{1}{G}$, equation (2.15) can be written as

$$J = \frac{3\pi}{2} \cdot \frac{R^4}{d^3} \cdot \frac{1}{K^*} - \frac{3}{2} \cdot \frac{R^2}{d^2} \cdot \frac{1}{K} \qquad (2.16)$$

or $$J = J_{meas} - \frac{3}{2} \cdot \frac{R^2}{d^2} \cdot k^* \qquad (2.17)$$

Where J_{meas} is the measured value of complex shear compliance. It is obtained from equation 2.6 by neglecting the inertial term. The second term on right hand side is called the compressibility correction term.

With $$k^* = \frac{1}{K} = k' - ik" \qquad (2.18)$$

Where, k^* stands for the complex compressibility of the sample.

Note that the correction term (equation 2.17) is higher than 10% (table 2.1) for spacers of thickness 300µm or lower, and should not be neglected for such spacers.

Spacer (µm)	Correction
500	9%
300	24%
200	34%

Table 2.1: Compressibility correction term for different spacers.

Note that in the calculation of correction term in equation 2.17, we have taken the value $K = 1.10^{-9}$ Pa^{-1} for different spacers.

2.4. Measurement procedure

The first step in the measurement procedure is the calculation of optimal amount of sample. The optimal amount of sample is calculated by using the following formula.

$$V = \pi . R^2 . d \qquad (2.19)$$

Where d is given by

$$d = d_{spacer} + \varepsilon \qquad (2.20)$$

Here, d_{spacer} is the spacer thickness, and $\epsilon = 10 \mu m$ is the residual gap when cell is closed without spacer (Fig. 2.7). In fact, the inner part of the PAV lower plate where we place the sample is a little bit lower than the border.
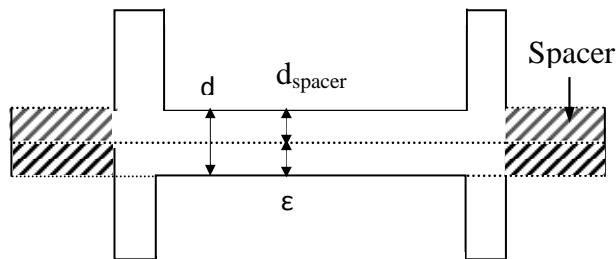
Fig. 2.7: Schematic diagram showing the gap correction thickness

This residual gap correction must be taken into account for each spacer, in order to have correct sample volume especially for thin spacers. However, what will be the effect on the rheological measurements if we do not respect the criterion that is if the amount of sample injected is more or less than the optimal amount for each spacer. This section is designed to answer this question. For this purpose, we have done a series of measurements in order to determine the effect of the filling.

The process consists of three series of measurements performed with each of the spacers 500µm, 300µm, 200µm, 100µm and 75µm respectively at 22°C. For first series, the amount of sample injected is equal to optimal amount (equation 2.19), for second series it is two times the optimal amount, while for third series it is taken to be one half of the optimal amount.

The results for 300-µm spacer can be observed in figure 2.8.
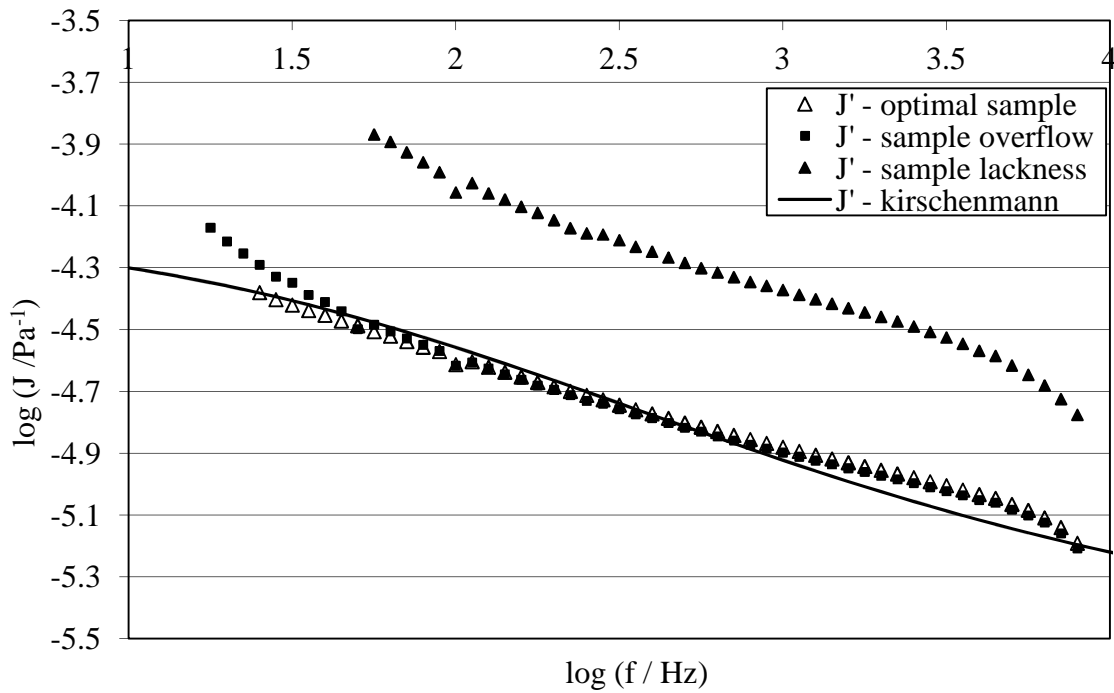
Fig. 2.8: Effect of bad filling for 300µm spacer.

Figure 2.8 shows that if there is an excess amount of sample, it does not affect very much the results, as the flow curves superimpose almost with the master curves. However, the results are not good if the amount of sample is not sufficient. They show extreme deviation from the master curves. The results for other spacers are similar, although the figures have not been shown.

In fact, if there is a lack of sample, the results will be clearly erroneous because they are proportional to R^4, with R the radius of the sample drop, which must match with the radius of the cell's plate. This fact is evident from the equation (2.8) discussed previously. In case of lack of sample, the radius of sample is small as compared to the plate radius, which leads to erroneous results.

The other steps taken into account for the measurement process are the following:

- Pre-heat the device up to the required temperature we want to take measurements.
- Inject the optimal amount of sample with the help of syringe.
- Close the cell firmly.
- Wait for thermal equilibrium and relaxation of the sample. The waiting time depends on the type of the sample.
- Take a series of measurements after waiting the corresponding number of hours according to the measurement protocol.
- Open the cell slowly. Check if both plates are well covered with sample, and then clean them very well.

2.5. Sample stability

As soon as the sample is placed between the plates and the device is closed, sample is not in equilibrium state (thermal and mechanical). The objective of this section is to find the minimum time in hours at which the measurements will be stable for each spacer.

For this purpose, we have taken several measurements with the Silicon oil AK 60000, from WACKER SILICONES. These measurements are taken with spacers of thicknesses 1000µm, 500µm, 300µm, 200µm and 100µm at 22°C. A set consisting of 13 measurements is taken with each spacer. Twelve of these measurements are taken on the same day as the sample injection, while the last measurement is taken after the whole night wait. From all the 13 measurements, we have taken one frequency index and the corresponding value of U/U_0. Consider the plotting of U/U_0 verses time (Fig. 2.9) for the set of measurements taken with 1000-µm spacer.
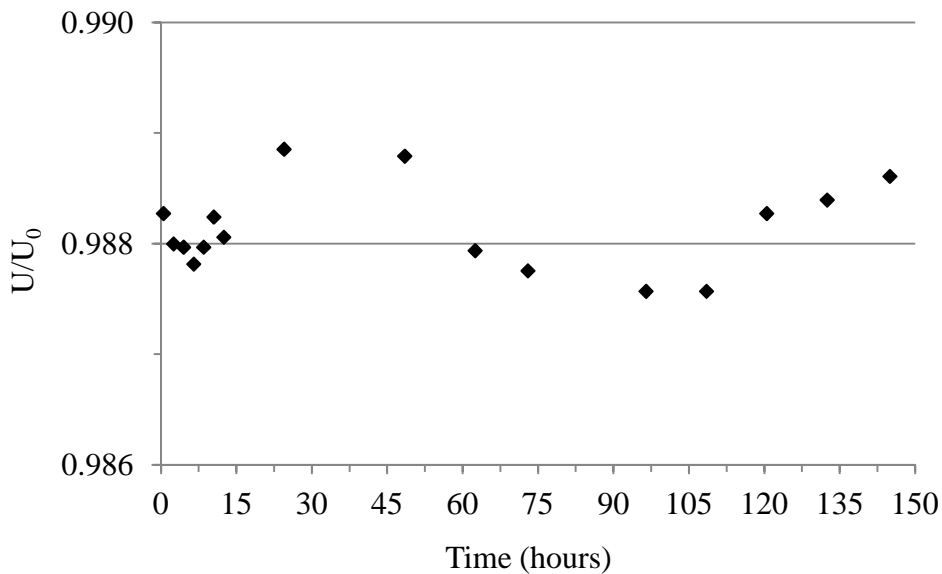
Fig. 2.9: Evolution of U/U_0 signal for a given frequency as a function of time;
1000-µm spacer (f = 2818 Hz)

Figure 2.9 shows that for 1000-µm spacer, the measurements seem to be stable immediately after putting the sample. It might be due to the fact that for 1000µm spacer, the sample molecules are not too much compressed and they have enough space to relax more rapidly.

Now consider the plotting of U/U_0 versus time (fig. 2.10) for the set of measurements taken with 500-µm spacer.
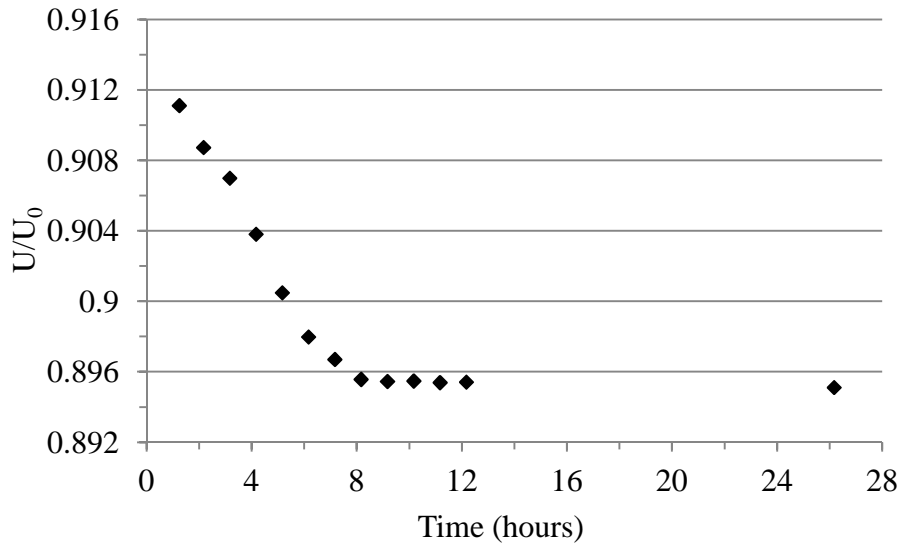
Fig. 2.10: Evolution of U/U_0 signal for a given frequency as a function of time;
500-µm spacer (f = 2818 Hz)

Figure 2.10 shows that the minimum time for measurements to be stable is about eight hours after the sample injection. The plotting of U/U_0 versus time for the measurements taken with 300-µm spacer and 200-µm spacer shows the same behavior. Spacers of thicknesses 100µm and 75µm show a different behaviour, where the measurements seem to be stable for a waiting time less than 1 hour. The result for 100µm spacer is shown in figure 2.11.
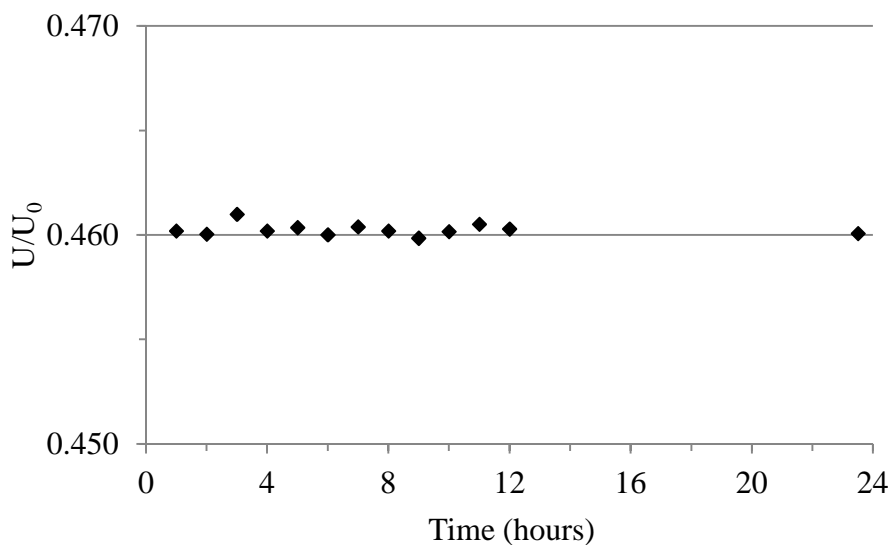
Fig. 2.11: Evolution of U/U_0 signal for a given frequency as a function of time;
100-µm spacer (f = 89 Hz)

This behavior (Fig. 2.11) may be due to the fact that for the thinner spacers, the sample molecules are very compressed and they do not have enough space for relaxing. Furthermore, for having good results, the limiting value of U/U_0 should be equal to 1 for frequencies approaching to zero. From figure 2.12, we see that the limiting value of U/U_0 is not equal to 1 for spacers of thickness 100 and 75 µm, which shows that the data obtained with these spacers is not useful for further calculations.
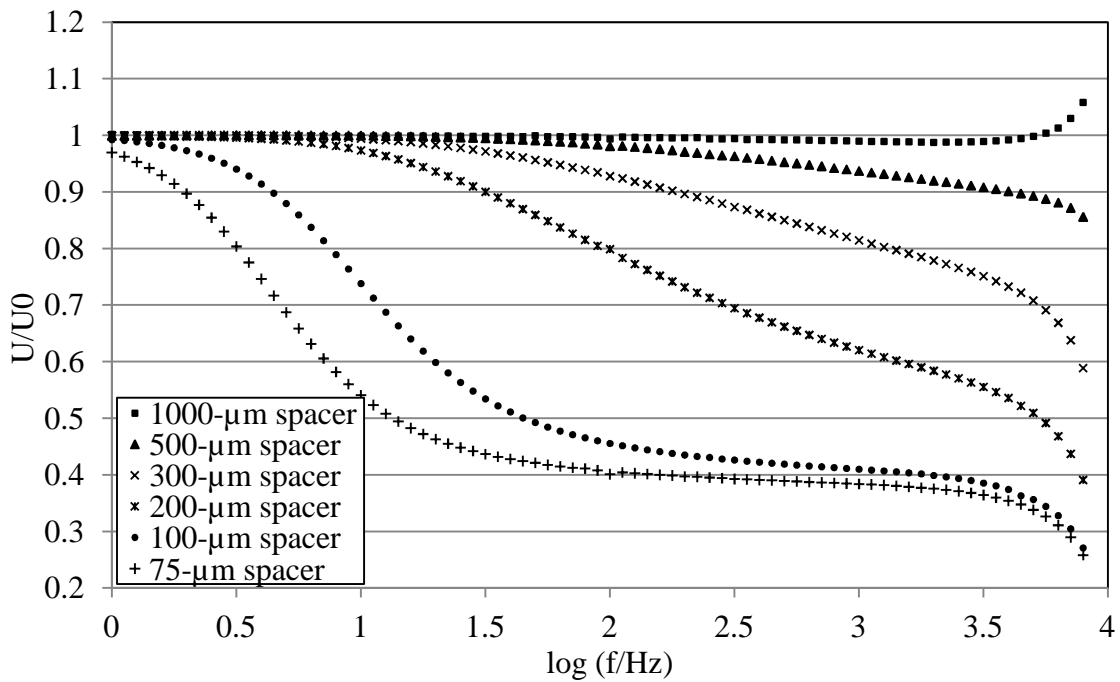
Fig. 2.12: Evolution of U/U_0 signal over frequency for different spacers

The results with all the spacers show that the thick spacers are more appropriate for SILICON AK60000 than the thinner ones. It is important to note that the measurement stability discussed above represents strictly the results only for 22°C. We can expect a different waiting time as a function of spacer thickness at other temperatures, although measurement stability at other temperatures have not been taken.

2.6. Repeatability and Reproducibility

Repeatability is the variation in measurements obtained with one device when used several times by one operator while measuring the same sample. It is commonly known as equipment variation (EV). Reproducibility is the variation in the average of measurements made by different operators (appraisers) using the same device when measuring the different samples. It is commonly known as appraiser variation (AV). The repeatability and reproducibility of a measuring system is used to determine the performance of a measurement instrument (Prevost S.L. et al, 2009). Figure 2.13 represents the flow chart for calculating the repeatability and reproducibility.
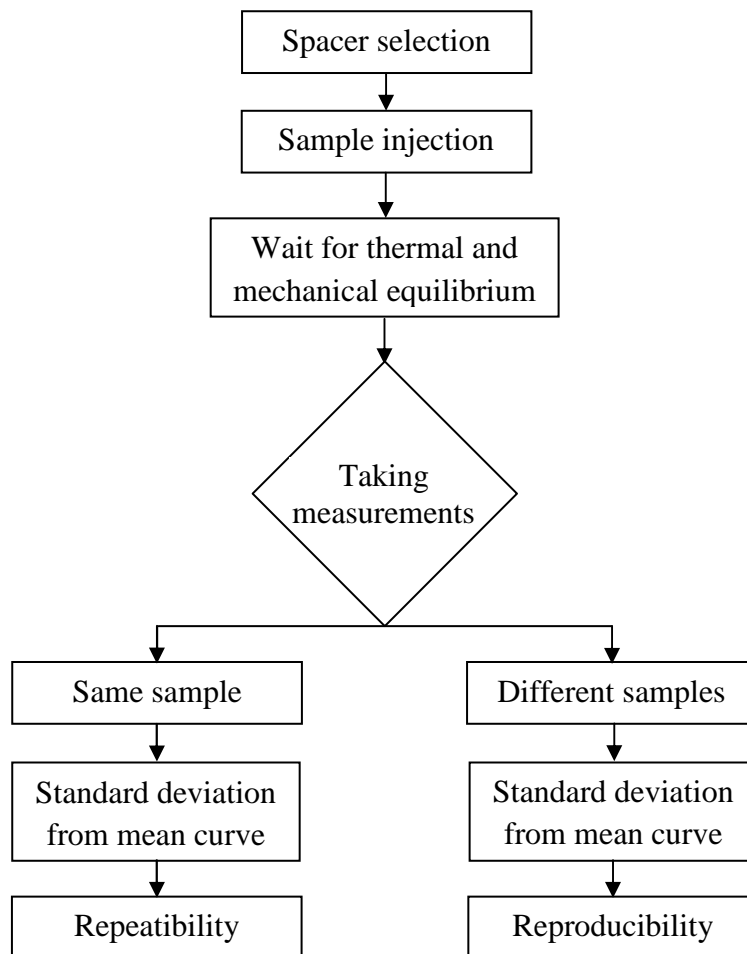
Fig. 2.13: Flow chart outlining how repeatability and reproducibility criteria are to be applied

2.6.1. Tests of repeatability

A series of measurements is conducted at 25 ° C and for spacers of thicknesses 500, 300, 200, 100, 75 and 50 µm respectively. All the chained measurements taken after the equilibrium is reached and without changing the sample have been used to calculate repeatability. For each set of measurements at a temperature and a given spacer, we have calculated deviations between the experimental points and the average curve. These deviations are shown in the table 2.2.

Spacer (µm)	No. of deviation data	Standard deviation (%)	Standard Deviation (Mean)
500	152	0.0252	0.019%
	152	0.0149	
	152	0.0174	
	156	0.0186	
300	208	0.0153	0.016%
	204	0.0166	
	204	0.0161	
200	220	0.0184	0.017%
	220	0.0158	
	220	0.0157	
100	136	0.0221	0.022%
	140	0.0196	
	137	0.0233	
75	108	0.0275	0.031%
	108	0.0252	
	108	0.0320	
	108	0.0303	
	108	0.0233	
	104	0.0338	
	104	0.0421	
50	56	0.0466	0.050%
	56	0.0444	
	56	0.0501	
	56	0.0609	
	56	0.0337	
	56	0.0600	
	56	0.0563	

Table 2.2: Standard deviation of deviations; repeatability case.

Figure 2.14 gives the standard deviation as a function of spacer.
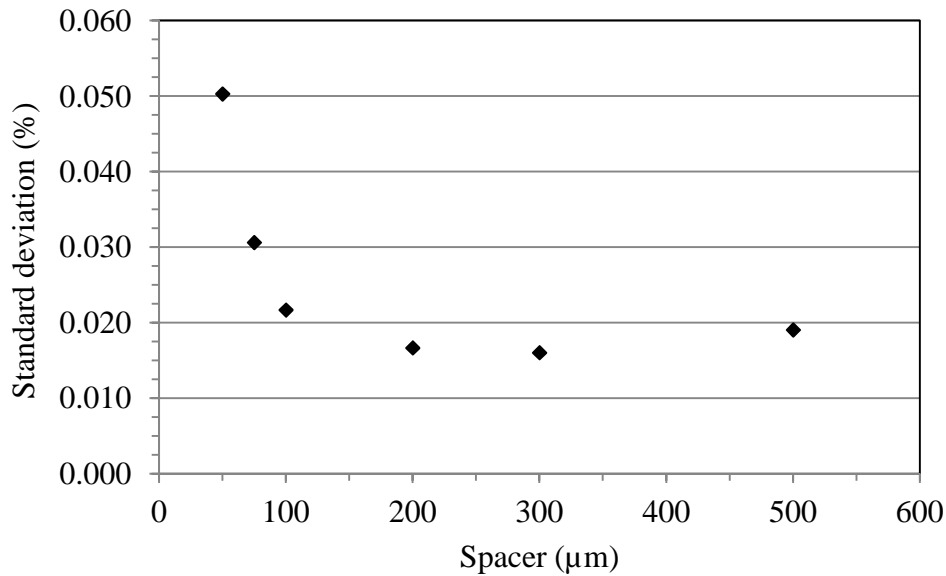
Fig. 2.14: Standard deviation as a function of spacer; repeatability case

From this graph, we see that maximum standard deviation (σ) is about 0.05%, which is for 50-µm spacer. This shows that the accuracy of the device in repeatability is less than 0.16% (3σ). The decreasing behavior of the graph shows that the results are more reliable with thicker spacers.

2.6.2 Tests of reproducibility

A series of measurements is conducted at 25 ° C and 35 ° C for spacers of thicknesses 500, 300, 200, 100, 75 and 50 µm respectively. After each measurement, the sample is replaced by a new sample. Measurements were taken after the equilibrium is reached. For each set of measurements at a temperature and a given spacer, we have calculated deviations between the experimental points and the average curve. These deviations are given in table 2.3.

Temperature (°C)	Spacer (µm)	No. of deviation data	Standard deviation (s.d)
25°C	500	154	0.1004%
	300	154	0.0849%
	200	165	0.0964%
	100	103	0.1551%
	75	187	0.5230%
	50	98	0.6823%
35°C	500	68	0.0147%
	300	145	0.1093%
	200	110	0.0488%
	100	70	0.0486%
	75	140	0.2392%
	50	60	0.3905%

Table 2.3: Standard deviation of deviations; reproducibility case

Figure 2.15 gives the standard deviation as a function of spacer.
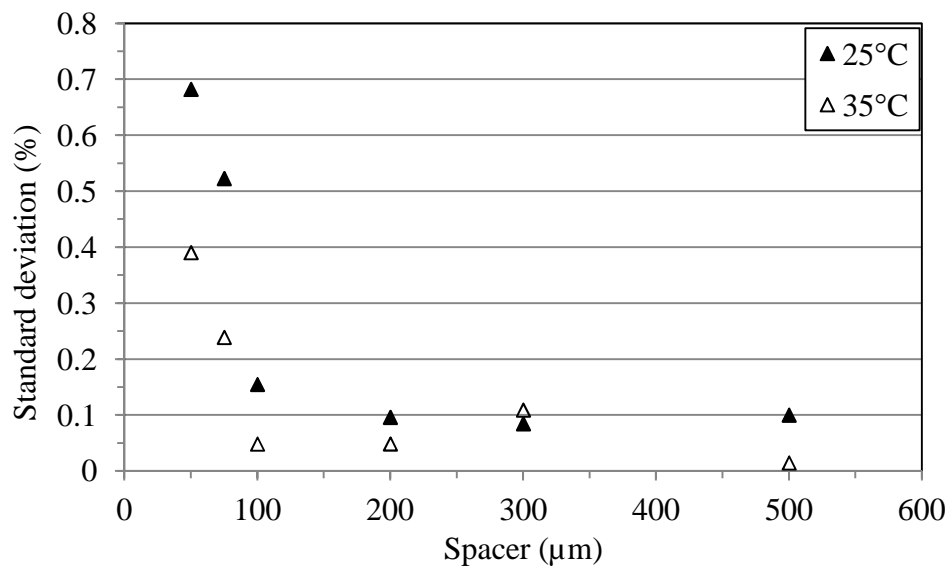
Fig. 2.15: Standard deviation as a function of spacer; reproducibility case

From this graph, we see that maximum standard deviation (σ) is about 0.7%, which is for 50-µm spacer. This shows that the device has an accuracy of less than 2.1% (3σ) in reproducibility. Again, the decreasing behavior of the graph shows that the results are

more reliable with thicker spacers. Furthermore, the deviation seems to decrease when temperature rises.

2.7. First measurements – Comparison with reference data

The first measurements are performed with AK 60000 SILICON OIL at 22°C, with the 500-µm, 300-µm and 200-µm spacers. The value of the density, given by supplier is set at 0.97 g.cm^{-3}. The results are presented in figure 2.16, where they are compared to the master curve obtained by Kirschenmann L. (2003).
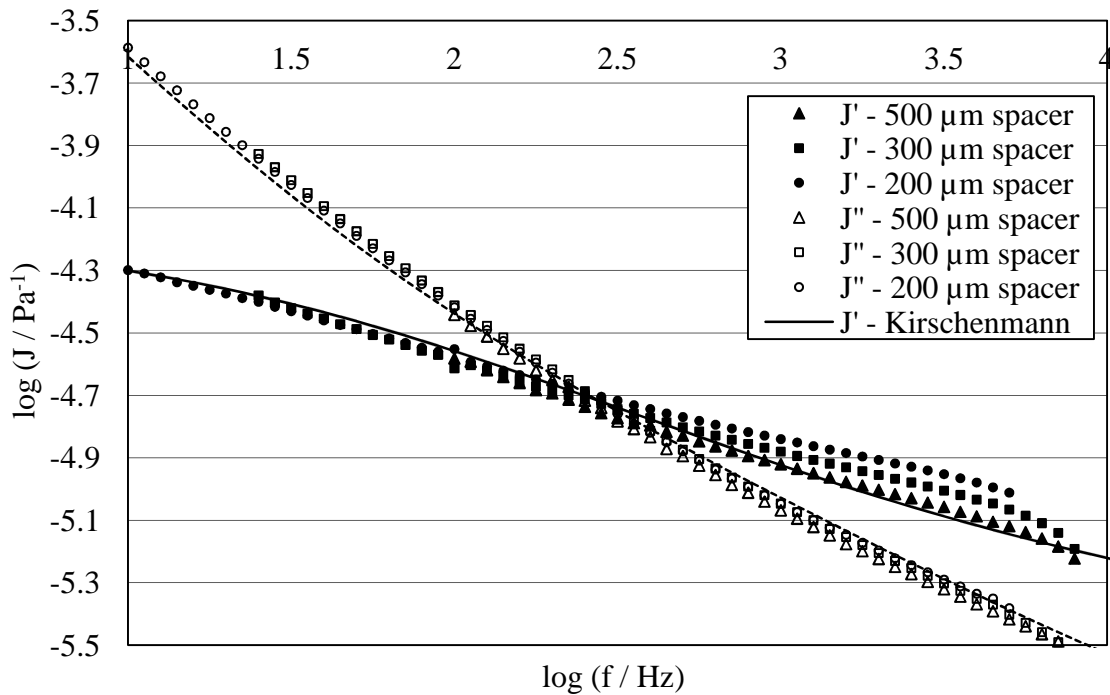
Figure 2.16 – Measurements on AK 60000 with three spacers and comparison with the data from Kirschenmann L. (2003).

Figure 2.16 shows that J' is lower than J'' at lower frequencies, which shows that the sample has more liquid type behaviour. But at high frequencies, J'' is lower than J', which shows that the sample has more solid like behaviour. We also note that the experimental data agree well with the master curve, but we also see small deviations at

higher frequencies and the data obtained with different spacers do not superimpose each other. These deviations may occur due to the sample compressibility effect. Now, let consider the effect of compressibility and the induced correction of the data.
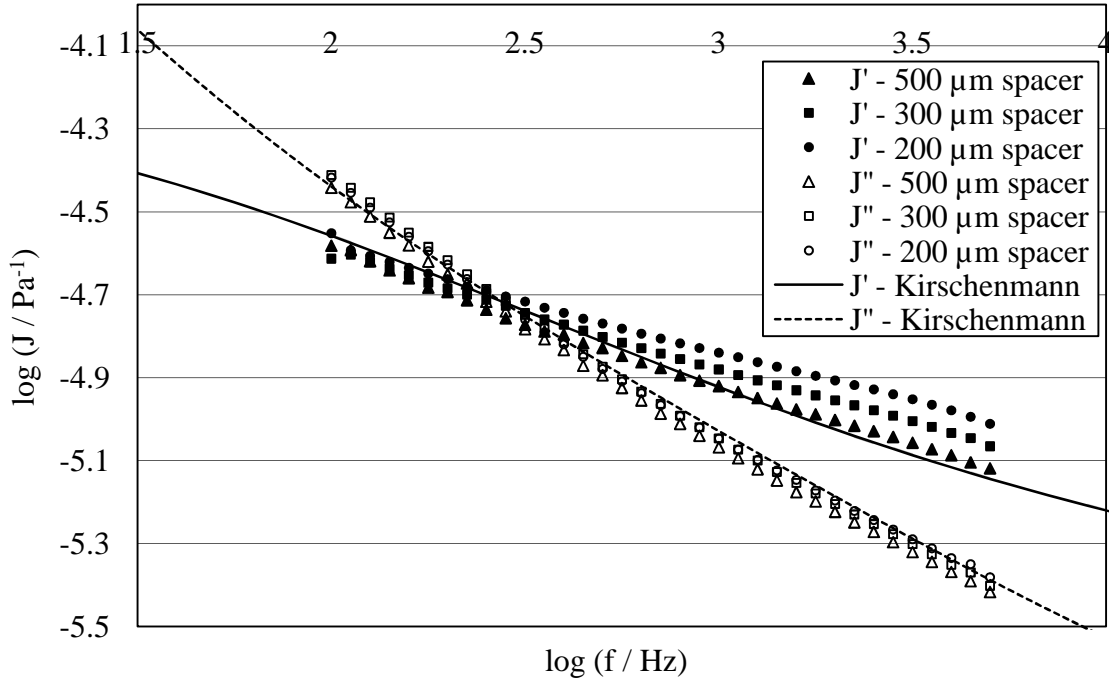
Figure 2.17 – Measurements on AK 60000 with three spacers (without compressibility) and comparison with the data from Kirschenmann L.

Recall to equation 2.17, which takes into account the sample compressibility.

$$J^* = J^*_{meas} - \frac{3}{2} \cdot \frac{R^2}{d^2} \cdot k^* \qquad (2.21)$$

With
$$k^* = k' - i\,k'' \qquad (2.22)$$

Where k' and k'' are the real and the imaginary part of complex compressibility. These parameters are fitted in such a way that the curves obtained with different spacers match together. The objective function for the minimization process is

$$F = \sum_{i=1}^{N} \sum_{j=1}^{M-1} \sum_{k=j+1}^{M} \left| \log(J_{i,j}) - \log(J_{i,k}) \right| \qquad (2.23)$$

Where $J_{i,j}$ is the shear compliance measured at the ith frequency with j^{th} spacer, N is the number of measurements per spacer, and M is the number of spacers. One must note that the different curves must have some common parts for the calculation of the function F, because the different compliances are compared at equal frequency. Once the values of compressibility are determined by minimizing the objective function, the different curves match together as shown in figure 2.18.
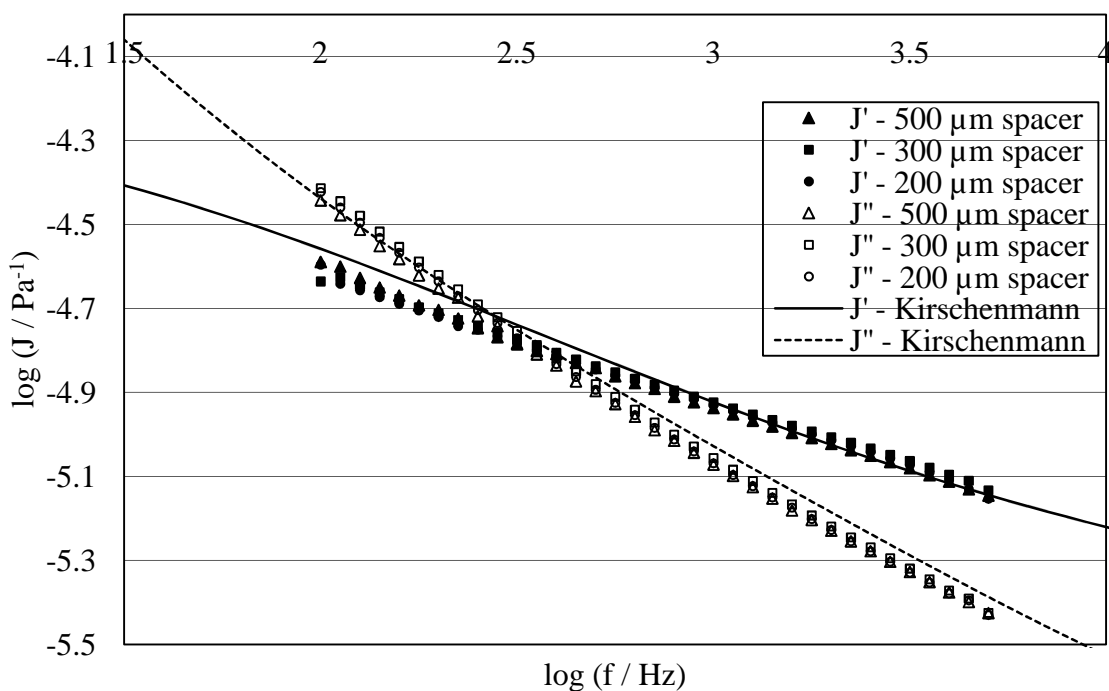
Figure 2.18 – Measurements on AK 60000 with three spacers (after compressibility correction) and comparison with the data from Kirschenmann L., with $k^* = (7.25 - 1.41i) \cdot 10^{-10}$ Pa^{-1}.

Here we see that after taking into account the sample compressibility, different curves are almost superimposed.

2.8. Effect of temperature on rheological properties

A series of measurements are taken at varying temperatures, with spacers of thicknesses 500-µm, 300-µm and 200-µm. The measurements are taken for silicon oil AK60000.

The effect of temperature on the rheological quantities such as complex shear modulus G and complex dynamic viscosity η is discussed in this section.

Consider the effect of temperature on G, for measurements taken with using 300-µm spacer (fig. 2.19). At high frequencies, the values of G' and G'' tend to superimpose each other at different temperatures respectively. For a given frequency, the values of G' and G'' are translated to lower values when temperature increases. We can also observe that intersection goes to high frequencies as temperature increases.
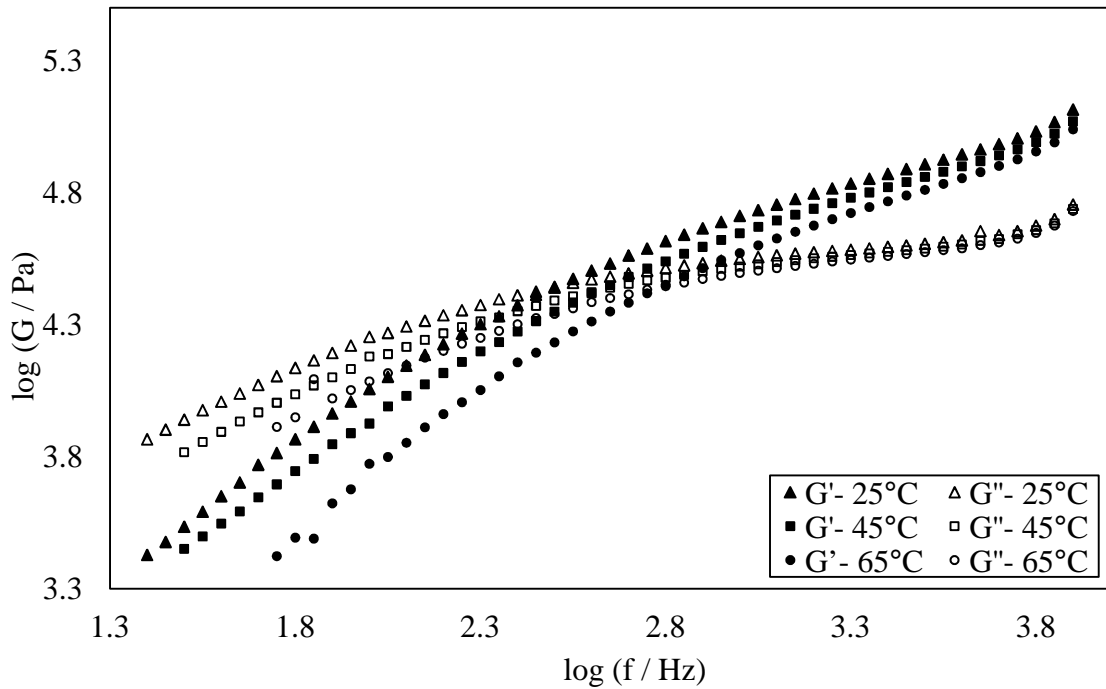
Fig. 2.19: Effect of temperature on complex shear modulus; 300-µm spacer

Similarly, the effect of temperature on η, for measurements taken with using 300-µm spacer (fig. 2.20), which shows that viscosity decreases as temperature increases. The measurements with other spacers show the similar effect of temperature on rheological properties, although the results are not shown.
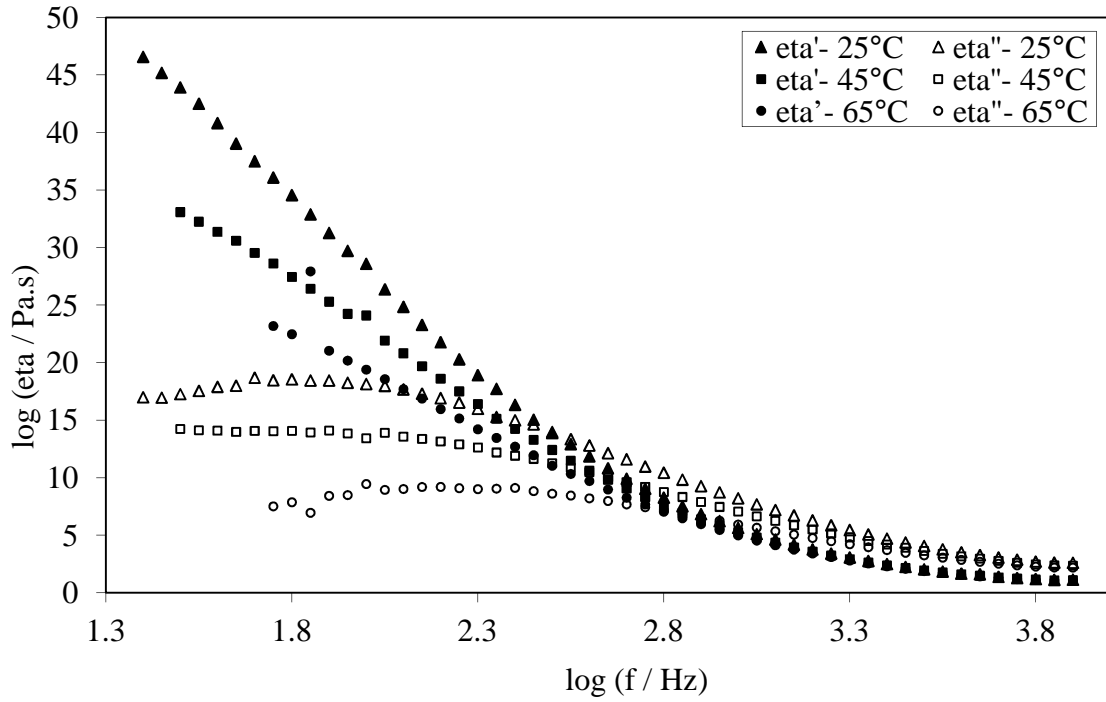
Fig. 2.20: Effect of temperature on complex dynamic viscosity; 300-μm spacer

2.9. Acoustic applications of PAV

The value of compressibility correction (section 2.7) may be used to determine the acoustic P-wave velocity using the following formula (Mavko G. et al., 1998).

$$V_p = \sqrt{\frac{K + \frac{4}{3}G}{\rho}} \qquad (2.24)$$

Where K is the bulk modulus (bulk modulus), G is the shear modulus (modulus of rigidity) and ρ is the density. The value of G is so small (in the order of 10^4 to 10^5) as compared to K (in the order of 10^{10}) that it does not affect the P-wave velocity, therefore it can be neglected. The bulk modulus K is the inverse of modulus of compressibility k, and can be calculated as

$$K = \frac{1}{k} = \frac{1}{\sqrt{k'^2 + k''^2}} \qquad (2.25)$$

95

The value of V_p calculated by using equation 2.24, equation 2.25 and the values of $k' = 7.25 \cdot 10^{-10}$ Pa^{-1} and $k'' = 1.41 \cdot 10^{-10}$ Pa^{-1} is found to be $1130\ m/s$. Using the same process, the values of V_p calculated for other temperatures are found out, and are given in the following table.

Temp (°C)	k' (Pa^{-1})	k'' (Pa^{-1})	V_p (m/s)
22	$0.725 \cdot 10^{-9}$	$0.141 \cdot 10^{-9}$	1130±170
25	$0.862 \cdot 10^{-9}$	$0.154 \cdot 10^{-9}$	1090±160
35	$0.922 \cdot 10^{-9}$	$0.130 \cdot 10^{-9}$	1050±160
45	$0.897 \cdot 10^{-9}$	$0.103 \cdot 10^{-9}$	1070±160
55	$1.097 \cdot 10^{-9}$	$0.134 \cdot 10^{-9}$	970±150

Table 2.4: PAV technique: P-wave velocity calculation at different temperatures; 15% uncertainty

In order to verify the validity of our measurement method, we have also measured the P-wave velocities using the ultrasonic technique (Annex A). In this technique, a single transducer functioning as emitter and sensor is used. Ultrasonic wave signal from the transducer is used to pass through the material. This signal is then received by the transducer. The time between the emission and reception of ultrasonic signal is measured. The P-wave velocity can be calculated using the formula (Khelladi H. et al., 2009).

$$V_p = \frac{2x}{\Delta t} \tag{2.26}$$

Where, x is the distance sample thickness, and $\Delta t = t_2 - t_1$ is the time between two consecutive signals on the transducer. The velocity values calculated using equation 2.26 at different temperatures are given in table 2.5.

T (°C)	t_1 (µs)	t_2 (µs)	x (cm)	V_p (m/s)
25	31.58	93.83	3.1312	1010±2.0
35	32.45	96.42	3.1291	980±2.0
45	33.34	99.08	3.1273	950±1.9
55	34.24	101.85	3.1237	920±1.8

Table 2.5: Ultrasonic technique: P-wave velocity calculation at different temperatures; 0.2% uncertainty

The values of V_p obtained by using the two techniques are shown together in figure 2.21. The values of P-wave velocities found by ultrasonic method are very precise, and the uncertainty in measurements is so small that the addition of error bars can be neglected.
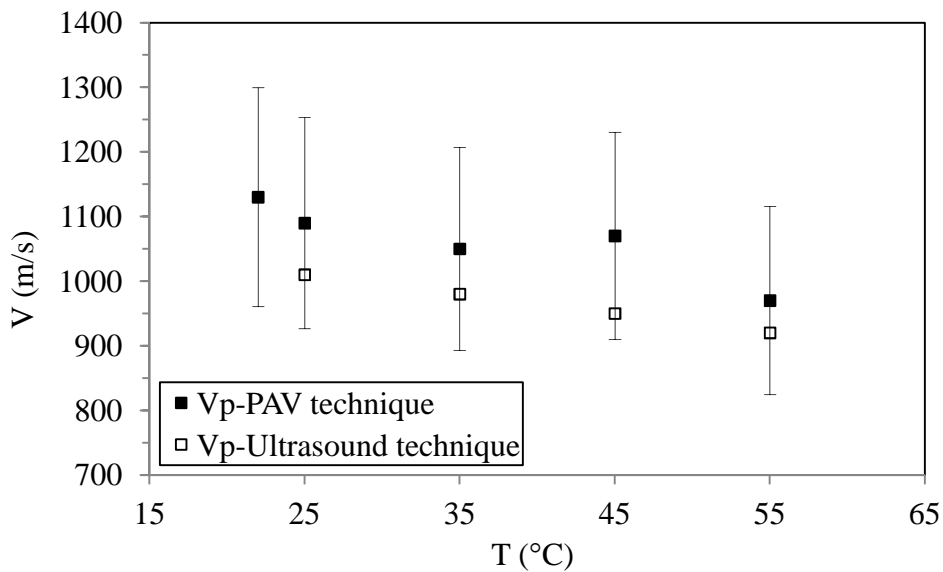
Figure 2.21 – Comparison of P-wave velocity measured by PAV technique and ultrasonic technique

It is important to note here that we do not know exactly the uncertainty in the P-wave velocity values measured by PAV. It is an indirect method that takes many steps to calculate the velocities. That is why we have taken here 15% uncertainty. Since all the

97

velocity values measured by direct method (ultrasound technique) fall within this uncertainty range, it shows that PAV device gives quite good results and is very promising. We have also applied the same PAV technique to find the compression wave velocities for other samples (Annex A), but these systems appeared to be inadequate for study in PAV.

2.10. Application of Viscoelastic models

Model fitting is an important part of any experimental measurement. As we have seen that AK 60000 Silicon oil is viscoelastic, therefore we need to fit a viscoelastic model against the experimental data. A short review about different kind of viscoelastic models is given in chapter 1. In this section, we will see the model fitting for measurements performed at 22°C and with 200-µm spacer. Figure 2.21 represents the graph of complex shear modulus G against angular frequency ω for 200-µm spacer, and the result of the application of single-element Maxwell model (equations 2.27, 2.28) to the experimental data.

$$G' = \sum G_i \frac{(\omega T_{ri})^2}{1+(\omega T_{ri})^2} \qquad (2.27)$$

$$G'' = \sum G_i \frac{\omega T_{ri}}{1+(\omega T_{ri})^2} \qquad (2.28)$$
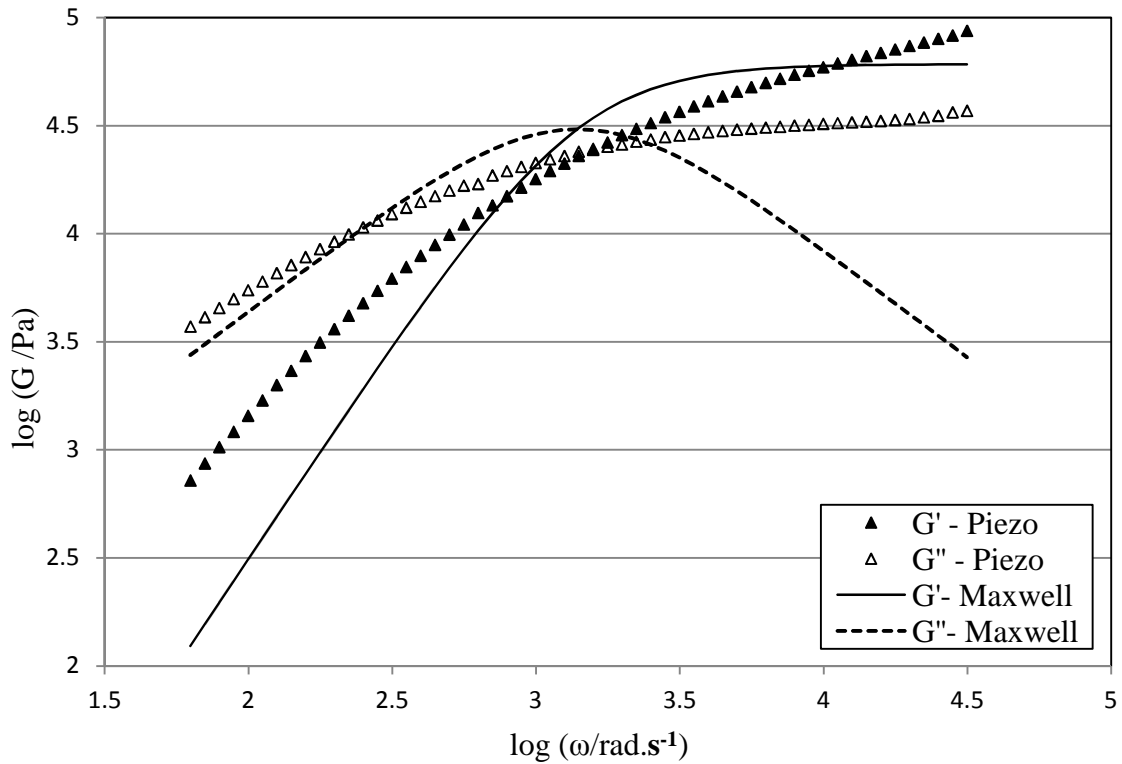
Figure 2.22 – Complex shear modulus over frequency ω. Application of the single -
element Maxwell model (AK60000 Silicon oil)

The constants of the Maxwell model found by the fitting process are found to be
$G = 6 \cdot 10^4 \ Pa$, and $T_r = 7 \cdot 10^{-4} \ s$. From the figure, it is clear that the single – element
Maxwell model does not fit at all the experimental data. The material may have more
than one relaxation times. We will now try to find the number of relaxation times of our
sample. For this purpose, if we apply double – element Maxwell model (equations 2.27,
2.28), and the results are shown in figure 2.23.
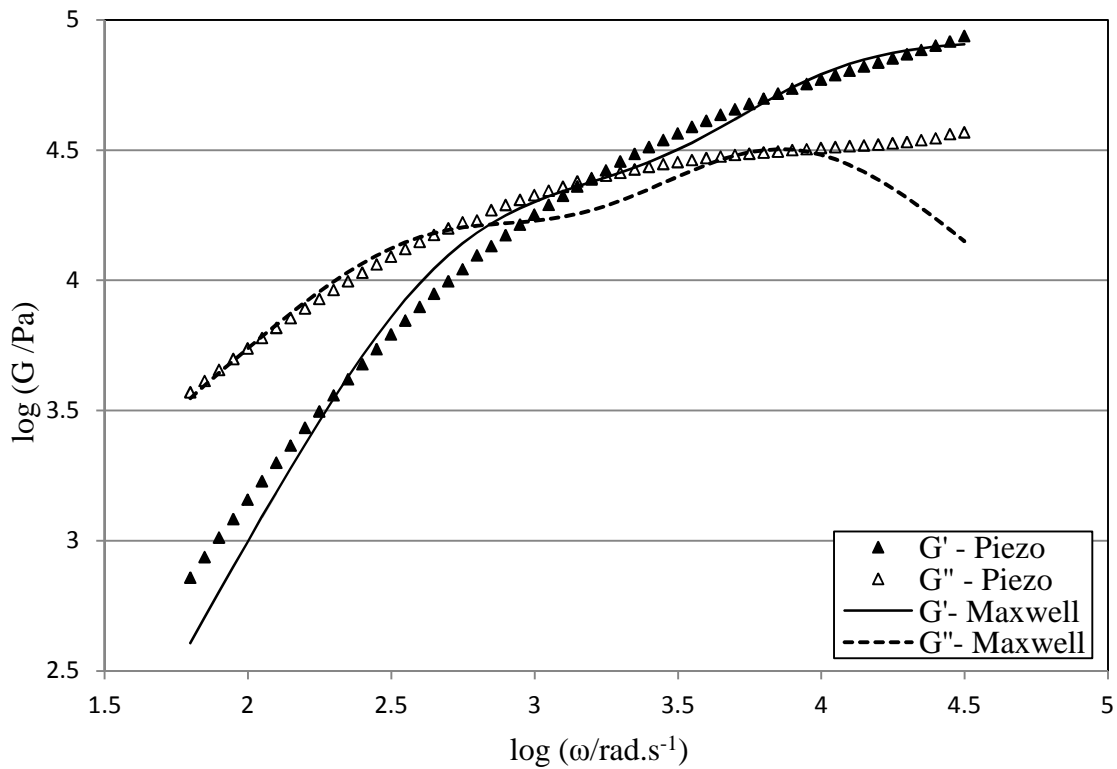
Figure 2.23 – Complex shear modulus over frequency ω. Application of the double - elements Maxwell model

The constants of the Maxwell model found by the fitting process are $G_1 = 6 \cdot 10^4$ Pa, $G_2 = 2 \cdot 10^4$ Pa, $T_{r1} = 1 \cdot 10^{-4}$ s and $T_{r2} = 2 \cdot 10^{-3}$ s. From the figure, it is clear that the double – element Maxwell model appears to be better than the single-element model but it does not fit well experimental data. It makes obvious that our sample has more than two relaxation times. By the continuous application of the Maxwell model, it reveals that it has at least five numbers of relaxation times. And the results of the application of five – element Maxwell model are shown in figure 2.24.
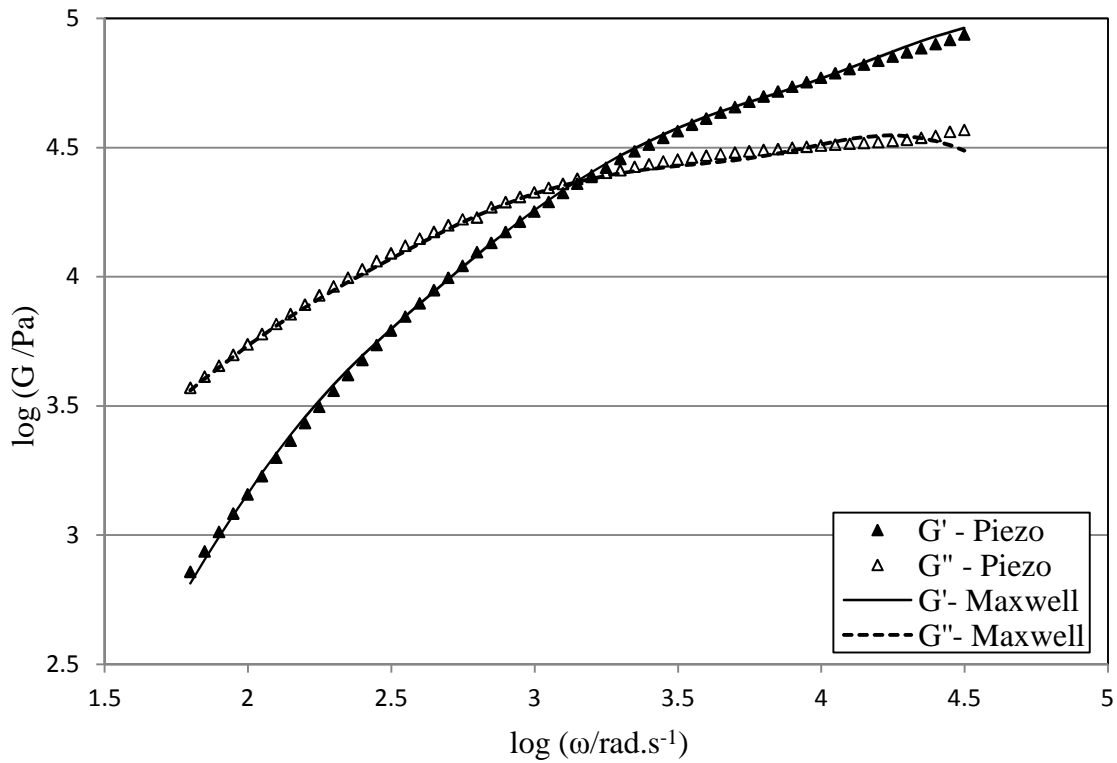
Figure 2.24 – Complex shear modulus over frequency ω. Application of the
five - elements Maxwell model

From figure 2.24, it is clear that the five - element Maxwell model fits very well the
experimental data. It is normal, as many materials are polydisperse, having molecules of
different sizes and mass. All the relaxation times are given in table 2.6, given below.

Index (n)	Maxwell model constants	
	Spring constant $G\ (Pa)$	Relaxation time $T_r\ (s)$
1	$6 \cdot 10^4$	$5 \cdot 10^{-5}$
2	$2 \cdot 10^4$	$4 \cdot 10^{-4}$
3	$1 \cdot 10^4$	$9 \cdot 10^{-4}$
4	$8 \cdot 10^3$	$1 \cdot 10^{-3}$
5	$5 \cdot 10^3$	$5 \cdot 10^{-3}$

Table 2.6: Relaxation time and spring constant for five – element Maxwell model

2.11. Chapter summary

In this chapter, we have seen that PAV atmospheric squeeze flow rheometer is very useful in the study of rheological properties of viscoelastic substances. Its capacity to work at a broad range of frequency (upto 8 KHz) makes it unique than the step motor rheometers. It can take measurements for volumes as small as 10-µL. Once the sample is in thermal and mechanical equilibrium, testing is very rapid as the results for 79 frequencies are obtained in about 10 minutes. It is equally useful for materials for which time-temperature superposition principle is difficult to apply. However, the study of rheological properties at reservoir conditions requires a high-pressure device. Chapter 3 is therefore about the study of the development of a high-pressure rheometer device.

CHAPTER 3

PAV: HIGH PRESSURE RHEOLOGY

In the previous chapter, we described a piezo axial vibrator device working at atmospheric pressure. Its advantages have been highlighted and it offers some possibilities that other kind of rheometers cannot. Furthermore, its design seems to be suitable for high-pressure adaptation. In this chapter, we present the development of a new rheometer device, based on the PAV device previously studied. This apparatus allows not only the study of the rheological measurements in the same frequency and temperature ranges as the atmospheric pressure one, but extends the acquisition of data up to 50 MPa (500 bars).

First, we will discuss the design of the new high pressure PAV, knowing that high-pressure constraint requires several modifications. Next, the working equations will be recalled and some corrections will be applied in order to take into account the physical changes of the cell. Finally, the calibration of the device will be explained, and some measurements on reference oils will be exposed.

3.1. Design of the High Pressure PAV

The atmospheric pressure PAV cannot be used, as it is if one wants to study pressurized samples. Actually, two inadequacies can be highlighted immediately.

First, in order to allow a good transmission of the vibrations to the sample, a thin metallic ring surrounds the central vibrating plate, screwed and glued to the piezo probe. Actually, the central plate and the surrounding ring are machined in a single metallic piece (figure 3.1).
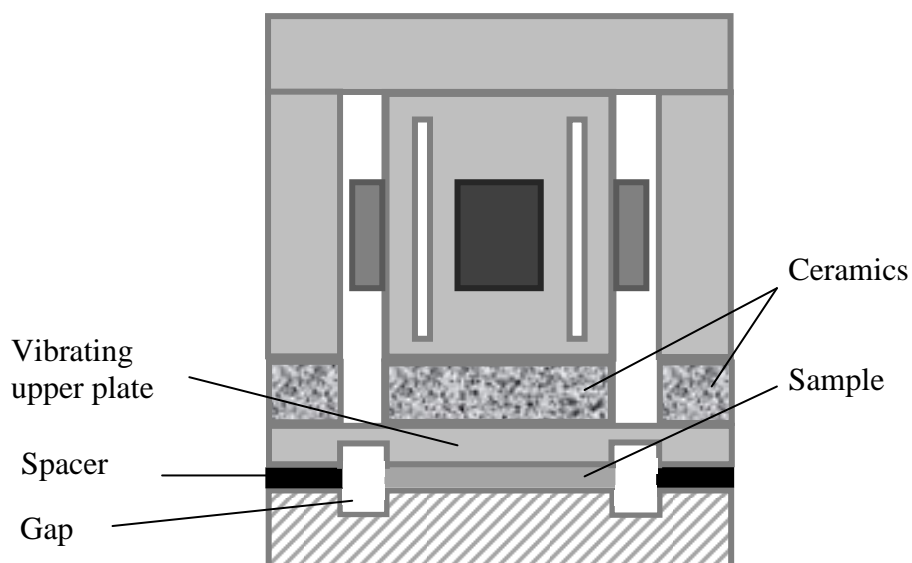
Fig. 3.1: Structure diagram of atmospheric pressure PAV device

The narrowing of the material is necessary to dissociate the central active part from the static border and make the plate vibrate correctly. In the case of high-pressure measurements, the sample will be injected under pressure in the cell, invading the whole space. Consequently, the thin metallic ring will bend due to the stress exerted by the sample and may be seriously damaged or even totally broken. Thus, in order to avoid the bending of this fragile metallic part, a counter pressure needs to be applied in the opposite side, i.e. in the surrounding of the piezo probe.

Now it appears the second inadequacy of the atmospheric pressure PAV. The ceramic used for thermal insulation cannot bear high pressure, as they will be irretrievably crashed. As the counter pressure is indispensable, the ceramics have to be discarded and we decided to make the entire high-pressure cell in a metallic material.

Of course, the heat transfer between the heating part or the sample and the piezo probe is now extremely strong especially if the sample is studied at high temperature and if the

piezo part is cooled as mentioned in the previous chapter. In this case, the thermal gradient will be very high and this phenomenon should be avoided in vibrating systems such as PAV because the physical properties of the device could not be known. Therefore, we will have to work in isothermal conditions, with the same temperature in the sample part as in the piezo part.

However, one may remember that in the previous chapter, the eight piezos were stuck on a copper tube with glue, the glass transition of which is quite low (140°C). Thus, as the high pressure PAV needs to run in isothermal conditions, some problems may occur at high temperatures: the glue being altered, the piezos can more or less come off and the PAV device can become useless.

For all these reasons, an adaptation of the atmospheric pressure PAV is required for high-pressure measurements. We had to rethink the design of the whole device, starting from the piezo probe by itself.

In order to avoid gluing piezos on the square-shaped copper tube, we replaced the whole copper tube by two cylindrical hollow tubes directly made in piezo material (figure 3.2).

Sensor piezo tube

Actuator piezo tube
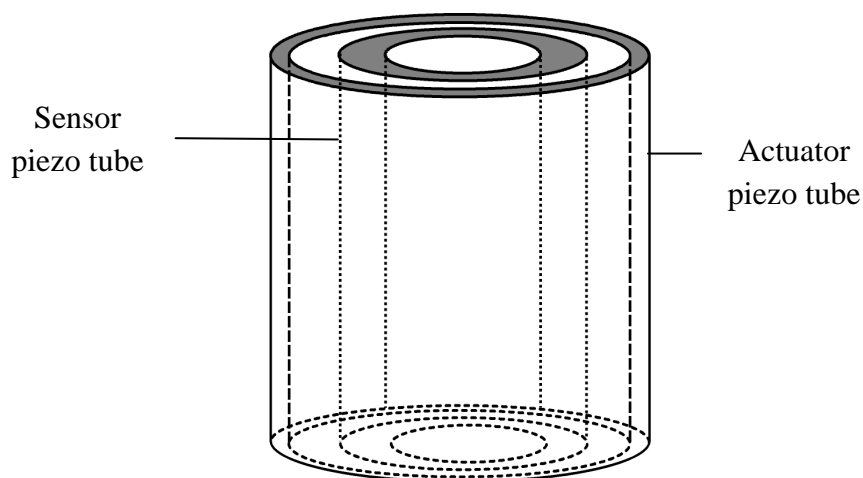
Fig. 3.2: Structure of piezos inside HP-PAV

Both piezos are concentric and have been cut to vibrate in a longitudinal way. The outer one is the actuator and the inner one is the sensor. These tubes are inserted in a metallic bloc, screwed and glued to the top and bottom surfaces (figure 3.3). This assemblage contributes the piezo probe.
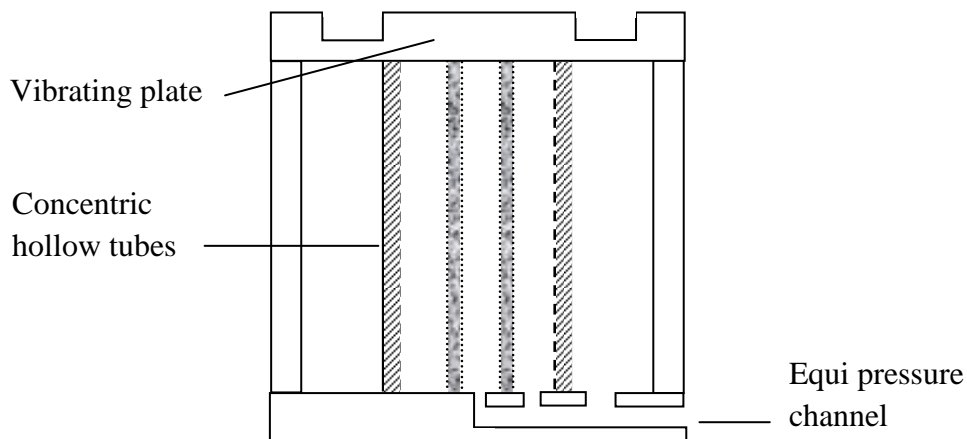
Fig. 3.3: Piezo probe inside HP-PAV

Note that the piezo tubes are slightly constrained (under stress) during assembling in order to ensure better contact with the top and bottom parts. A tiny channel drilled in the bottom metallic bloc ensures equal pressure in all parts of the piezo probe and outside the probe. This piezo probe is then inserted in a high-pressure cell (figure 3.4).

Before closing the cell, the thickness of the gap where the sample will be injected is set, thanks to thin metallic spacers from 15µm to 300µm. The cell is surrounded by a water jacket, which allows thermal regulation through a refrigerating/heating circulator. A temperature probe inserted in the top metallic part as near as possible to the sample measures the temperature of the system.
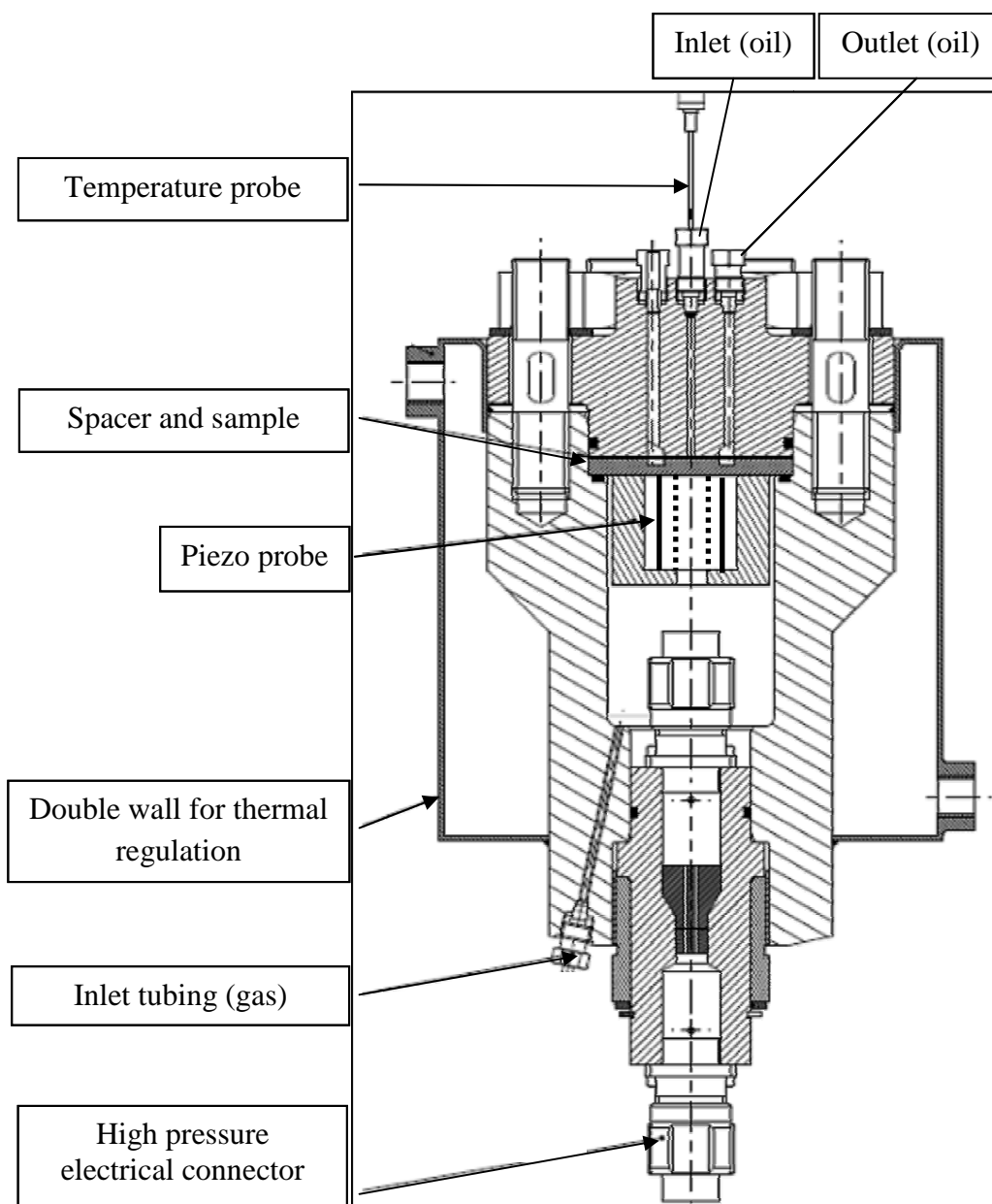
Fig. 3.4: High-Pressure PAV cell

Once the cell is closed, the sample under high pressure can be injected through the central inlet of the top metallic bloc. At each time, the pressure in the upper part must be compensated by an equal counter pressure in the lower part. Now let see how this counter pressure is managed in the schematic diagram of the whole HP-PAV device (figure 3.5).
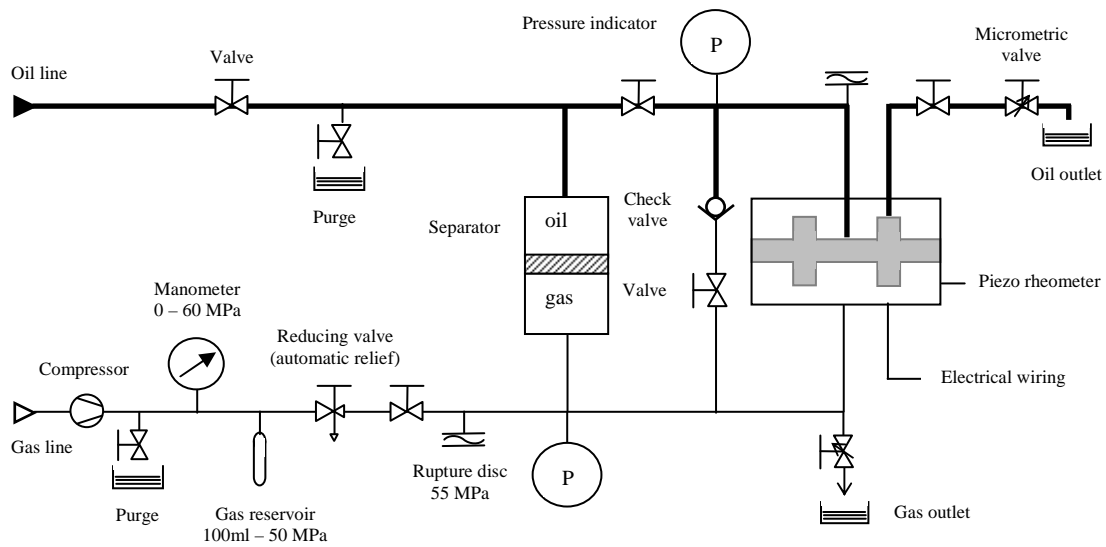
Fig. 3.5: Schematic diagram of HP-PAV device

Figure 3.5 shows that the HP-PAV device can be roughly divided into two parts: the sample line, including all the tubings necessary for sample injection in the HP-PAV and the gas line leading gaseous nitrogen in the bottom part of the PAV cell for counter pressure. The necessary equi-pressure required to save the cell from damaging is handled by two connections existing between both the sample and the gas lines.

The first connection is the check valve, which is used before injection of pressurized samples. Let us consider a sample, i.e. a crude oil, at a pressure P greater than the atmospheric pressure. Before injection, the sample line must be pressurized at a pressure P to avoid a pressure drop of the sample, which could lead to irreversible phase transition. For this purpose, nitrogen is pressurized by the compressor. It is then injected in the gas line at the same time as it is injected in the sample line via the check valve, ensuring an equal pressure in both the lines and thus in the top and bottom parts of the PAV cell.

The second and more important connection between both lines for controlling the equi-pressure is the separator. It consists of a metallic hollow cylinder containing a mobile piston inside. Before injection of the sample and during pressurization of the sample line with nitrogen, the piston is kept in the upper position. After the sample injection, the piston is pulled back to lower position and the top chamber of the separator is filled with sample. Now, if one wants to adjust the pressure of the sample, it is possible to increase or decrease the gas pressure in the gas line. The pressure variations are then transmitted to the sample line through the separator. Note that both the pressures, respectively in the gas and sample lines are not exactly the same due to friction of the piston against the metallic cylinder. But the separator, if used correctly, avoids high pressure differences between the upper and lower parts of the PAV device. Of course, except before the sample injection the piston should not be at the extreme top or bottom positions during the experiments, as it could not balance pressure variations if they occur in the wrong side.

In a future version of the HP-PAV device, this separator should be replaced by a motorized one, controlled by the pressure sensors already in place. This operation will allow to get a real equi-pressure in the whole device and increase its security. Finally, note that a gas reservoir is placed in the gas line in order to smooth the rude increments in pressure due to the compressor.

The measurements are made via a LockIn amplifier, which supplies the excitation voltage to the excitation piezos, and measures the detection voltage of the detection piezos (figure 3.6). The LockIn amplifier is connected to a computer, which takes up the measured values. Water bath K6-CC-NR is used as temperature measuring and controlling device. In addition, there is a pressure indicator device, which indicates the

pressure of oil, pressure of gas, and the pressure difference between the upper and lower part of PAV.
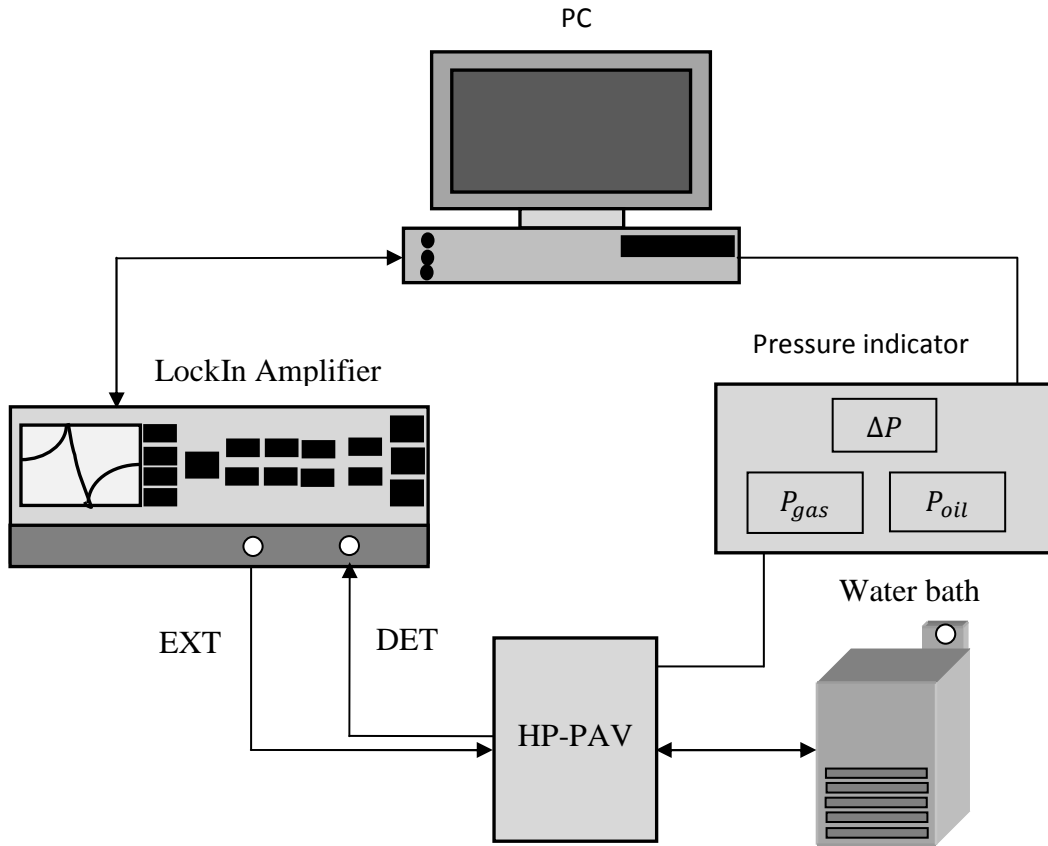
Fig. 3.6: Structure of the measuring position of HP-PAV device

3.2. Working equations for High Pressure PAV

As the atmospheric pressure PAV and the HP-PAV cell are quite similar, we used the same mechanical equivalent model as the one presented in chapter 2. Here we recall the final equations used for the calculation of complex shear compliance in the previous chapter.

$$\left(\frac{K_0}{K^*}\right)' = \frac{U}{U_0} \cdot \frac{1}{1-\frac{f^2}{f_0^2}} \cdot \frac{\frac{1}{1+B\left(1-\frac{f^2}{f_0^2}\right)}\left(cos\Delta\varphi - \frac{U}{U_0}\right) + \frac{sin\Delta\varphi}{Q_0\left(1-\frac{f^2}{f_0^2}\right)}}{1-2\frac{U}{U_0}cos\Delta\varphi + \left(\frac{U}{U_0}\right)^2} - \frac{B}{1+B\left(1-\frac{f^2}{f_0^2}\right)} - \frac{K_0}{K_1} \cdot \frac{1}{\left(1-\frac{f^2}{f_1^2}\right)} \quad (3.1)$$

$$\left(\frac{K_0}{K^*}\right)'' = \frac{U}{U_0} \cdot \frac{1}{1-\frac{f^2}{f_0^2}} \cdot \frac{\frac{sin\Delta\varphi}{1+B\left(1-\frac{f^2}{f_0^2}\right)} - \frac{1}{Q_0\left(1-\frac{f^2}{f_0^2}\right)}\left(cos\Delta\varphi - \frac{U}{U_0}\right)}{1-2\frac{U}{U_0}cos\Delta\varphi + \left(\frac{U}{U_0}\right)^2} \qquad (3.2)$$

Of course, the constants that appear in these equations will be different from the ones previously found. Some of them can be calculated directly but the others need a complete calibration process in order to be estimated. However, as the mechanical model is not strictly the same because of differences in the configuration of sample area, some terms need to be corrected.

The first correction term, as for the atmospheric pressure PAV, is the residual gap ε, which remains once the cell is closed without spacer (figure 3.7). Therefore, for each spacer of thickness d_{spacer}, the sample thickness is

$$d = d_{spacer} + \varepsilon \qquad (3.3)$$

Where ε is found by calibration.
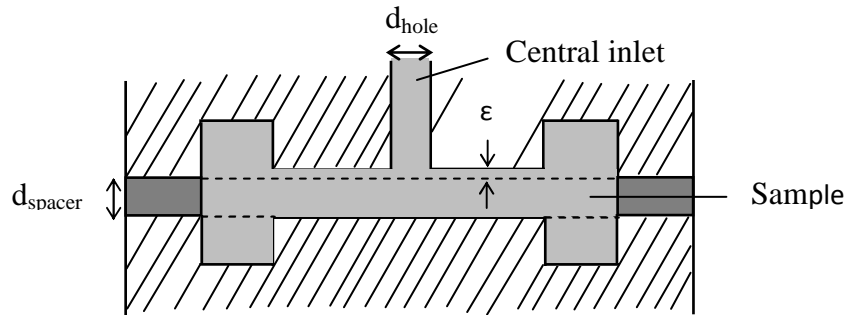
Fig. 3.7: Zoom in of the sample area; sample appears in light gray shaded area

The second correction term is related to the presence of the inlet tubing in the centre of vibrating area (figure 3.7). Actually, when the bottom plate vibrates, the squeeze flow is not only radial but also longitudinal through the inlet tubing for the inner part of the

sample. Consequently, the presence of the inlet tubing alters the mechanical behavior of the sample. In the equation:

$$\frac{1}{K^*} = \frac{2d^3}{3\pi R^4}\left[J^*\left(1 + \frac{\rho\omega^2 d^2 J^*}{10} + \cdots\right) + \frac{3R^2}{2d^2}\kappa^*\right] \tag{3.4}$$

The spring constant K^* of the sample artificially becomes smaller (or the complex compliance J^* higher). It means that for the PAV probe the sample appears thicker than it is really. Thus, in order to correct this effect, we consider that the sample has an effective thickness of

$$d_{eff} = \frac{d_{spacer} + \varepsilon}{\alpha} \qquad \text{with } \alpha \in\ ]0; 1[\tag{3.5}$$

This coefficient α will be determined from calibration in the same time as ε in a further section.

The third correction to be brought is linked to the presence of sample in the surrounding ditch. As mentioned in the first section of this chapter, the sample invades the whole available space because of pressure, contrarily to the atmospheric pressure PAV where the circular shaped sample was surrounded by air. Obviously, this extra-connected fluid will also influence the measured data.

Actually, the spring constant of the gap K^*_{gap} is parallel shunted by compression of the surrounding due to the gap volume change when the plates are vibrating. So, the PAV probe measures:

$$K^* = K^*_{gap} + K^*_{surrounding} \tag{3.6}$$

The latter can be calculated as follows:

$$K^*_{surrounding} = \frac{A^2}{K_L V_0} \qquad (3.7)$$

Where

$A = \pi R^2$ is the surface of the vibrating plate. With R=8.75 mm, it gives out 2405 cm^2.

$K_L \simeq 0.5.10^{-9}$ Pa^{-1} is the compressibility of the sample.

$V_0 = 2.2$ cm^3 is the surrounding volume.

Thus $K^*_{surrounding} \simeq 5.27.10^7$ N/m. This quantity must be subtracted from the measured K^* to get K^*_{gap}.

3.3. Calibration of HP-PAV probe

As seen in the previous section, the equations leading to viscoelastic properties show many parameters, which are characteristics of the device. Some of them can be easily calculated or obtained with sample experiments, e.g. coefficient A, the resonance frequency f_0 and the bandwidth D_0. Others are independent and tuning one of these parameters affects the final value of the other parameters (e.g. α, ε).

3.3.1 Determination of f_0 and D_0

The resonance frequency f_0 and -3dB bandwidth D_0 of the HP-PAV probe are obtained thanks to a simple frequency scanning. For this purpose, the probe is got out of the high pressure cell, the actuators are excited by sinusoidal voltage $v_a(t)=V_a\sin(\omega t)$ with variable frequency and the voltage $v_s=V_s\sin(\omega t+\varphi)$ of the sensor is recorded. The figure 3.8 shows the variations of the ratio v_s/v_a and the phase φ as a function of frequency.
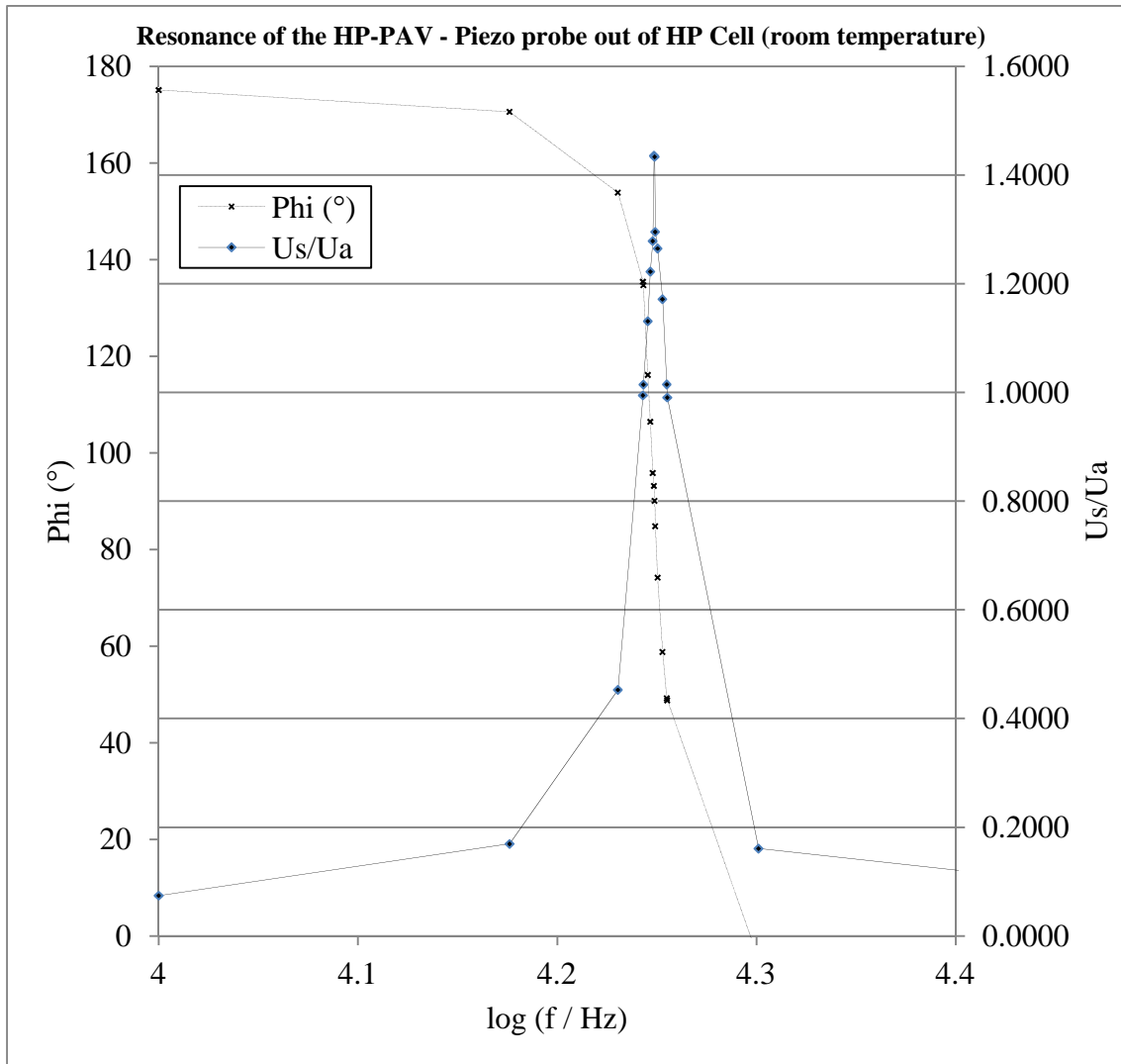
Fig. 3.8: Ratio v_s/v_a and the phase φ as a function of frequency

From figure 3.8, we get

$$
\begin{cases}
f_0 = 17725 \text{ Hz} & (3.8) \\
\\
D_0 = 480 \text{ Hz} & (3.9)
\end{cases}
$$

3.3.2 Determination of A

This parameter corresponds to the lower limit of the U/U_0 detectable by the HP-PAV probe. In order to access this value, one have to make a loaded measurement U with a

given sample and an empty measurement U_0, using a spacer thin enough for the chosen sample.

Here we used the HP-PAV device without any spacer. Gap thickness is then ε, and we measured the ratio U/U_0 as a function of frequency for many reference oils of various viscosities (Table 3.1).

Name	Viscosity (mPa.s, cP)	Density (g/mL)	Trademark
2B	2.119	0.7736	PTB
S6	7.679	0.8569	Cannon
S20	28.25	0.8467	Cole-Parmer
S20	28.95	0.8557	Cannon
N35	55.64	0.8569	Cannon
S200	398.5	0.868	Cole-Parmer
N350	760.7	0.8846	Cannon
S600	1368	0.8888	Cannon
N1000	1991	0.8461	Cannon
S2000	5018	0.8744	Cannon
N4000	10209	0.8844	Cole-Parmer
S30000	72680	0.8954	Cole-Parmer

Table 3.1: Reference oils used in this work; data given at 25°C

The U/U_0 range for different spacers is shown in figure 3.9. This figure clearly indicates that for high viscosity oils, the U/U_0 curve tends to a lower limit of 0.15 for higher frequencies. Thus, the parameter A equals 0.15.
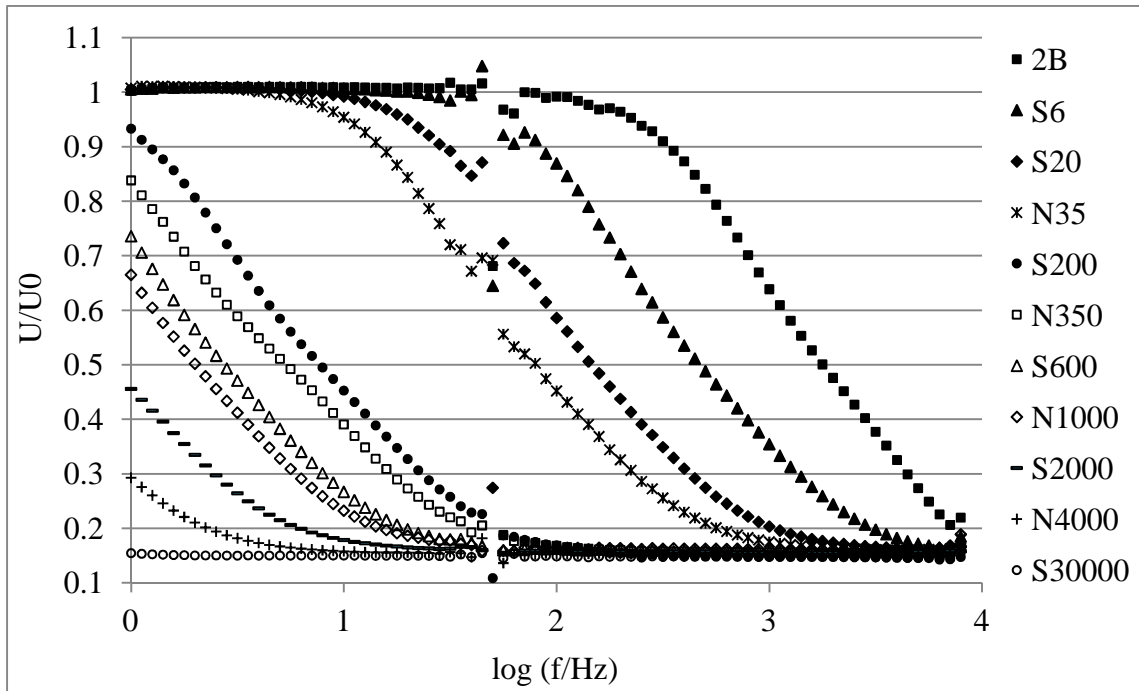
Fig. 3.9: U/U_0 verses log (f) for a number of reference oils

Figure 3.9 also gives important information about the validity range of $\frac{U}{U_0}$, which lies

within the interval $[0.30\text{-}0.90]$ if we take only the linear behavior of all the curves. Note

that we see some fluctuation of data at about 50 Hz. It may be due to the electric

network in France.

3.3.3 Determination of α and ε

Remind that these parameters correct the spacer thickness to take into account the

residual gap of the cell and the effect of the central hole of the inlet tubing. The

effective thickness perceived by the probe is given in equation 3.5.

In order to access these two parameters, we made measurements with all reference oils

(table 3.2) for various spacers, and we adjusted d_{eff} in such a way that the Newtonian

plateau matches with the expected results given by the supplier (figure 3.10). Table 3.2 gives the obtained values of d_{eff} for each oil and corresponding spacers.
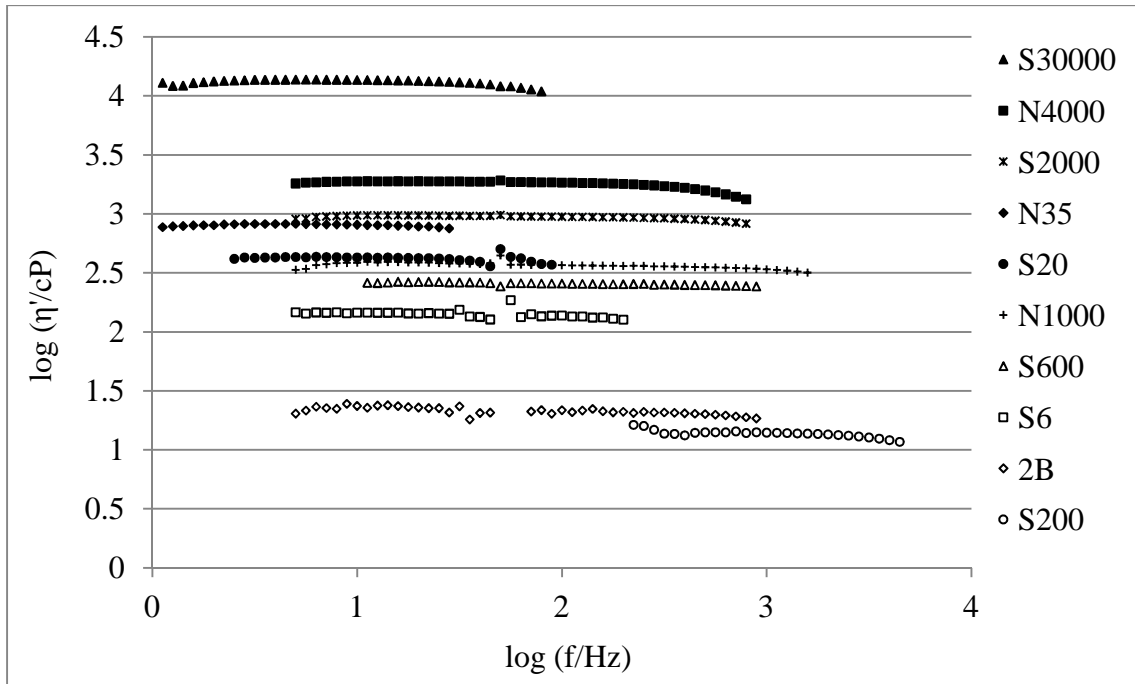
Fig. 3.10: Viscosity as a function of frequency for reference oils

Spacer (µm) / Oil	0	100	200	500
2B	11.7	-	-	-
S6	11.3	-	-	-
S20	12.2	-	-	-
N35	12.3	-	-	-
S200	-	123	-	-
N350	-	123	-	-
S600	-	122	230	528
N1000	-	122	227	530
S2000	-	121	224	529
N4000	-	123	224	534
S30000	-	121	224	530

Table 3.2: Values of d_{eff} (µm) for each oil and spacer

Figure 3.11 plots the values of d_{eff} as a function of d_{spacer} and clearly shows a linear trend of the curve.
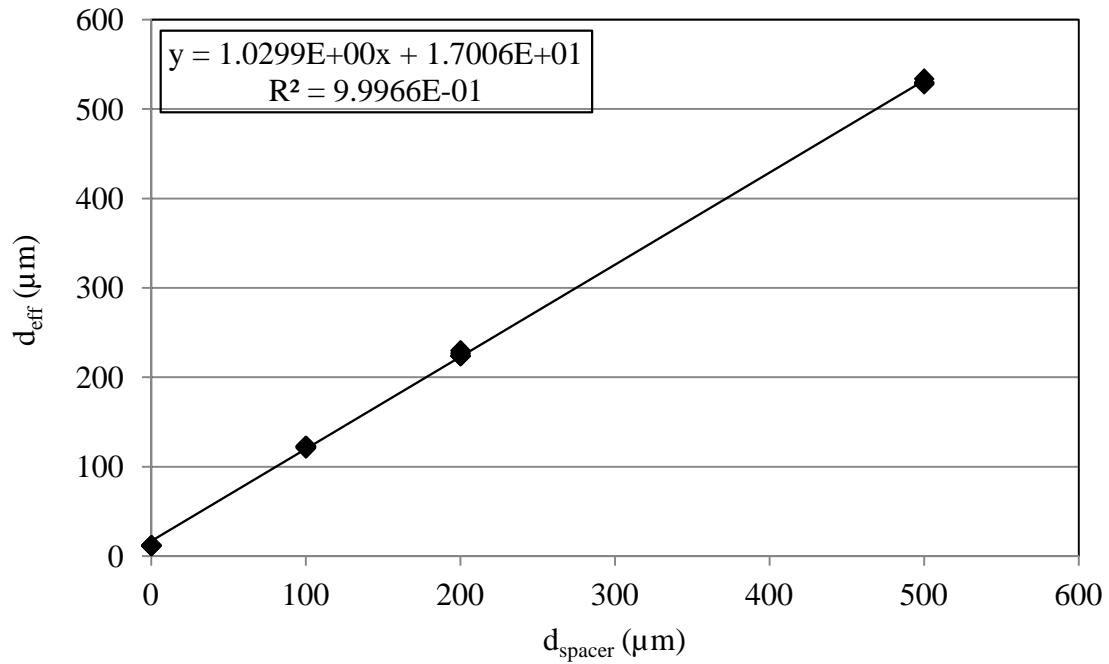
Fig. 3.11: Plot of effective thickness as a function of spacer thickness

The linear approximation of these data leads to the following equation:

$$d_{eff} \; (\mu m) = \frac{d_{spacer}(\mu m) + 16.512}{0.9710} \tag{3.9}$$

It shows that residual gap is around about 17µm and that the effect of the central hole induces a virtual increase of the thickness of around 3%.

Though this linear approximation gives rather good estimations of viscosities for 100 to 500 µm-spacers (less than 10% error), the results are bad for measurements without spacer and shows error between 58% and 100%. Actually, a bad estimation of the effective gap size, even with a low error strongly alters the final result due to its dependence on $(1/d^3)$.

In order to increase the accuracy of the calculations, we proceeded to a polynomial approximation of degree 2. In the following sections, the effective gap size will be

calculated as follows

$$d_{eff} = -1.2053.\,10^{-4}d_{spacer}^2 + 1.0951\,d_{spacer} + 12.684 \qquad (3.10)$$

Here d_{eff} and d_{spacer} are given micrometers. Table 3.3 displays the errors obtained by using this polynomial correlation. The results have been largely improved. For 100 to 500 µm-spacers, the error falls down to less than 5%. Without spacer, the results are still approximated but the error is now less than 41%.

Oil	Viscosity by Supplier at 25°C	Experimental deviations			
		0µm	100µm	200µm	500µm
2B	2.119	+26%	-	-	-
S6	7.679	+41%	-	-	-
S20	28.25	+13%	-	-	-
N35	55.64	+10%	-	-	-
S200	398.5	-	-4.6%	-	-
N350	760.7	-	-4.3%	-	-
S600	1368	-	-2.9%	-3.5%	+1.0%
N1000	1991	-	-3.4%	-0.3%	-0.1%
S2000	5018	-	-0.7%	+3.9%	+0.5%
N4000	10209	-	-3.8%	+3.7%	-2.4%
S30000	72680	-	-0.7%	+4.2%	+0.3%

Table 3.3: Deviations between viscosities calculated with polynomial approximation and reference data

Now we have a good approximation of d_{eff} and good viscosity values for Newtonian reference oils, let see the results for the AK60000 silicon oil which presents viscoelastic behaviour.

In order to avoid the connected volume effect, not studied yet, we made measurements at atmospheric pressure in the same configuration as for the atmospheric pressure PAV,

i.e. by injecting a drop of AK60000 and letting the surrounding space empty. Figure 3.12 shows the J' and J" curves as a function of frequency.
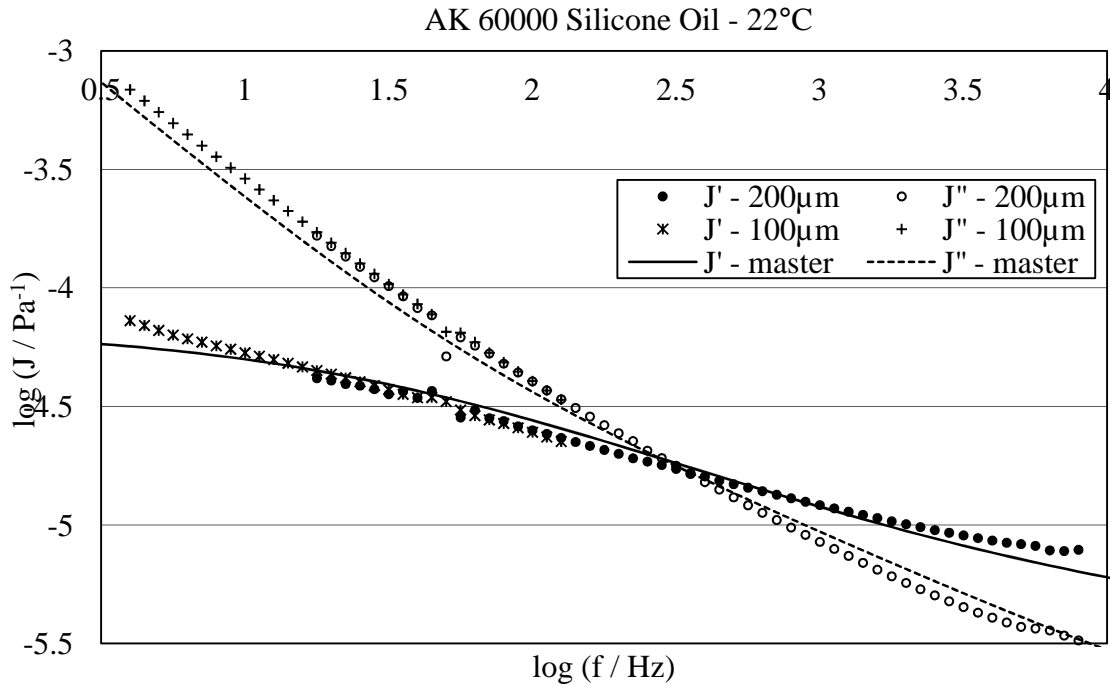
Fig. 3.12: HP-PAV; Complex shear compliance as a function of frequency

The curves correspond quite well. However, we can remark that the frequency of the intersection between both curves is slightly overestimated. The master curves interest at f=280 Hz, while the experimental curves intersect at 355 Hz. However, this overestimation remains rather low as regard of the experimental errors.

3.4. Repeatability and reproducibility

The repeatability and reproducibility for HP-PAV is found in the same way as for the repeatability and reproducibility for atmospheric pressure device. For repeatability, measurements of AK60000 oil are taken at 25°C with different spacers. Table 3.4 gives the standard deviation for each spacer.

Spacer (µm)	No. of deviation data	Standard deviation (%)
500	159	0.192
400	182	0.133
300	219	0.168
200	258	0.337
100	147	0.731

Table 3.4: Standard deviation as a function of spacer; repeatability case for HP-PAV

The following figure gives the standard deviation as a function of spacer.
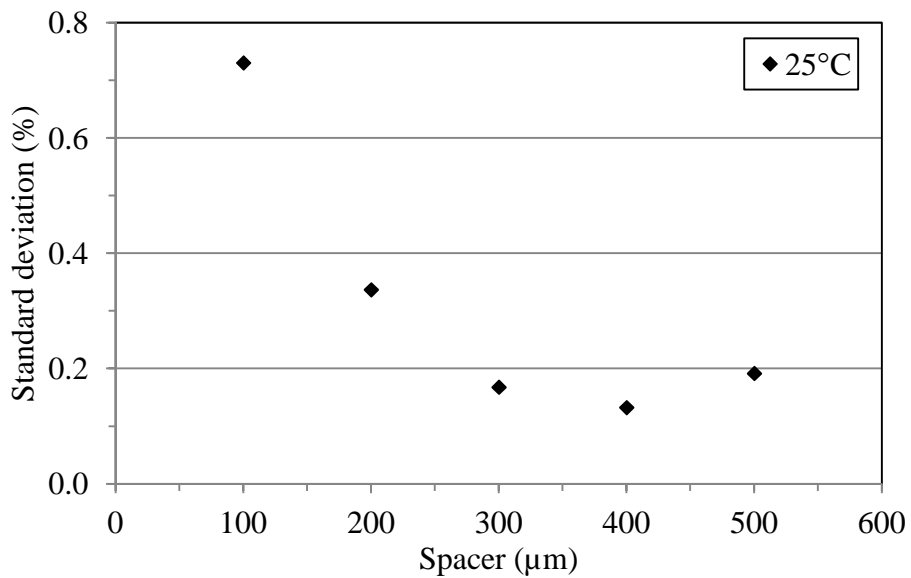
Fig. 3.13: Standard deviation as a function of spacer; repeatability case for HP-PAV

From table 3.4, we see that the maximum standard deviation (σ) is 0.73%, which is for

100-µm spacer. This shows that the device has an accuracy of less than 2.2% (3σ) in

reproducibility. The decreasing behavior of the graph (figure 3.10) shows that the results are more reliable with thicker spacers for a given sample.

In case of reproducibility, the measurements are taken with AK60000 oil at 22°C for different spacers and a number of references oils at 25°C without spacer. Table 3.5 represents the standard deviation for AK60000 oil and reference oils.

Spacer (µm)	No. of deviation data	Standard deviation (%)
500	120	0.227
400	123	0.116
300	131	0.567
200	160	0.647
100	74	1.32

Table 3.5: Standard deviation AK60000; reproducibility case for HP-PAV.

From table 3.5, we see that the maximum standard deviation (σ) is 1.32%, which is for 100-µm spacer. This shows that the device has an accuracy of less than 4.0% (3σ) in reproducibility.

The measure of standard deviation using different reference oils having viscosities lower than that of AK60000 is given in table 3.6. It shows that the value of maximum standard deviation is 4.95%, which is for the reference oil N35. This shows that the accuracy of the device in reproducibility is less than 15.0% (3σ).

Spacer	Reference oil	Viscosity (cP)	No. of deviation data	Standard deviation (%)
	S20	28.25	66	3.15
	N35	55.64	72	4.95
	S6	7.679	66	2.44
0 µm	S200	398.5	62	2.12
	N350	760.7	50	3.03
	S20	28.95	69	4.39
	S600	1368	33	1.66
	N1000	1991	22	4.00

Table 3.6: Standard deviation reference oils; reproducibility case for HP-PAV.

The standard deviations given by table 3.5 and table 3.6 can be represented by the following figure.
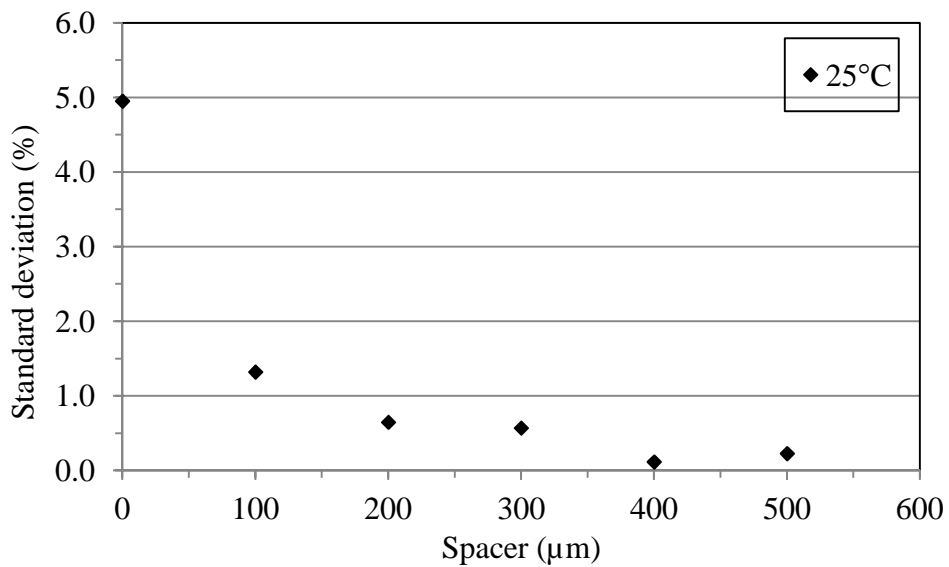
Fig. 3.14: Standard deviation as a function of spacer; reproducibility case for HP-PAV

Figure 3.14 shows that the standard deviation increases as the spacer thickness decreases. It is the same result as was seen with the atmospheric pressure PAV. Therefore, it can be concluded that the device is more reliable for thicker spacers as compared to thinner spacers.

3.5. Chapter summary

In this chapter, we have adapted the atmospheric pressure PAV rheometer in the development of a new high-pressure PAV rheometer. This high-pressure rheometer works in the same frequency and temperature ranges. It allows rheological measurements up to 500 bars (50 MPa). Its calibration is accomplished in order to find the important parameters. The repeatability and reproducibility measurements show that the device is very reliable.

Annex A

P-wave velocity in viscous suspension

In this part, we have calculated the P-wave velocity for viscous suspension. The objective of this part is to understand the variation of velocity as a function of quantity of particles in suspension. For this purpose, we have prepared a sample which composes of a mixture of vegetable oils (50% volume sunflower oil, 50% volume hydrogenated coconut oil) with {0; 2; 3; 4; 5; 7} weight percentage of clay.

The velocity is determined by acoustic and PAV technique. In the acoustic technique, we have used the well known pulse transmission method. This method consists of a pulse generator/receiver SOFRANEL MODEL 500PR, two acoustic transducers and a personal computer. The measuring setup is shown in figure 1.
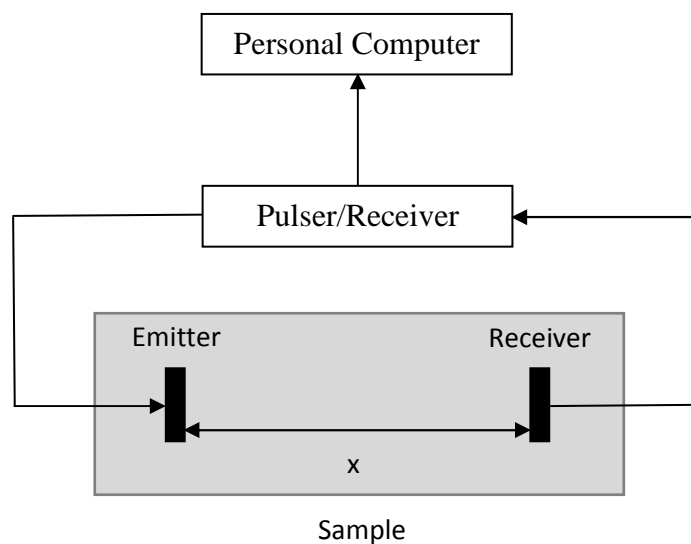
Fig. 1: Measuring setup for pulse transmission method

The pulse generator/receiver generates electrical pulses, which are sent to the emitter transducer, which converts electrical energy to ultrasonic waves. After passing through

the sample, these ultrasonic waves are converted back to electrical signals by the receiving transducer. These electrical signals can be recorded on the computer. The P-wave velocity is then calculated by using the formula in the following.

$$V_p = \frac{x}{\Delta t}$$

Where, x is the distance between the emitting transducer and receiving transducer, and Δt is the duration of wave propagation through the sample. The velocities are given in table 1.

Mass fraction of clay	T (°C)	x (cm)	Δt (µs)	V_p (m/s)
0%	30	10.7±0.6	72.8±0.4	1470±90
2%	25	10.0±0.6	64.8±0.4	1540±100
3%	25	10.0±0.6	62.4±0.4	1600±110
4%	25	5.0±0.6	29.2±0.4	1710±220
5%	27	10.7±0.6	72.5±0.4	1480±90
7%	27	10.7±0.6	54.9±0.4	1940±120

Table 1: Ultrasonic technique: P-wave velocity calculation at different temperatures

The P-wave velocity calculations using PAV technique are taken at 25°C. The results are given in table 2, which shows that he velocities found by PAV technique are too small than that the velocities determined by acoustic technique.

Mass fraction of clay	k' (Pa^{-1})	k'' (Pa^{-1})	V_p (m/s)
0%	$14.091 \cdot 10^{-9}$	$16.54 \cdot 10^{-9}$	220±36
2%	$9.683 \cdot 10^{-9}$	$12.472 \cdot 10^{-9}$	260±39
4%	$11.025 \cdot 10^{-9}$	$9.291 \cdot 10^{-9}$	280±44
5%	$11.025 \cdot 10^{-9}$	$19.600 \cdot 10^{-9}$	220±33
7%	$3.675 \cdot 10^{-9}$	$11.216 \cdot 10^{-9}$	300±46

Table 2: PAV technique: P-wave velocity calculation at 25°C

The values of V_p obtained by using the two techniques are shown together in figure 2.
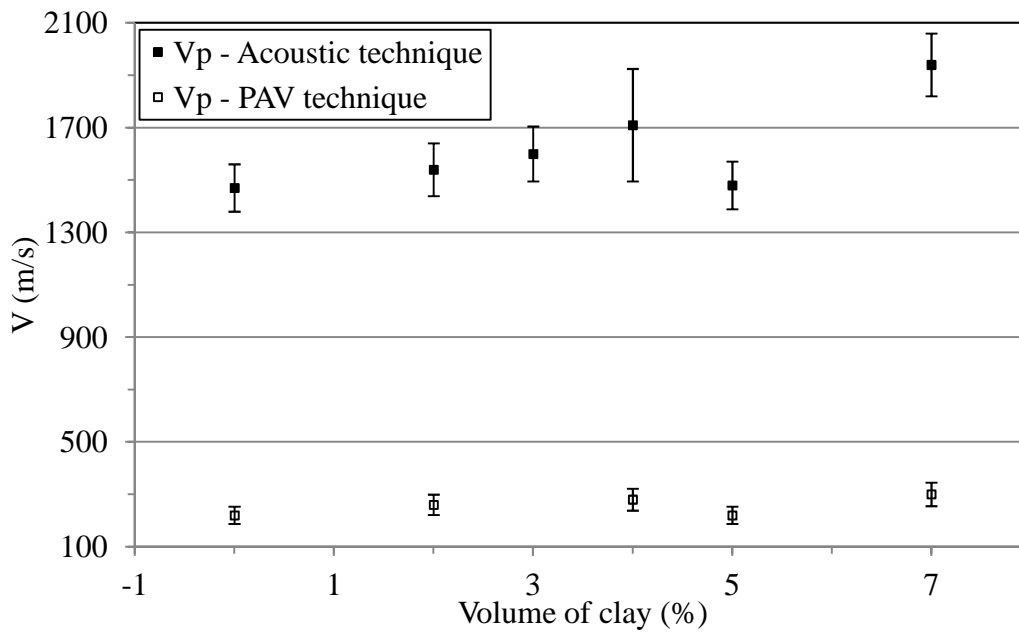
Fig. 4: Comparison of P-wave velocity measured by PAV technique and acoustic technique.

Figure 4 shows the measurement of P-wave velocity with the PAV technique is not good as compared to acoustic technique. It may be due to the following reasons. Firstly: the effect of putting bad amount of sample, because when we took these measurements we were not used to put the optimal amount of sample. Instead, it was used to put by

hand. Secondly: the sample is not homogeneous, and the presence of clay particles may block the vibrating plate.

Conclusion and perspectives

Rheology of complex fluids is growing topic in applied research. However, the conventional rheometers are often large, require large volumes of fluid in their measurements, and are limited to low frequencies (lower than 100 Hz) if used in the oscillation mode. There is also a drive to test complex fluids at higher and higher frequencies so that the fundamental processes that occur within the fluid at short time scales can be analyzed. Sometimes, these higher frequencies can be obtained by using time-temperature principle, but it is not always possible, especially if the material possesses a phase or glass transition state in the studied temperature range. On the other side, the torsional resonators and quartz resonators can also be used to acquire high frequency data. However, the disadvantage of these kinds of devices is that they are only operated at a single frequency.

Therefore, it is obvious that there is a need for a rheometer that can be operated at a continuous high frequency range rheometer, which can use small volumes of sample. For this purpose, we have presented a rheometer, which fulfills the above requirements. This device is based on the Piezo Axial Vibrator (PAV) principle. It is a kind of squeeze flow rheometer. It is very useful to study the rheological properties of viscoelastic materials, within the linear viscoelastic range. During the dynamic squeeze flow, the complex spring constant K^* of the sample is determined using the phase and amplitude of the induced voltage, and under the condition that no wall slip takes place and the disc radius R is very much larger than the sample thickness d. From K^*, we are then able to calculate the viscoelastic properties i.e. the complex shear modulus $G = G' + iG''$, the complex shear compliance $J = J' + iJ''$, and the complex viscosity $\eta = \eta' + i\eta''$. In

PAV, the sample effect is proportional to $(1/d^3)$, so that with small d one can also measure low viscous substances. It can work in the temperature range of 5°C to 150°C, and the frequency range of 1 Hz to 8 kHz at the atmospheric pressure. It requires very small amount of sample (down to 10µm). The disadvantage of this rheometer is that it requires a number of actuators and sensors that need to be assembled very carefully making the instrument expensive.

However, the study of rheological properties of petroleum fluids at reservoir conditions requires a high-pressure device. Therefore, to achieve this goal, the atmospheric pressure device is adapted to fit in a newly developed high-pressure cell (chapter 3). This high-pressure device has the advantage that it measures the viscoelastic properties not only in the same temperature and in frequency range as the atmospheric pressure one, but also extends the pressure range up to 500 bars (50 MPa). For atmospheric pressure measurements, it uses the same sample amount as the atmospheric pressure PAV. It possesses the disadvantage that for high-pressure measurements, the HP-PAV needs a big amount of sample.

The work undertaken in development of high-pressure PAV device shows that there is a great potential for this rheometer to be improved further to the point where it can be industrially useful. For the present, we have only studied the viscoelastic properties at atmospheric pressure. Measurement should be done at high pressures and high temperatures. Note that for high-pressure measurements, the ditch around the plates will also be filled with sample; therefore, a study needs to be done to measure the effect of the connected volume. Furthermore, the range of U/U_0 for valid data should be taken into account, which can vary from Newtonian to non-Newtonian fluids. Finally yet

importantly, since we do not know the behavior of HP-PAV for measurements at high pressures and high temperatures, therefore, extreme care should be taken for such measurements to avoid any unexpected incident.

REFERENCES:

Abu-Jdayil B. (2003). *"Modelling the time-dependent rheological behavior of semisolid food stuffs"*. Journal of Food Engineering, **57**: p. 97–102.

Ahmed J. and Ramaswamy H.S. (2007). *"Dynamic rheology and thermal transitions in meat-based strained baby foods"*. Journal of Food Engineering, **78**: p. 1274–1284.

Arabo E.Y.M. (2011). *"Shear and extensional viscosities of hard wheat flour dough using a capillary rheometer"*. Journal of Food Engineering, **103**: p. 294–298.

Barnes H.A., Hutton J.F., and Walters K. (1989). *"An Introduction to Rheology"*. ELSEVIER SCIENCE PUBLISHERS B.V.

Barnes H.A. (1999). *"The yield stress — a review or 'παντα ρει'— everything flows?"*. Journal of Non-Newtonian Fluid Mechanics. **81**: p. 133–178.

Barnes H.A. (2000). *"A Handbook of Elementary Rheology"*. University of Wales Institute of Non-Newtonian Fluid Mechanics.

Behura J., Batzle M., Hofmann R., and Dorgan J. (2007). *"Heavy oils: Their Shear Story"*. Geophysics, **72**(5): p. 175-183.

Bell D., Binding D.M. and Walters K., (2005). *"The Oscillatory Squeeze Flow Rheometer – Comprehensive Theory and a New Experimental Facility"*. Rheologica Acta, **46**(1): p. 111-121.

Bird R.B., Dai G.C., and Yarusso B.J. (1983). *"The rheology and flow of viscoplastic materials"*. Review Chemical Engineering. **1**: 1-70.

Bird R.B., Armstrang R.C., and Hassager O. (1987). "Dynamics of Polymeric Liquids". <u>A Wiley –Interscience Publication</u>.

Bylund G. (1995). "*Dairy Processing Handbook*". 2nd Edition. <u>Tetra Pak Processing systems AB,S-221 86 Lund, Sweden</u>.

Chan T.W., and Baird D.G. (2002). "*An evaluation of squeeze flow rheometer for the rheological characterization of a filled polymer with a yield stress*". <u>Rheologica Acta</u>, **41**: p. 245-256.

Chhabra R.P. and Richardson J.F. (1999). "*Non-Newtonian Flow in the Process Industries, Fundamentals and Engineering Applications*". <u>Butterworth-Heinemann</u>.

Cheneler D. (2009). "*The design and Analysis of a Micro Squeeze Flow Rheometer*". *PhD thesis.* <u>The university of Birmingham</u>.

Cheneler D., Bowen J., Ward M.C.L., Adams M.J. (2011). "Micro squeeze flow rheometer for high frequency analysis of nano-litre volumes of viscoelastic fluid". <u>Microelectronic Engineering</u>, **88**: p. 1726–1729.

Cheng L.X. (1998). "*Experimental Study of Rheological Behavior of Heavy Oil Under Reservoir Conditions*". <u>Jianghan Research Institute of Petroleum Exploration and Development, Jianghan, China</u>. No.1998.029.

Choi S.Y. (1968). "*Determination of melt viscosity as a function of hydrostatic pressurein an extrusion rheometer*". <u>J. Polym</u>. Sci. **6**(12): p. 2043-2049.

Coblas D., Broboana D. and Balan C. (2010). "*Rheological characterization of viscous fluids in oscillation squeezing flows*". <u>U.P.B. Sci. Bull., Series D</u>. **72**(3): p. 177-184.

Curtis C., Kopper R., Decoster E., Guzman-Garcia A., Huggins C., Knauer L., Minner M., Kupsch N., Linares L.M., Rough H., and Waite M. (2002). "*Heavy oil reservoirs*": Oilfield Review, **14**(3): p. 30–51.

Donsì G., Ferrari G., Maresca P. (2011). "*Rheological properties of high pressure milk cream*". Procedia Food Science, **1**: p. 868–868.

Elgibaly A.A.M., Nashawi I.S., and Tantawy M.A. (1997). "*Rheological characterization of Kuwaiti oil-lakes and their emulsions*". SPA 37259.

Ellis J. (1976). "*Ultrasonic and viscoelastic studies at different pressures*". Ph.D. Thesis, University of Salford.

Engmann J., Servais C., Burbidge A.S. (2005). "*Squeeze flow theory and applications to rheometry: A review*". Journal of Non-Newtonian Fluid Mechanics. **132**: p. 1–27.

Ferry J.D. (1980). "*Viscoelastic Properties of Polymers*", 3rd Edition, John Wiley & Sons New York, ISBN: 0-471-04894-1.

Field J.S., Swain M.V. and Phan-Thein N., (1996). "*An Experimental Investigation of the use of Random Squeezing to Determine the Complex Modulus of Viscoelastic Fluids*". J. Non-Newtonian Fluid Mech., **65**: p. 177-194.

Flugge W. (1967). "*Viscoelasticity*". Waltham, Massachusetts: Blaisdell Pub. Co.

Fritz G., Maranzano B.J., Wagner N.J., Willenbacher N. and (2002). "*High frequency rheology of hard sphere colloidal dispersions measured with a torsional resonator*". J. Non-Newtonian Fluid Mech, **102**: p. 149–156.

Hemeida A.M. and Al-Awad M.N.J. (1999). "Rheological behavior of high viscosity Saudi crude oil". <u>Journal of Engineering</u>, **9**(3): p. 51-60.

Henaut I., Argillier J-F., Pierre C., and Moan M. (2003). *"Thermal Flow Properties of Heavy Oils"*. <u>Offshore technology conference (OTC)</u> 15278, p.1-6.

Henson D.J. and Mackay M.E. (1995). "*Effect of gap on the viscosity of monodisperse polystyrene melts: Slip effects*". <u>Journal of Rheology</u>, **39**(2): p. 359-373.

Hinkle A. and Batzle M. (2006). "*Heavy oils: A worldwide overview*". <u>The Leading Edge</u>, **25**(6): p.742-749.

Jo C., Fu J., and Naguib H.E. (2005). "*Constitutive modeling for mechanical behavior of PMMA microcellular foams*" <u>Polymer</u>, **46**: p. 11896–11903.

Jo C., Fu J., and Naguib H.E. (2007). "*Constitutive modeling of HDPE polymer/clay nanocomposite foams*". <u>Polymer</u>, **48**: p. 3349–3360.

Kalita P., Schaefer R. (2008). "*Mechanical Models of Artery Walls*". <u>Arch Comput Methods Eng</u>, **15**: p. 1–36.

Kalyon D.M., Yaras P., Aral B., and Yilmazer U. (1993). "*Rheological behavior of a concentrated suspension: A solid rocket fuel stimulant*". <u>Journal of Rheology</u>, **37**(l): p.35-53.

Khandare P. M., Zondlo J.M., Stansberry P.B., Stiller A.H. (2000). "*Rheological investigation of pitch materials Part I: Design and development of a high-temperature high-pressure (HTHP) rheometer*". <u>Carbon</u>, **38**: p. 881–887.

Khelladi H., Plantier F., Daridon J.L., and Djelouah H. (2009). Measurement under high pressure of the nonlinearity parameter B/A in glycerol at various temperatures. Ultrasonics, **49**: p. 668–675.

Kimber K. D. (2007). "*Heavy oil*". Eighth U.S.-China Oil and Gas Industry Forum, September 9-11 2007 San Francisco California.

Kirschenmann L. (2003). "*Structure of two piezoelectric devices (PRV/PAV) to measure the visco-elastic properties of soft substances in the frequency range 0.5 Hz - 2 kHz or 0.5 Hz - 7 kHz*" PhD thesis University of Ulm Germany.

Kolitawong C., Giacomin A.J. (2002). "*Dynamic response of a shear stress transducer in the sliding plate rheometer*". J. Non-Newtonian Fluid Mech, **102**: p. 71–96.

Lawal A. and Kalyon D.M. (1998). "*Squeezing Flow of Viscoplastic Fluids Subject to Wall Slip*". POLYMER ENGINEERING AND SCIENCE, **38**(11): p. 1793-1804.

Lawal A. and Kalyon D.M. (2000). "*Compressive Squeeze Flow of Generalized Newtonian Fluids with Apparent Wall Slip*". Intern. Polymer Processing, **XV** (1): p. 63-71.

Lewandowski R., Chorazyczewski B. (2010). "*Identification of the parameters of the Kelvin–Voigt and the Maxwell fractional models, used to modeling of viscoelastic dampers*". Computers and Structures, 88: p. 1–17.

Mackley M.R., Marshal R.T.J., Smeulders J.B.A.F (1995). "*The multipass rheometer*". J. Rheol, **39**(6): p. 1293-1309.

Macosko, C.W. (1994). "*Rheology principles, measurements and applications*". Wiley. VCH, Inc.

Manconi M., Aparicio J., Seyler D., Vila A.O., Figueruelo J., and Molina F. (2005). "*Effect of several electrolytes on the rheopectic behaviour of concentrated soy lecithin dispersions*". Colloids and Surfaces A: Physicochem. Eng. Aspects 270–271: p. 102–106.

Mavko G., Mukerji T., and Dvorkin J. (1998). "*The Rock Physics Handbook; Tools for Seismic Analysis in Porous Media*". Cambridge University Press: p. 51-75.

Meeten G.H. (2004). "*Squeeze flow of soft solids between rough surfaces*". Rheol Acta, **43**:p. 6-16

Morita A.T., Toma M.S., Marco-Aurelio P. (2006). "*Low cost capillary rheometer, transfer molding and die-drawing module*". Polymer Testing, **25**: p.197-202.

Nehdi M. and Rahman M.A. (2004). "*Estimating rheological properties of cement pastes using various rheological models for different test geometry, gap and surface friction*". Cement and Concrete Research. **34**: p. 1993–2007.

Nwankwo E., Durning C.J. (1999). "*Fluid property investigation by impedance characterization of quartz crystal resonators Part I: Methodology, crystal screening, and Newtonian fluids*". Sensors and Actuators, A72: p. 99–109.

Ortman K.C., Agarwal N., Eberle A.P.R., Baird D.G., Wapperom P., Giacomin A.J. (2011). *"Transient shear flow behavior of concentrated long glass fiber suspensionsin a sliding plate rheometer"*. Journal of Non-Newtonian Fluid Mechanics, **166**:p. 884–895.

Oswald P. (2005). *"Rhéophysique ou comment coule la matière"*. Edition Belin.

Plegue, T.H., Frank, S.G., and Zakin, J.L., (1989). *"Studies of water-continuous emulsions of heavy crude oils prepared by alkali treatment"*. SPE Prod. Eng, **4** (2): p. 181–183.

Prevost S.L., Bernatchez H.M., Jackson K.A., Arbour N.A., Harder C.J. (2009). Spartan DX-12 TM Instrument Repeatability and Reproducibility. DX12 AN001 VER 1.0 Nov 09.

Rao M.A. (1999). *"Rheology of Fluid and Semisolid Foods: Principles and applications"*. Aspen publishers Inc. Maryland.

Romoscanu A.I., Sayir M.B., Häusler K. and Servais C. (2003). *"High frequency probe for the measurement of the complex viscosity of liquids"*. Meas Sci Technol, **14**(4): p. 451-462.

Sablani S.S., Shayya W.H., and Kacimov A. (2003). *"Explicit calculation of the friction factor in pipeline flow of Bingham plastic fluids: a neural network approach"*. Chemical Engineering Science, **58**: p.99-106.

Sadeqi S., Khabazi N., and Sadeghy K. (2011). *"Blasius flow of thixotropic fluids: A numerical study"*. Commun Nonlinear Sci Numer Simulat, **16**: p. 711–721.

Saowapark S., Apichartsrangkoon A., Bell A.E. (2008). "*Viscoelastic properties of high pressure and heat induced tofu gels*". Food Chemistry, **107**: p. 984–989.

Schramm G. (2000). "*A Practical Approach to Rheology and Rheometery*". 2nd Edition.

Seyssiecq I., Ferrasse J-H., and Roche Nicolas (2003). "*State-of-the-art: rheological characterization of wastewater treatment sludge*". Biochemical Engineering Journal, **16**: p. 41–56.

Shah N. A. (2008). "*Ideal Fluid Dynamics for Scientists and Engineers*". A-One Publishers Lahore.

Shaw M.T. and Liu Z.Z. (2006). "*Single-point Determination of Nonlinear Rheological Data from Parallel-Plate Torsional Flow*". Applied Rheology. **16**(2): p.70– 79.

Shenoy A.V. (1999). "*Rheology of Filled Polymer Systems*". Kluwer Academic Publishers.

Sherwood J.D. (2005). "*Model-free inversion of squeeze-flow rheometer data*". J. Non-Newtonian Fluid Mech, 129:p. 61–65.

Son Y. (2008). "*Development of a pressure-driven micro-rheometer*". Polymer Testing, **27**: p. 243–247.

Steffe J.F. (1996). "*Rheological Methods in Food Process Engineering*". Freeman press USA.

Steffe J.M. and Daubert C.R. (2006). "*Bioprocessing Pipelines: Rheology and Analysis*". <u>Freeman press USA</u>.

Swamee P.K., and Aggarwal N. (2011). "*Explicit equations for laminar flow of Bingham plastic fluids*". <u>Journal of Petroleum Science and Engineering</u>, **76**(3): p. 178-184.

Tadmor Z. and Gogos C.G. (2006). "*Principles of polymer processing*". Wiley Interscience. 2nd Edition.

Ungerer P., Batut C., Moracchini G., Sanchez J., De Sant'Anah H.B., Carrier J., Jensen D. M. (1998). "*Measurement and prediction of volumetric and transport properties of reservoir fluids at high pressure*". <u>Revue de l'Institut Français du Pétrole</u>. **53**(3): Mai-Juin

Valtorta D., Mazza E. (2005). "*Dynamic measurement of soft tissue viscoelastic properties with a torsional resonator device*". <u>Medical Image Analysis</u>, **9**: p. 481–490.

Venerus D.C. (2007). "*Free Surface Effects on Normal Stress Measurements in Cone and Plate Flow*". <u>Applied Rheology</u>, **17**(3): p. 36494-1-- 36494-6.

Walters K. (1975). *"Rheometry"*. <u>Chapman and Hall Ltd</u>.

Wang B. and Chen L.Q. (2009). "*Asymptotic stability analysis with numerical confirmation of an axially accelerating beam constituted by the standard linear solid model*". <u>Journal of Sound and Vibration</u>, **328**: p. 456–466.

Wang B., Li D., Wang L-J., and Özkan N. (2010). "*Anti-thixotropic properties of waxy maize starch dispersions with different pasting conditions*". Carbohydrate Polymers, **79** : p. 1130–1139.

Wang J., Dong M., and Asghari K. (2006). "*Effect of Oil Viscosity on Heavy-Oil/Water Relative Permeability Curves*". SPE 99763.

Zhang J.J., Liu X. (2008). "*Some advances in crude oil rheology and its application*". J. Cent. South Univ. Technol. **15**(s1): p. 288-292.

Zhao Y. and Machel H.G. (2012). "*Viscosity and other rheological properties of bitumen from the Upper Devonian Grosmont reservoir, Alberta, Canada*". AAPG Bulletin, **96**(1): p. 133-153.

RÉSUMÉ

La rhéologie des fluides complexes est un sujet à l'intérêt grandissant dans le domaine de la recherche appliquée. Toutefois, les rhéomètres classiques nécessitent de grands volumes d'échantillons et sont généralement limités à une plage relativement étroite de fréquences de fonctionnement. En outre, seuls quelques rhéomètres sont dédiés à des mesures à hautes pressions, qui sont pourtant essentielles pour résoudre certains des problèmes rencontrés dans l'industrie pétrolière. Par conséquent, dans le cadre de cette thèse, un rhéomètre piézo-électrique à vibrations axiales est présenté. Il peut produire des données sur une large gamme de fréquences continues (1 Hz à 8 kHz). Il peut être utilisé avec de faibles quantités d'échantillons (jusqu'à 10 µL) et a servi pour la caractérisation d'huiles de synthèse. Enfin, cet appareil a été adapté pour faire face à des conditions de haute pression. Pour ce faire, une nouvelle conception de la cellule a été nécessaire et est présentée dans ce travail. Ce projet de thèse permettra d'étudier les propriétés de transport des huiles lourdes et de concilier les données obtenues dans les domaines de la sismique et de la pétro-acoustique.

ABSTRACT

Rheology of complex fluids is growing topic in applied research. However, the conventional rheometers require large sample volumes and are usually limited to a relatively narrow range of operating frequencies. Furthermore, only few rheometers are dedicated to high pressures conditions, which are nevertheless crucial to tackle some of the petroleum industry problem. Therefore, in this thesis, a piezoelectric axial vibrator rheometer is presented which can produce data for a large continuous frequency range (1 Hz to 8 kHz). It can be used for very small amount of samples (down to 10µL) and has been employed to characterize synthetic oil. Then, this apparatus has been adapted to deal with High Pressure conditions. To do so, a new design of the cell has been required and is presented in this work. This thesis project will allow studying the transport properties of heavy oils to conciliate the data obtained in the areas of seismic and petro-acoustic.